

FRIEDRICH-SCHILLER-UNIVERSITÄT JENA  
FAKULTÄT FÜR MATHEMATIK UND INFORMATIK



# Numerical bifurcation analysis of the asymmetric spring-mass model

DISSERTATION

zur Erlangung des Akademischen Grades  
doctor rerum naturalium (Dr. rer. nat.)

vorgelegt dem Rat der Fakultät für Mathematik und Informatik  
der Friedrich-Schiller-Universität Jena

von Dipl.-Math. ANDREAS MERKER,  
geboren am 25.11.1975 in Kustanai

1. Gutachter: Prof. Dr. Martin Hermann (FSU Jena)
2. Gutachter: Prof. Dr. Andre Seyfarth (TU Darmstadt)
3. Gutachter: Prof. Dr. Gerhard Zumbusch (FSU Jena)

Tag der Disputation: 03.07.2014

# Contents

<b>Zusammenfassung</b>	<b>vi</b>
<b>Abstract</b>	<b>vii</b>
<b>1. General introduction</b>	<b>1</b>
<b>2. Stable walking with asymmetric legs</b>	<b>5</b>
2.1. Introduction . . . . .	5
2.2. Motivation . . . . .	6
2.2.1. Robot experiment . . . . .	6
2.2.2. Prosthetic walking . . . . .	8
2.2.3. Aims of this study . . . . .	8
2.3. Methods . . . . .	9
2.3.1. Symmetric model . . . . .	9
2.3.2. Asymmetric model . . . . .	12
2.3.3. System analysis . . . . .	12
2.4. Results . . . . .	13
2.4.1. Period-one gaits with symmetric legs . . . . .	13
2.4.2. Period doubling . . . . .	14
2.4.3. Asymmetry of angle of attack . . . . .	14
2.4.4. Asymmetry of leg stiffness . . . . .	16
2.4.5. Asymmetry of rest length and dimensionless energy . . . . .	16
2.5. Discussion . . . . .	16
<b>3. Spring-mass model</b>	<b>22</b>
3.1. Introduction . . . . .	22
3.2. The model as a hybrid dynamical system . . . . .	24
3.2.1. Running . . . . .	24
3.2.2. Walking . . . . .	26
3.3. Periodic solutions . . . . .	27
3.3.1. Running . . . . .	28

3.3.2. Walking . . . . .	29
3.4. Transformation into a boundary value problem . . . . .	29
3.4.1. Running . . . . .	30
3.4.2. Walking . . . . .	31
3.4.3. Period-2 solutions . . . . .	33
3.5. Results . . . . .	34
3.5.1. Running . . . . .	34
3.5.2. Walking . . . . .	36
3.6. Discussion . . . . .	37
<b>4. Numerical bifurcation analysis of the spring-mass model</b>	<b>41</b>
4.1. Introduction . . . . .	41
4.2. Some topics of the analytical bifurcation theory . . . . .	42
4.2.1. Definitions and important theorems . . . . .	43
4.2.2. Lyapunov-Schmidt reduction . . . . .	45
4.2.3. Simple turning points . . . . .	47
4.2.4. Double turning points . . . . .	47
4.2.5. Secondary bifurcation points . . . . .	48
4.2.6. Continuation . . . . .	50
4.3. Bifurcations in the spring-mass model . . . . .	51
4.3.1. Simple turning point . . . . .	51
4.3.2. Transcritical bifurcation . . . . .	52
4.3.3. Period-doubling bifurcation . . . . .	52
4.3.4. Hopf bifurcation . . . . .	53
4.3.5. Double turning point . . . . .	53
4.3.6. Implementation . . . . .	54
4.4. Results . . . . .	55
4.4.1. Running . . . . .	55
4.4.2. Walking . . . . .	56
4.5. Discussion . . . . .	58
<b>5. Stable running with asymmetric legs</b>	<b>60</b>
5.1. Introduction . . . . .	60
5.2. The asymmetric spring-mass model for running . . . . .	61
5.3. Transformation into a boundary value problem . . . . .	62
5.4. Results . . . . .	62
5.4.1. Asymmetry of angle of attack . . . . .	62
5.4.2. Asymmetry of leg stiffness . . . . .	64
5.4.3. Asymmetry of rest length . . . . .	64

---

5.5. Discussion . . . . .	66
<b>6. General conclusions</b>	<b>70</b>
6.1. Summary . . . . .	70
6.2. Outlook . . . . .	71
<b>A. Computation of adjointed matrices</b>	<b>72</b>
<b>Danksagung</b>	<b>87</b>
<b>Ehrenwörtliche Erklärung</b>	<b>88</b>

# Zusammenfassung

Das Feder-Masse-Modell und deren zahlreichen Erweiterungen gehören derzeit zu den besten Kandidaten für das Template der menschlichen Fortbewegung. Mit der steigenden Komplexität wird jedoch deren Anwendung sehr aufwendig. Da Bifurkationen die Gebiete der stabilen Bewegung begrenzen, kann das Studium des Stabilitätsverhaltens auf die Berechnung entsprechender Grenzpunkte zurückgeführt werden. In dieser Dissertation wird ein Verfahren präsentiert, das auf der Berechnung von Bifurkationspunkten im Feder-Masse-Modell beruht. Im Original basiert das Modell auf einem hybriden dynamischen System. Das hier vorgeschlagene Verfahren besteht aus der Transformation der Folge von Anfangswertproblemen in ein einziges Randwertproblem. Mit der neuen Methode lassen sich Unstetigkeiten vermeiden. Weiterhin ist die Anwendung fortgeschrittener numerischer Verfahren zur Lösung parameterabhängiger Zwei-Punkt-Randwertprobleme möglich. Außerdem können sachgemäße erweiterte Systeme benutzt werden, um Umkehrpunkte, sowie transkritische und Periode-verdoppelnde-Bifurkationspunkte zu bestimmen. Es wird gezeigt, dass die entstehenden Randwertprobleme mit dem Einfachschießverfahren gelöst werden können, was die Anwendung des aufwendigeren Mehrfachschießverfahrens überflüssig macht. Das vorgestellte Verfahren ist schnell, robust gegenüber numerischen Störungen und erlaubt die Berechnung hochgradig instabiler periodischer Lösungen des Originalproblems.

Die asymmetrische Beinfunktion ist oft ein unerwünschter Seiteneffekt in künstlichen Beinsystemen und kann funktionale Defizite und Variationen der mechanischen Konstruktion widerspiegeln. Sie findet sich ebenfalls in der Fortbewegung von Menschen und Tieren nach einem Unfall oder in spezifischen Gangmustern. Bis jetzt ist nicht klar, inwiefern die Unterschiede in der Beinfunktion der gegenüberliegenden Gliedmaße während des Rennens oder Gehens toleriert werden können. In dieser Dissertation wird diese Fragestellung unter Verwendung des Feder-Masse-Modells für die Simulation von Rennen und Gehen mit nachgiebigen Beinen untersucht. Wir zeigen mit Hilfe der ursprünglichen Realisierung des Modells und des neuen Randwertproblem-Verfahrens, dass beträchtliche Unterschiede zwischen den gegenüberliegenden Beinen toleriert werden können und dass sie sogar von Vorteil für die Robustheit der Systemdynamik sein können. Ein besseres Verständnis der Mechanismen und der potenziellen Vorteile einer asymmetrischen Beinfunktion kann helfen, die Entwicklung von künstlichen Gliedmaßen und neuartiger therapeutischer Konzepte und Rehabilitationstrategien voranzutreiben.

# Abstract

The spring-mass model and its numerous extensions are currently some of the best candidates for templates of human locomotion. However, with increasing complexity, their applications can become very computationally costly. Since the bifurcations limit the region of stable locomotion, the study of stability can be reduced to the computation of the corresponding boundaries. In this thesis, an approach is presented that is based on the calculation of bifurcations in the spring-mass model. Originally, the realization of the model was based on a hybrid dynamical system. The new approach consists of the transformation of the series of initial value problems on different intervals into a single boundary value problem. Using this technique, discontinuities can be avoided and sophisticated numerical methods for studying parameterized nonlinear boundary value problems can be applied. Thus, appropriate extended systems are used to compute transcritical and period-doubling bifurcation points as well as turning points. We show that the resulting boundary value problems can be solved by the simple shooting method with sufficient accuracy, making the application of the more extensive multiple shooting superfluous. The proposed approach is fast, robust to numerical perturbations and allows to determine highly unstable periodic solutions of the original problem.

Asymmetric leg function is often an undesired side-effect in artificial legged systems and may reflect functional deficits or variations in the mechanical construction. It can also be found in legged locomotion in humans and animals, for example after an accident or in specific gait patterns. So far, it is not clear to what extent differences in the leg function of contralateral limbs can be tolerated during walking or running. Here, we address this issue using the spring-mass model for simulating walking and running with compliant legs. With the help of the original realization of the model and the boundary value problem approach, we show that considerable differences between contralateral legs can be tolerated and may even provide advantages to the robustness of the system dynamics. A better understanding of the mechanisms and potential benefits of asymmetric leg operation may help to guide the development of artificial limbs or the design novel therapeutic concepts and rehabilitation strategies.

# 1. General introduction

In natural sciences, mathematical models are tools, which provide a simplistic description of complex processes. The greatest challenge is to create a simple model, which is nonetheless powerful enough to describe sophisticated relationships. One of the most successful templates for the simulation of human walking, running and hopping is the spring-mass model. Here, the utterly complex human locomotion [Maus, 2012] is reduced to three control parameters. The model for running and hopping consists of a mass point representing a center of mass of the human body riding on a linear leg spring [Blickhan, 1989; McMahon & Cheng, 1990]. For the study of walking gaits, a second leg spring was introduced [Geyer et al., 2006]. While the simplicity of the model allows efficient study of a general locomotive behaviour, its great strength is also the possibility of extensions [Seyfarth et al., 2012, 2013]. For instance, the influence of different parts of a leg on locomotion can be simulated by a suitable segmentation of the leg spring [Maykranz et al., 2009; Rummel & Seyfarth, 2008].

Human locomotion is a complex process characterized by immense variability, e.g. Maurer et al. [2013]. The external variability provides the necessary adaptation of the locomotor system to the environment like rough terrain, stairs etc [Grimmer et al., 2008]. The human locomotor system has also a natural internal variability, which can be roughly separated in three parts: stochastical fluctuations (*noise*), change of leg properties during ground contact (*drift*) and leg asymmetry (*offset*) [Riese, 2013]. Drift occurs because the human leg is not a perfect linear spring. For instance, the leg stiffness changes during ground contact [Lipfert, 2010]. Stochastic fluctuations may have certain influence on the neural control of locomotion [Dingwell & Cusumano, 2010; Hausdorff, 2007]. The left-right leg asymmetry, which is one of the main subjects of this thesis, is not only observed in locomotion gaits of people with prosthetic limbs or unilateral injuries [Schaarschmidt et al., 2012] but also in legged robots with construction limitations [Merker et al., 2011b]. Gait asymmetry also occurs in healthy humans [Sadeghi et al., 2000]. A better understanding of the mechanisms and potential benefits of asymmetric leg operation may help to guide the development of artificial limbs [Grimmer & Seyfarth, 2011a,b] or the design of novel therapeutic concepts and rehabilitation strategies [Hreljac, 2004]. Most investigations do not address whether leg asymmetry must be handled as a limiting constraint, or instead should be exploited to help maximize task performance, e.g. Valderrabano et al. [2007]. The aim of this



study is to determine, whether the growing discrepancy between two contralateral legs has any positive effect on the stability of running or walking. Thus, leg asymmetry is considered as a fundamental system property.

The original spring-mass model contains three control parameters: the leg angle, the leg stiffness and the leg length. Leg asymmetry is simulated by an additional set of asymmetric parameters. Running is defined as the gait pattern with a flight phase and a single-support phase, i.e. when only one leg spring has a ground contact, e.g. [Seyfarth et al. \[2002\]](#). Walking is a combination of a single- and a double-support phase, e.g. [Rummel et al. \[2010b\]](#). Periodic solutions of the model often correspond to continuous locomotion patterns. The investigations of stable periodic solutions is of particular interest. While there are many ways to measure stability of human locomotion experimentally, e.g. [Bruijn \[2010\]](#), the mathematical definition of stability is considered as the property of the system to absorb small perturbations [[Marx & Vogt, 2011](#)]. The increased complexity makes the stability analysis of the asymmetric model to a challenging mathematical problem. The combination of the leg asymmetry with any other type of variability would additionally raise the computational effort. Therefore, for further efficient studies it is necessary to develop an approach, which reduces the complexity of the computation and still preserves the significance of the model.

The general idea is to reduce the computation of stable solutions to the study of the boundaries of the stability regions. This concept leads to a non-trivial mathematical problem, since the areas of stability are mostly confined between bifurcation points. Bifurcations often denote important qualitative changes (like gain and loss of stability) in the dynamics of physical systems. Thus, their study is important for many research fields like fluid sloshing [[Hermann & Timokha, 2005, 2008](#)], structural mechanics [[Ikeda & Murota, 2002](#)] or synthetic biology [[Strelkova, 2014](#)]. Bifurcation points are parameter values, where these changes happen. In particular, they are singularities in the given problems and can only be determined using special numerical methods. In this thesis, we use a method of *extended systems*, which is based on the Lyapunov-Schmidt reduction [[Lyapunov, 1906](#); [Schmidt, 1908](#)]. Here, the strategy is to embed the problem into a higher dimensional boundary value problem, which still can be solved using standard numerical techniques [[Wallisch & Hermann, 1987](#)]. To apply this approach for the study of asymmetric locomotion, an appropriate implementation of the spring-mass model is required.

The original realization of the model is based on a sequence of initial value problems (also called hybrid dynamical systems). There exist numerical methods for the computation of bifurcation points in hybrid systems. However, they often require the application of a specific software package, e.g. [Thota & Dankowicz \[2008\]](#). In this thesis, we propose a more general approach, which is based on boundary value problems [[Hermann, 2004](#); [Hermann & Saravi, 2014](#); [Stoer & Bulirsch, 1993](#)]. The implementation of the model as a parametrized two-point boundary value problem

can be extended for computation of bifurcation points as it described in [Wallisch & Hermann \[1987\]](#). There exist a number of efficient boundary value problem solvers for different platforms like AUTO [[Doedel et al., 2005](#)] or the MATLAB solver bvp4c [[Shampine et al., 2000](#)]. In this thesis, we propose the well-approved software package RWPM [[Hermann & Kaiser, 1993](#); [Hermann et al., 1999](#); [Hermann & Timokha, 2005](#)]. This package uses the fast and efficient shooting method for solving boundary value problems and provides a routine for the numerical continuation [[Hermann & Ullrich, 1992](#)]. Compared to the difference methods, e.g. [Hermann \[2004\]](#), and the variational methods, e.g. [Gottlieb & Orszag \[1977\]](#), the multiple shooting method and its modifications are the only feasible methods for the treatment of nonlinear boundary-value problems for ordinary differential equations [[Stoer & Bulirsch, 1993](#)].

Investigation of human locomotion is an interdisciplinary research field. Scientists from different areas of science, who are not familiar with advanced mathematical theory, may be interested in the predictions of mathematical modeling. Thus, our first aim was to develop an approach, that can be general enough to be understood by people, whose mathematical training does not extend beyond the classical methods of applied mathematics. Some basics of functional analysis and topology can nevertheless be helpful to get a better view on the problematic. Additionally, we intended to solve the resulting problem without the application of any specific software. For the systems presented in this work, any boundary value problem solver can be used without restriction by platform. Finally, a clear visual presentation of results is crucial for their intuitive understanding. Therefore, we present our most important outcomes in detailed bifurcation diagrams.

During the work on this thesis, three publications were submitted to scientific journals. The paper [Merker et al. \[2011b\]](#) was written in collaboration with Jurgen Rummel and Prof. Dr. Andre Seyfarth. The PogoWalker experiments were conducted by Dr. Horst-Moritz Maus. The numerical bifurcation analysis of the bipedal model [Merker et al. \[2013\]](#) was developed together with Dr. Dieter Kaiser and Prof. Dr. Martin Hermann. The study of the asymmetric model [Merker et al. \[2014\]](#) was done with the additional support by Prof. Dr. Andre Seyfarth. Last but not least, the poster [Merker et al. \[2011a\]](#) from the Dynamic Walking conference (Jena, 2011) arose in cooperation with Dr. Sebastian Riese and Prof. Dr. Andre Seyfarth.

**This thesis is organized as follows.** In the next chapter, the paper [Merker et al. \[2011b\]](#) is presented. The chapter describes in detail the importance of the study of asymmetric locomotion and provides strong biomechanical background for the asymmetric model. Using the asymmetric model, we investigated to what extent the left-right leg asymmetry can be tolerated during walking. The model was implemented as a sequence of initial value problems. Bifurcation points were found in a heuristic way. First, the neighbouring points of the desired bifurcation point were calculated as precisely as possible. Then, the bifurcation point was found as the intersection point

of corresponding solution branches. In particular, all required stable solutions had to be computed explicitly. During the work on this paper, we noticed that the applied heuristic approach is slow and expensive. This observation led to the development of a new method based on boundary value problems.

In Chapter 3, we give a detailed mathematical description of the spring-mass model and present its transformation into a boundary value problem. Although the new implementation of the model is a necessary intermediate step for the computation of bifurcation points, it has useful properties on its own.

Chapter 4 starts with some basic topics of the numerical bifurcation theory. In particular, the techniques of extended systems for the numerical determination of various types of bifurcation points are presented. Then, the extended systems are applied to the boundary value problem implementation of the spring-mass model. Finally, we show how the new approach can be used to compute the manifolds of stable solutions of the symmetric spring-mass model.

In Chapter 5, we apply the boundary value problem approach from Chapter 3 to the asymmetric spring-mass model. Using the extended systems from Chapter 4, we compute bifurcation points and thus the regions of stability of the asymmetric model. With results of Chapter 3 as a reference, we investigate the influence of the asymmetric parameters on the stability of running. Moreover, we demonstrate the superiority of the boundary value problem approach to the heuristic method from Chapter 2.

In the last chapter, the main results of this thesis are summarized and discussed.

**The aims of this thesis are:**

- Development of a new boundary value problem approach for the spring-mass model.
- Extension of the boundary value problem for the computation of different types of bifurcation points.
- Application of the bifurcation analysis to the investigation of the stability behaviour of the asymmetric spring-mass model.

## 2. Stable walking with asymmetric legs

### 2.1. Introduction

For locomotion humans usually select the most efficient bipedal gait, namely walking [Cavagna & Kaneko, 1977]. Beside efficiency, an equally important property of the chosen gait is stability. Human walking has inspired engineers to build bipedal robots, which should walk as stable as humans. Humans stabilize walking in a rather unconscious and intuitive way. In artificial legged systems, it is still a challenge to achieve stability during the highly dynamic gait.

The symmetry between contralateral legs is considered an appropriate condition for achieving stable locomotion. However, human legs are adaptable and offer much more possibilities than used during walking like when moving over slightly uneven terrain or walking up- and downstairs. Additionally, human legs have to deal with unexpected situations, for example if an unexpected step down arises. However, in most cases leg mechanics and neural system are able to master such critical situations.

The human locomotor system is not only able to deal with external disturbances, it may also need to manage internal challenges. One such issue is the asymmetry between the left and right leg, which is found prominently in people with prostheses or orthoses. Here, it is obvious that the dynamics of both legs are different. One reason could be the differences in leg masses, which results in gaits of periods greater than two, as predicted in a compass-gait model [Moon & Spong, 2010]. Interestingly, a left-right asymmetry during locomotion is observed also in able-bodied human subjects, even with equal leg masses [Sadeghi et al., 2000]. Herzog et. al. have reported that asymmetries of ground reaction force (GRF) of about 4% are observable in normal walking [Herzog et al., 1989]. Another common issue found in humans is leg length inequality [Gurney, 2002]. The left-right differences in gait patterns are most visible for slower speeds [Goble et al., 2003; Nolan et al., 2003]. Beside left-right asymmetries, small stochastic stride-to-stride fluctuations are reported [Dingwell et al., 2010], which could also contribute to dynamical asymmetries of the gait. Stride-to-stride fluctuations might even be important to increase robustness of walking while minimizing energetic costs. In artificial walking devices, they can also be used for learning algorithms that improve robustness and top speed [Faber & Behnke, 2007; Kohl & Stone, 2004].

These observations indicate that gait asymmetries are a key feature of human motion. Nevertheless, during the design process of a bipedal robot, engineers take care of identical leg properties and joint control on both sides. But in practice, dynamic properties of the legs are often not exactly equal, for instance the wear at the joints could be different. Such imperfections in the hardware (mechanics, actuators) could lead to a left-right asymmetry of leg dynamics. In this chapter, we investigate to what extent asymmetric leg function may challenge walking stability. For this, we use a simulation model, i.e. the bipedal spring-mass model, that resembles the dynamics, and therefore the resulting center of mass (CoM) kinematics of human walking [Geyer et al., 2006]. Following the concept of Full & Koditschek [1999] and Jordan [1990], we aim at subsequentially increasing the complexity of a gait template such that the scientific question can be addressed while features of the underlying body dynamics are preserved. Here, the additional complexity is achieved by introducing asymmetry parameters into the model.

Human walking is characterized by single- and double-support phases, while the body is lifted during single-support around midstance. It is further distinguished from other gaits by the pattern of ground reaction force, where a double humped pattern with two force maxima is observed [Lipfert, 2010]. Although human and artificial legs are very complex in their structure, their function during walking can be described mechanically in a surprisingly simple way. At preferred walking speed, a fairly linear force-length relationship is found [Lipfert, 2010]. Thus, the human leg can be understood as a simple prismatic leg spring supporting the body.

This chapter is organized as follows. To motivate our study, we give two examples of asymmetric walking in the next section. In Section 2.3 the methods used in our investigations are presented. In Section 2.4 the results of simulations are described followed by their discussion in Section 2.5.

## 2.2. Motivation

### 2.2.1. Robot experiment

One motivation for this study is the customized conceptual bipedal walking robot, PogoWalker (Figure 2.1(a)), which was developed at the Laufflabor Locomotion Laboratory, Friedrich-Schiller-Universität Jena. The legs of PogoWalker have the same stiffness and length. Each leg is moved by two motors: the first one actuates the hip and the second one shortens the leg during the swing phase (Figure 2.1(b)). The motors for the leg rotation are arranged in the front and the back of the upper body to align the center of mass in the geometric center. As there was a slight mechanical coupling between leg rotation (first motor) and leg shortening (second motor), this construction approach led to different leg angles of left and right leg. Due to the shifted leg

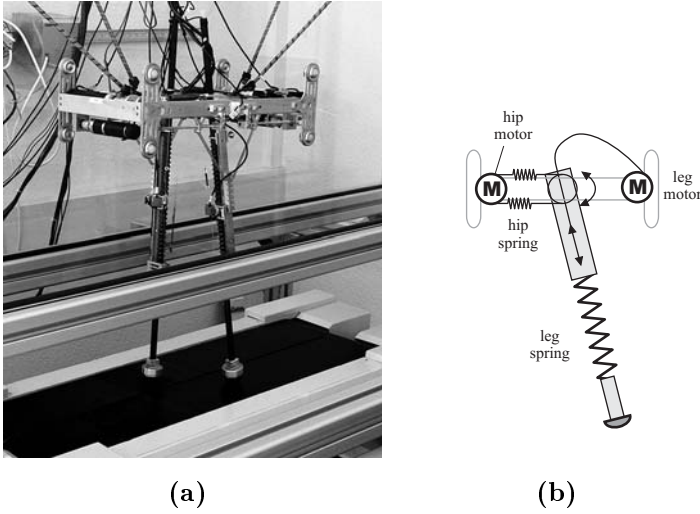


**Figure 2.1.** The bipedal PogoWalker in (a) with compliant telescoping legs walking on the instrumented treadmill. The schematic in (b) illustrates the motor configuration for one leg.

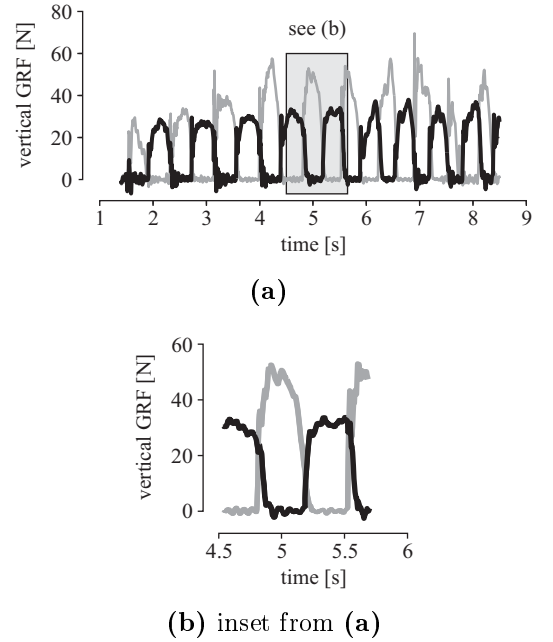


**Figure 2.2.** Vertical ground reaction forces (GRF) of PogoWalker measured with treadmill sensors. The forces are separated for both legs and were recorded with 200 Hz. Here, only the first ten strides are shown.

placements, the leg compressions vary, which results in different maxima of the ground reaction forces (Figure 2.2).

The robot has two equal prismatic legs with fixed rest length of  $L_0 = 0.58$  m and fixed average normalized leg stiffness of  $\tilde{k}_0 = 20$ . The leg angle  $\alpha_0$  was adjusted at about  $70^\circ$ . The mass of PogoWalker is 4.1 kg, which is concentrated in the upper body. During the experiments, about 10% of the robot weight was suspended by elastic cords as a prevention from falling. PogoWalker walked on an instrumented treadmill (Tecmachine, Andrezieux Boutheon, France) with integrated 3D force sensors (Kistler, Winterthur, Switzerland). In this study, a treadmill speed of 0.46 m/s was used. Thus, average dimensionless energy in this experiment with PogoWalker was about 1.017.

The control consists of three phases. In the stance phase, the leg is retracted with a speed matching the treadmill speed. After take-off, the leg is actively shortened and protracted until  $\alpha_0 = 70^\circ$  is reached. In the last phase, the leg remains in this position until touch-down. Ground contact of the leg is detected by foot force sensors. Since the gait pattern is not predefined, PogoWalker needs some steps to develop a continuous gait pattern. After some introducing steps the robot adapts to the motion and shows asymmetrical vertical GRF patterns (Figure 2.2). Even so, PogoWalker is able to walk over a considerable number of steps ( $>100$ ) without stumbling.

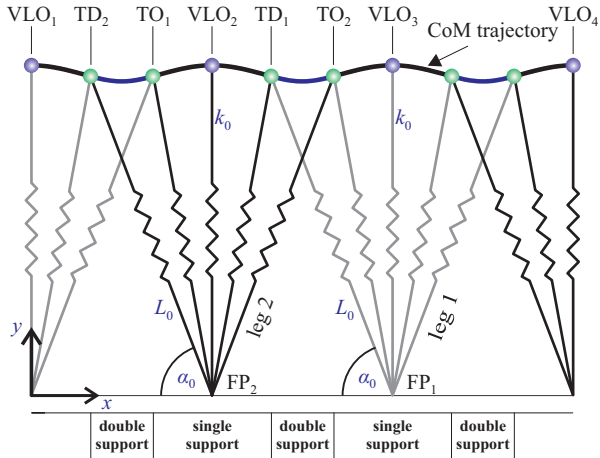


**Figure 2.3.** The symmetric bipedal spring-mass model for walking (i.e. with  $\alpha_1 = \alpha_2 = \alpha_0$ ,  $k_1 = k_2 = k_0$  and  $L_1 = L_2 = L_0$ ). The points on the center of mass (CoM) trajectory show events vertical leg orientation (VLO), touch-down (TD) and take-off (TO). Black and blue parts of the CoM trajectory represent single- and double-support phases, respectively.

### 2.2.2. Prosthetic walking

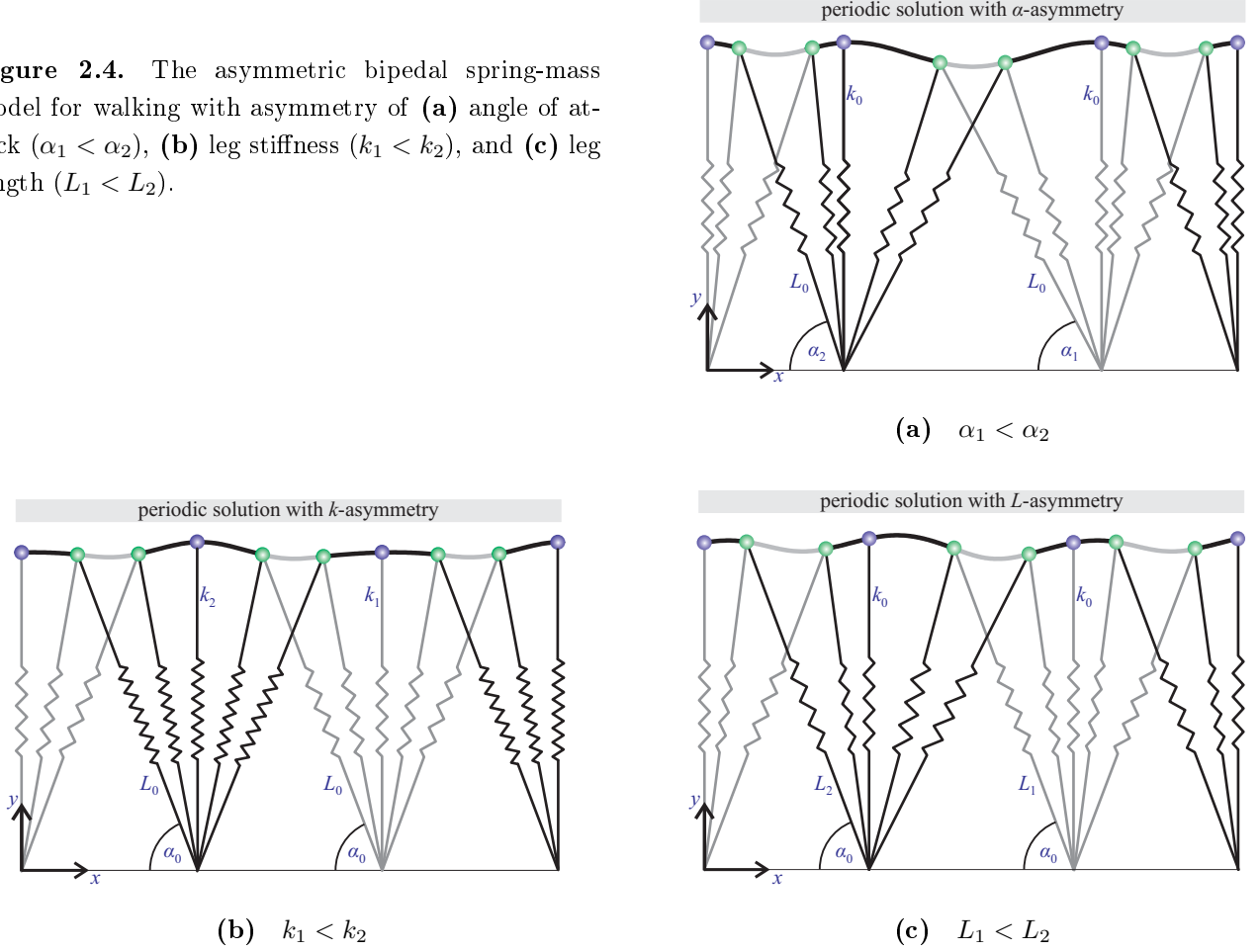
In human walking, asymmetric gaits are typically found when the leg function is restricted due to amputation of a limb. In [Schaarschmidt et al. \[2012\]](#), five subjects with unilateral transfemoral amputations were analyzed when walking at 1.1 m/s on an instrumented treadmill (ADAL-WR, HEF Tecmachine, Andrezieux, Boutheon, France) with integrated 3D force sensors (Kistler, Winterthur, Switzerland). For each subject, two trials were obtained, starting with the computerized artificial knee joint C-Leg, followed by the non-computerized 3R80 (both Otto Bock HealthCare). The asymmetry between both limbs was observed in the pattern of the vertical and horizontal GRFs with longer contacts on the intact side. All subjects were able to walk by selecting an asymmetric gait pattern.

### 2.2.3. Aims of this study

As demonstrated by the examples described above, asymmetric walking is a commonly observed gait pattern in both humans or artificial legged systems. So far, it is not clear to what extent asymmetry should be avoided or whether for certain conditions gait asymmetry could be accepted. For instance, Hof *et. al.* suggested that symmetric leg function is not necessarily required to be an aim of gait rehabilitation [[Hof et al., 2007](#)].

In order to approach this question, we will use a conceptual model for bipedal locomotion based on spring-like leg function [[Geyer et al., 2006](#)] to investigate effects of asymmetric leg parameters on stability of walking patterns. In order to facilitate the comparison of the model with robot data we used similar leg parameters in the model as in the PogoWalker. We expect, that within certain ranges asymmetric leg configurations are tolerated in the walking model, while stability is expected to decrease with increasing gait asymmetry.

**Figure 2.4.** The asymmetric bipedal spring-mass model for walking with asymmetry of **(a)** angle of attack ( $\alpha_1 < \alpha_2$ ), **(b)** leg stiffness ( $k_1 < k_2$ ), and **(c)** leg length ( $L_1 < L_2$ ).



## 2.3. Methods

Since walking with symmetric legs is a reference for our study, we first introduce the symmetric spring-mass model.

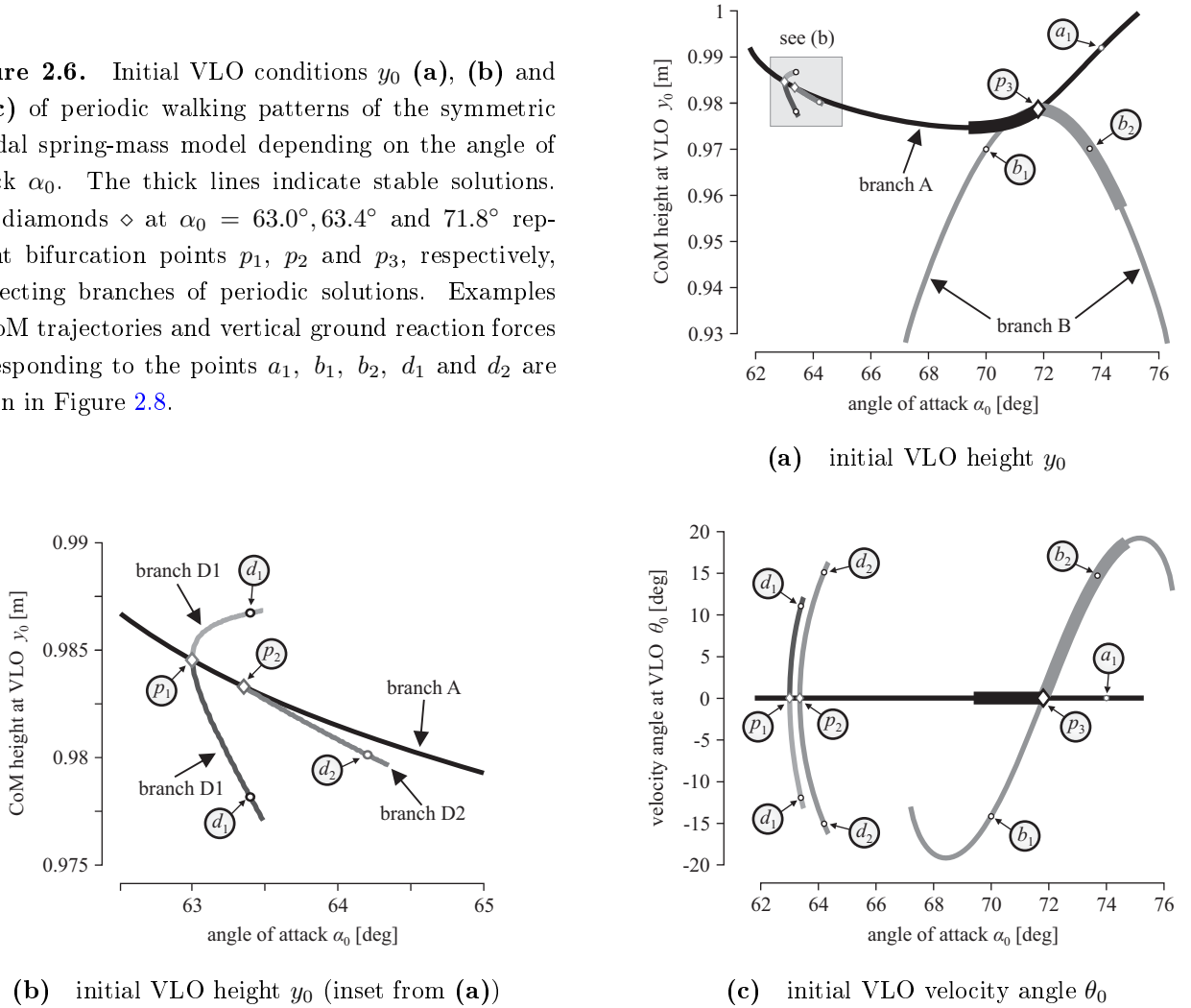
### 2.3.1. Symmetric model

The bipedal spring-mass model (Figure 2.3) consists of two linear massless leg springs and a point mass  $m$  representing the center of mass of the body. In the symmetric model, both leg springs are assumed to have the same properties: the rest length  $L_0$  and the stiffness  $k_0$  (Figure 2.3). During the step the system energy  $E_0$  remains constant. Location and velocity of the center of mass are given by  $r = (x, y)^T$  and  $\dot{r} = (\dot{x}, \dot{y})^T$ , respectively. We set the initial state of the system to  $r_0 = (x_0, \dot{x}_0, y_0, \dot{y}_0)^T$ . The motion of the center of mass is then described by equation

$$m\ddot{r} = F_1 + F_2 + mg, \quad (2.1)$$



**Figure 2.6.** Initial VLO conditions  $y_0$  (a), (b) and  $\theta_0$  (c) of periodic walking patterns of the symmetric bipedal spring-mass model depending on the angle of attack  $\alpha_0$ . The thick lines indicate stable solutions. The diamonds  $\diamond$  at  $\alpha_0 = 63.0^\circ, 63.4^\circ$  and  $71.8^\circ$  represent bifurcation points  $p_1, p_2$  and  $p_3$ , respectively, connecting branches of periodic solutions. Examples of CoM trajectories and vertical ground reaction forces corresponding to the points  $a_1, b_1, b_2, d_1$  and  $d_2$  are shown in Figure 2.8.



with the gravitational acceleration  $g = (0, -9.81)^T$  and the force  $F_i$  generated by leg  $i$  during stance. The force  $F_i$  is given by

$$F_i = k_0 \left( \frac{L_0}{|r - r_{FP_i}|} - 1 \right) (r - r_{FP_i}). \quad (2.2)$$

Here,  $r_{FP_i}$  is the position of the foot point  $FP_i$  of leg  $i$ . In the swing phase of leg  $i$ , the force  $F_i$  is zero. The transition from swing phase to stance phase (touch-down) happens when the landing condition  $y = L_0 \sin(\alpha_0)$  is fulfilled, where  $\alpha_0$  is the angle of attack (Figure 2.3). The transition from stance phase to swing phase (take-off) of leg  $i$  occurs, when the extending leg length reaches  $L_0$ .

Any gait of the spring-mass model is completely characterized by three fundamental system parameters (i.e. the dimensionless leg stiffness  $\tilde{k}_0 = (k_0 L_0)/(mg)$ , the angle of attack  $\alpha_0$  and the dimensionless system energy  $\tilde{E}_0 = E_0/(mgL_0)$ ) and the four-dimensional vector  $r_0$  of initial conditions [Geyer et al., 2006]. We start the simulations at the instant of the vertical leg orientation (VLO, [Rummel et al., 2010a]) during single support. Here, the number of independent initial

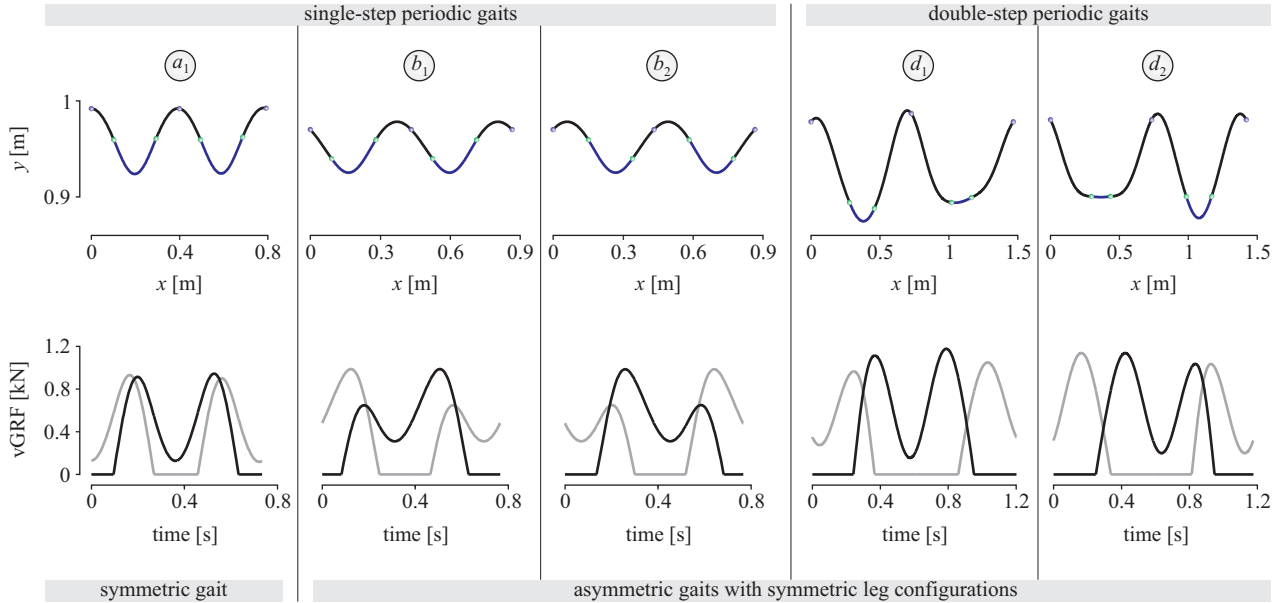


**Figure 2.8.** Examples of CoM trajectories (upper row) and vertical ground reaction forces (vGRF) of both legs (lower row) corresponding to the points  $a_1$ ,  $b_1$ ,  $b_2$ ,  $d_1$  and  $d_2$  in Figure 2.6. The points in the upper row indicate events vertical leg orientation (VLO), touch-down (TD) and take-off (TO) (Figure 2.3).

conditions can be reduced to two, i.e. the height  $y_0$  and the velocity angle

$$\theta_0 = \arctan\left(\frac{\dot{y}_0}{\dot{x}_0}\right). \quad (2.3)$$

The model parameters  $L_0$  and  $m$  are chosen according to human data ( $L_0 = 1$  m,  $m = 80$  kg). The average dimensionless stiffness of PogoWalker legs is  $\tilde{k}_0 = 20$ . Using dimensional analysis [Geyer et al., 2006], we convert  $\tilde{k}_0$  to the dimensional stiffness  $k_0$  with respect to the model parameters  $m$  and  $L_0$  and round it to 16 kN/m.

The average dimensionless energy  $\tilde{E}_0$  in the PogoWalker experiments is about 1.017. However, for this energy the bipedal symmetric model has no stable periodic solutions [Rummel et al., 2010b]. Thus, we did all calculations in our investigation with constant dimensional energy  $E_0 = 820$  J corresponding to the dimensionless energy  $\tilde{E}_0$  of 1.045. The difference between the system energy in experiment and simulations is less than 3%, which is still within an acceptable tolerance.

The model is implemented in MATLAB (The MathWorks Inc., Natick, MA, USA). The differential equations are solved using Runge-Kutta method (ode45) with absolute and relative tolerance of  $10^{-13}$ . Unless otherwise mentioned, the steps of  $\alpha_0$  of  $0.1^\circ$  were used in all our calculations.

### 2.3.2. Asymmetric model

To investigate the asymmetric behaviour, each leg is described by a different parameter set. Therefore, we introduce the asymmetry parameters  $\varepsilon_\alpha$ ,  $\varepsilon_k$ ,  $\varepsilon_L$  and  $\varepsilon_{\tilde{E}}$  of  $\alpha_0$ ,  $k_0$ ,  $L_0$  and  $\tilde{E}_0$ , respectively.  $\varepsilon_\alpha$ ,  $\varepsilon_k$ ,  $\varepsilon_L$  and  $\varepsilon_{\tilde{E}}$  are also called imperfection or perturbation parameters [Strogatz, 1994]. For leg 1 the perturbations are subtracted from the corresponding control parameters (Figure 2.4):

$$\alpha_1 = \alpha_0 - \varepsilon_\alpha, \quad k_1 = k_0 - \varepsilon_k, \quad L_1 = L_0 - \varepsilon_L, \quad \tilde{E}_1 = \tilde{E}_0 - \varepsilon_{\tilde{E}}. \quad (2.4)$$

For leg 2 the perturbations are added (Figure 2.4):

$$\alpha_2 = \alpha_0 + \varepsilon_\alpha, \quad k_2 = k_0 + \varepsilon_k, \quad L_2 = L_0 + \varepsilon_L, \quad \tilde{E}_2 = \tilde{E}_0 + \varepsilon_{\tilde{E}}. \quad (2.5)$$

We call  $\varepsilon_\alpha$  the  $\alpha$ -asymmetry,  $\varepsilon_k$  the  $k$ -asymmetry,  $\varepsilon_L$  the  $L$ -asymmetry and  $\varepsilon_{\tilde{E}}$  consequently the  $\tilde{E}$ -asymmetry.

The  $\tilde{E}$ -asymmetry  $\varepsilon_{\tilde{E}}$  affects dimensional stiffness  $k_0$  and leg length  $L_0$ . However, the values of  $\varepsilon_{\tilde{E}}$  were chosen in such way that the dimensionless stiffness  $\tilde{k}_0$  remains equal for both legs. For each  $\varepsilon_{\tilde{E}}$ , the corresponding value of  $\varepsilon_L$  was calculated using  $\tilde{E}_0 = E_0/(mgL_0)$  with constant dimensional energy  $E_0 = 820$  J. Next, the stiffness asymmetry  $\varepsilon_k$  was calculated using  $\tilde{k}_0 = (k_0L_0)/(mg)$  with  $\tilde{k}_0 = 20$ . Notice, that although the dimensionless system energy  $\tilde{E}_0$  is different for left and right leg, the dimensional energy  $E_0$  remains the same for both legs.

We consider positive perturbations of leg asymmetry only ( $\varepsilon_\alpha > 0$ ,  $\varepsilon_k > 0$ ,  $\varepsilon_L > 0$  and  $\varepsilon_{\tilde{E}} > 0$ ). Switching the order of the steps, i.e. beginning with the step 2 and following by the step 1, we achieve the case of negative perturbation with exactly the same stability behaviour.

In this study we used steps of  $\varepsilon_\alpha$ ,  $\varepsilon_k$ ,  $\varepsilon_L$  and  $\varepsilon_{\tilde{E}}$  of  $0.1^\circ$ ,  $0.1$  kN/m,  $10^{-4}$  m and  $10^{-4}$ , respectively.

### 2.3.3. System analysis

Stability is one of the most important properties of bipedal walking. Here, we give a short description of the stability analysis used in our investigations.

The system analysis of a single step is described in detail in Section 3.3.2. However, the investigation of walking in the asymmetric model requires the observation of a complete gait cycle, comprising two subsequent steps. For this, slight modifications of the system analysis had to be done. Since each gait pattern with single-step periodicity is also a double-step periodic pattern, these modifications do not affect the analysis of single-step periodic gaits.

The step 1 starts in  $VLO_1$  defined by the initial conditions. It lasts until  $VLO_2$  is reached. The gait cycle is completed when  $VLO_3$  is reached (Figure 2.3).

With VLO as Poincaré section we apply the Poincaré return map  $\mathbf{F}$ . If  $s_i = (y_i, \theta_i)$  is the state of the system in  $VLO_i$  then after the complete gait cycle the state in  $VLO_{i+2}$  is  $s_{i+2} = \mathbf{F}(s_i)$ . Using the Poincaré map we identify periodic walking solutions, which are represented as fixed points  $s^*$  in the map  $s^* = \mathbf{F}(s^*)$ . We calculate the fixed points as zeros of the function

$$\mathbf{G}(s) = s - \mathbf{F}(s) \quad (2.6)$$

applying a Gauss-Newton algorithm using the MATLAB function `fsolve` with relative and absolute tolerance of  $10^{-8}$ .

To determine the stability of a fixed point we calculate the Jacobi matrix  $\mathbf{J}_{\mathbf{F}}(s^*)$  of  $\mathbf{F}$  in  $s^*$ . The gait pattern corresponding to  $s^*$  is stable if the magnitude of both eigenvalues of  $\mathbf{J}_{\mathbf{F}}(s^*)$  is less than one [Guckenheimer & Holmes, 1983].

## 2.4. Results

### 2.4.1. Period-one gaits with symmetric legs

Periodic solutions of the symmetric model are shown in Figure 2.6. We consider two kinds of single-step periodic walking patterns, branches A and B, which were already presented in Rummel et al. [2010b]. The vertical ground reaction forces and center of mass trajectories of patterns on A are mirrored at VLO (example  $a_1$  in Figure 2.8 corresponding to the point  $a_1$  in Figure 2.6), in contrast to solutions of branch B ( $b_1$  and  $b_2$  in Figure 2.6 and Figure 2.8).

The branches A and B are connected by the transcritical bifurcation point  $p_3$  at  $\alpha_0 = 71.8^\circ$ . On branch A the stable solutions are found between  $\alpha_{\min} = 69.4^\circ$  and the bifurcation point  $p_3$ . The stable solutions are continued by branch B starting at the bifurcation point  $p_3$  and ending at  $\alpha_{\max} = 74.7^\circ$ . For parameter values  $\alpha_{\min}$  and  $\alpha_{\max}$ , the eigenvalues of the Jacobi matrix are complex-conjugate with magnitude equal to one. Together with change of stability this indicates that in  $\alpha_{\min}$  and  $\alpha_{\max}$  Hopf bifurcations occur [Marsden & McCracken, 1976].

In the following, we investigate the size of the region where locomotion is stable. Therefore, we define the continuous range of stable solutions  $\Delta\alpha = \alpha_{\max} - \alpha_{\min}$  and call it the  $\alpha$ -range. The symmetric model exhibits an  $\alpha$ -range of  $\Delta\alpha = 5.3^\circ$ , which provides a reference for investigations on the asymmetric model (Sections 2.4.3, 2.4.4 and 2.4.5).

### 2.4.2. Period doubling

Additionally, we present two kinds of double-step periodic patterns lying on branches D1 and D2 in Figure 2.7(b). D1 and D2 are connected to branch A by the bifurcation points  $p_1$  and  $p_2$ . Periodic solutions lying on branches D1 and D2 were calculated using steps of  $\alpha_0$  of  $0.01^\circ$ .

Starting at  $VLO_i$ , after the first step a fixed point lying on D1 reaches in  $VLO_{i+1}$  the corresponding point on the contrary part of D1 (example  $d_1$  in Figure 2.6 and Figure 2.8). E.g. the trajectory of  $d_1 = (0.978 \text{ m}, 11.033^\circ)$  has in  $VLO_{i+1}$  a different center of mass height  $y_{i+1} = 0.987 \text{ m}$  and velocity angle  $\theta_{i+1} = -11.943^\circ$  (Figure 2.7(c)). After the second step the starting point on D1 is reached again and periodicity is fulfilled.

The patterns on D2 are characterized by  $(y_i, \theta_i) = (y_{i+1}, -\theta_{i+1})$ . After one step these gaits have the same VLO height  $y_0$  and exactly the opposite sign of the velocity angle  $\theta_0$  (Figure 2.7(c)).

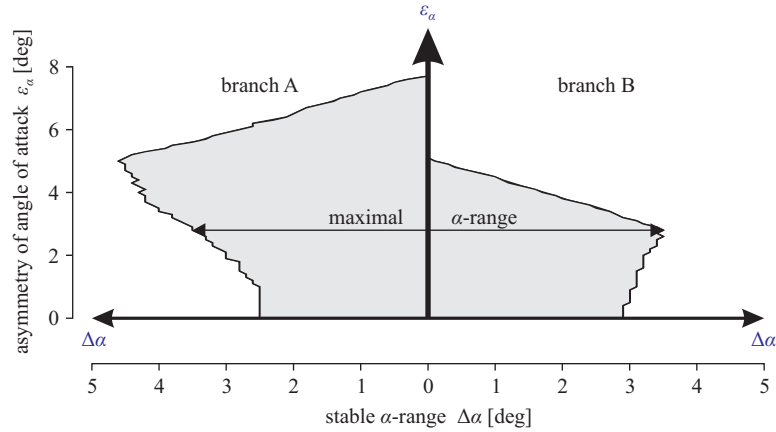
All double-step periodic patterns on D1 and D2 are unstable. Moreover, the magnitude of the velocity angle  $\theta_0$  increases rapidly (Figure 2.7(c)), which makes this pattern very sensitive to all kinds of asymmetric perturbations. In most cases, leg asymmetry causes the take-off of the supporting leg in a single-support phase. Since our definition of walking requires at least one leg always having ground contact this locomotion patterns cannot be treated as walking any more. Therefore, the further discussion of the influence of leg asymmetry on the walking patterns lying on D1 and D2 is omitted.

### 2.4.3. Asymmetry of angle of attack

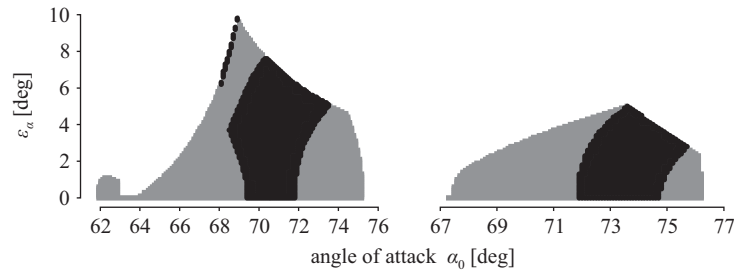
As can be seen in the Figure 2.11, moderate perturbations of  $\alpha_0$  do not affect the bifurcation. In this case,  $\varepsilon_\alpha$  is a bifurcation preserving imperfection [Shearer, 1980]. As long as this bifurcation exists, stable solutions can be found on both branches, A and B.

The branch B diminishes with increasing asymmetry. For  $\varepsilon_\alpha > 5^\circ$  no bifurcation and no second branch could be found. For perturbations larger than  $9.9^\circ$  no periodic solutions at all were determined. Compared to the symmetric case, we observed an increase of the  $\alpha$ -range for values of  $\varepsilon_\alpha$  less than  $4.5^\circ$ . The maximum value of  $\Delta\alpha = 6.9^\circ$  was found at  $\varepsilon_\alpha = 2.8^\circ$  (Figure 2.9(a)). Here, the left limit of the region of stable solutions is  $\alpha_{\min} = 68.8^\circ$  and the right one is  $\alpha_{\max} = 75.7^\circ$  (Figure 2.9(b)). For  $\varepsilon_\alpha > 3^\circ$  the  $\alpha$ -range is monotonically decreasing due to the reduction of the branch B.

For a small range of  $\alpha_0$  around  $70.3^\circ$  and an  $\alpha$ -asymmetry of  $7.8^\circ$  the walking gait not only remains stable (Figure 2.9(b)), but stability, i.e. the magnitude of both eigenvalues, is also improved



(a) Development of the  $\alpha$ -range  $\Delta\alpha$  with increasing asymmetry  $\varepsilon_\alpha$ .



(b) Development of periodic solutions of branches A (left) and B (right) (Figure 2.7(a)) with increasing  $\alpha$ -asymmetry. Gray and black regions show unstable and stable asymmetric patterns, respectively.

**Figure 2.9.** Asymmetry of angle of attack  $\varepsilon_\alpha$ .

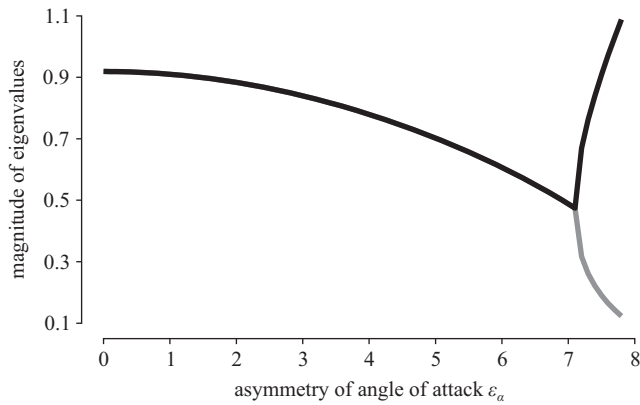


**Figure 2.10.** Magnitude of eigenvalues of periodic solutions for  $\alpha_0 = 70.3^\circ$  depending on the asymmetry of angle of attack  $\varepsilon_\alpha$ . For values of  $\varepsilon_\alpha$  up to  $7.1^\circ$  the eigenvalues are complex-conjugate. Thus, their magnitude is equal.

(Figure 2.10). For this value of  $\alpha_0$ , stable walking is still possible with the total left-right deviation of angle of attack of  $15.6^\circ$ .

One interesting result is that  $\alpha$ -asymmetry can stabilize previously unstable symmetric walking patterns. For example, the unstable symmetric gait for  $\alpha_0 = 69^\circ$  becomes stable for values of  $\varepsilon_\alpha$  greater than  $2.2^\circ$  and less than  $5^\circ$  (Figure 2.9(b)).

The main reason for vanishing periodic solutions at higher values of  $\alpha_0$  is that the length of the supporting leg spring in a single-support phase reaches the rest length  $L_0$ . Like in the case of double-step periodic patterns, we observe a rapid increase of magnitude of the velocity angle  $\theta_0$  (Figure 2.11) and an appearance of a flight phase during the step.

#### 2.4.4. Asymmetry of leg stiffness

Adding leg stiffness asymmetry  $\varepsilon_k$  to the system results in two branches of periodic solutions without any bifurcations (Figure 2.12), i.e.  $\varepsilon_k$  is a bifurcation destroying imperfection [Shearer, 1980]. Here, all stable solutions of the asymmetric system lie on one branch between two Hopf bifurcations.

Unlike the  $\alpha$ -asymmetry (Section 2.4.3), no gain of the  $\alpha$ -range was observed with  $k$ -asymmetry. As shown in Figure 2.13(a), under the effect of  $k$ -asymmetry the  $\alpha$ -range  $\Delta\alpha$  diminishes continuously. Increase of  $\varepsilon_k$  resulted first in loss of stable solutions at about  $\varepsilon_k = 2.6$  kN/m and finally in loss of any periodic solutions at about  $\varepsilon_k = 9.2$  kN/m (Figure 2.13(b)). Hence, stable walking is possible with a stiffness deviation between the contralateral legs less than 5.2 kN/m, which is 32.5% of the reference stiffness  $k_0 = 16$  kN/m of the symmetric system.

#### 2.4.5. Asymmetry of rest length and dimensionless energy

The rest length asymmetry  $\varepsilon_L$  affects the system in the similar way as leg stiffness asymmetry  $\varepsilon_k$  (Section 2.4.4). All stable solutions of the asymmetric system lie also on one branch between two Hopf bifurcations (Figure 2.14). We observe no increase of  $\alpha$ -range (Figure 2.15(a)). The stable solutions are lost at  $\varepsilon_L = 9$  mm and periodic solutions are lost at  $\varepsilon_L = 21$  mm (Figure 2.15(b)). Hence, considering the reference leg length  $L_0$  of 1 m, stable walking exists for the total difference in the length of contralateral legs of up to 1.8%.

A similar tolerance of 2% is predicted for asymmetries in dimensionless energy  $\varepsilon_{\tilde{E}}$ . Here, stable solutions exist for the values of  $\varepsilon_{\tilde{E}}$  up to 0.01. Periodic solutions are lost at  $\varepsilon_{\tilde{E}} = 0.023$ .

## 2.5. Discussion

In this study we investigated the effect of asymmetries in angle of attack  $\varepsilon_\alpha$ , leg stiffness  $\varepsilon_k$ , leg length  $\varepsilon_L$  and dimensionless energy  $\varepsilon_{\tilde{E}}$  between both legs on the dynamics and stability of spring-mass walking. We could demonstrate that asymmetric leg function does not necessarily reduce the

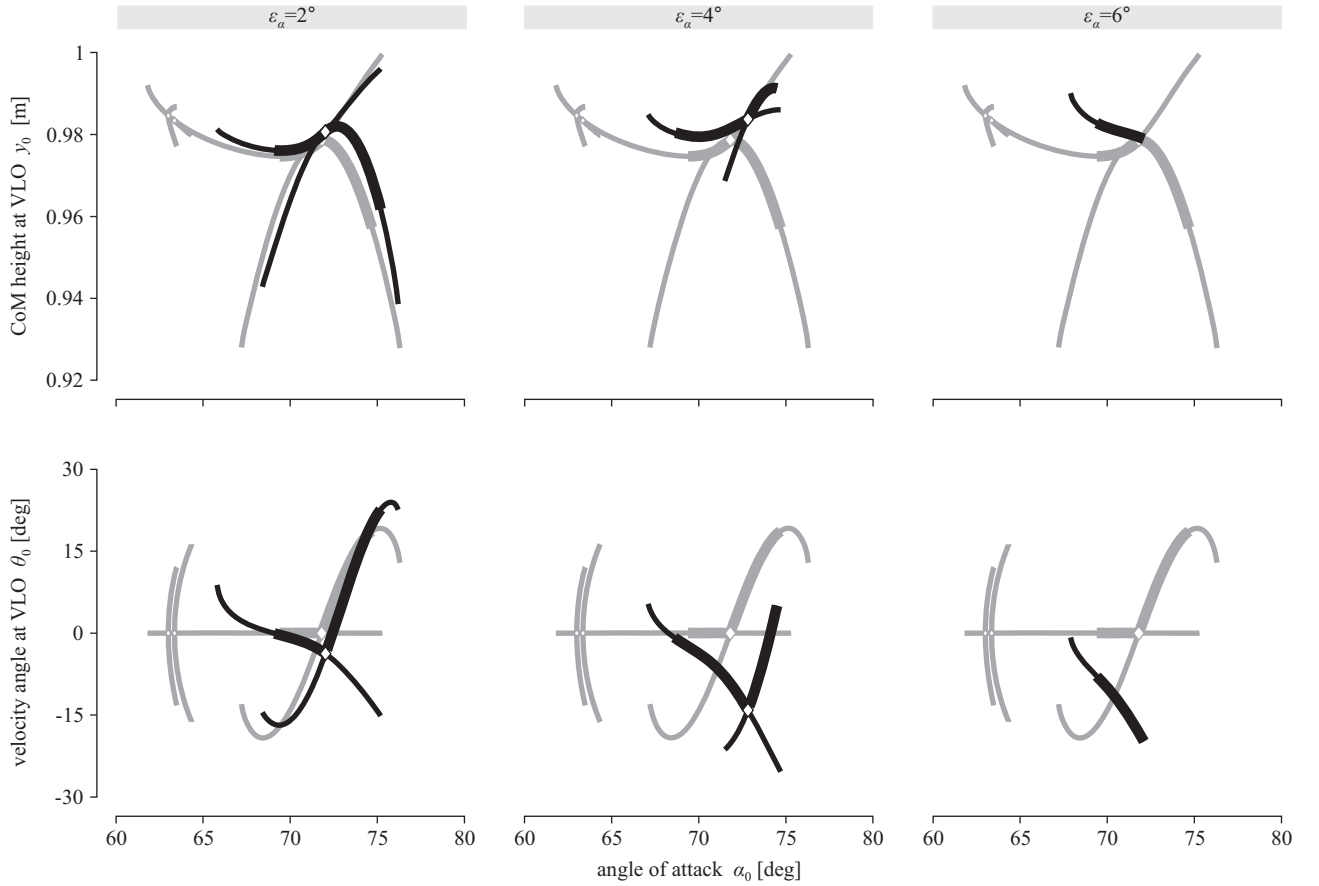


**Figure 2.11.** Initial VLO conditions depending on the reference angle of attack  $\alpha_0$  for  $\varepsilon_\alpha = 2^\circ$ ,  $4^\circ$ , and  $6^\circ$ . The upper row shows the height  $y_0$  of CoM at VLO. In the lower row the velocity angle  $\theta_0$  at VLO is represented. The grey curves are the initial conditions of the reference periodic gait patterns (see Figure 2.6). The thick lines indicate stable solutions. The diamonds  $\diamond$  are bifurcation points connecting each two branches of periodic solutions.

region of stable walking. The  $\alpha$ -asymmetry cannot only be tolerated during walking but may also result in advantages as demonstrated by the increased  $\alpha$ -range (Figure 2.9). For a small range of values of  $\alpha_0$  the  $\alpha$ -asymmetry can even stabilize symmetric walking gaits. Surprisingly, for values of  $\alpha_0$  around  $70^\circ$ , after applying  $\alpha$ -asymmetry to the symmetric system the gait not only remains stable, but stability also is improved (Figure 2.10). This indicates that asymmetric gaits could be a better solution for asymmetric leg configuration as was already suggested for amputees by Hof et al. [2007].

There are specific effects of asymmetries in  $\alpha_0$ ,  $k_0$ ,  $L_0$  and  $\tilde{E}_0$  on the region of stable walking. With increasing asymmetry of leg stiffness  $\varepsilon_k$ , of leg length  $\varepsilon_L$  and of dimensionless energy  $\varepsilon_{\tilde{E}}$  the  $\alpha$ -range  $\Delta\alpha$  diminishes continuously. Moreover, for  $\varepsilon_\alpha$  stable solutions were found as long as periodic solutions existed, while with  $\varepsilon_k$ ,  $\varepsilon_L$  and  $\varepsilon_{\tilde{E}}$  stability was lost even though periodic solutions were still present.

Experimental data on human walking [Bhave et al., 1999; Kaufman et al., 1996; Perttunen et al.,



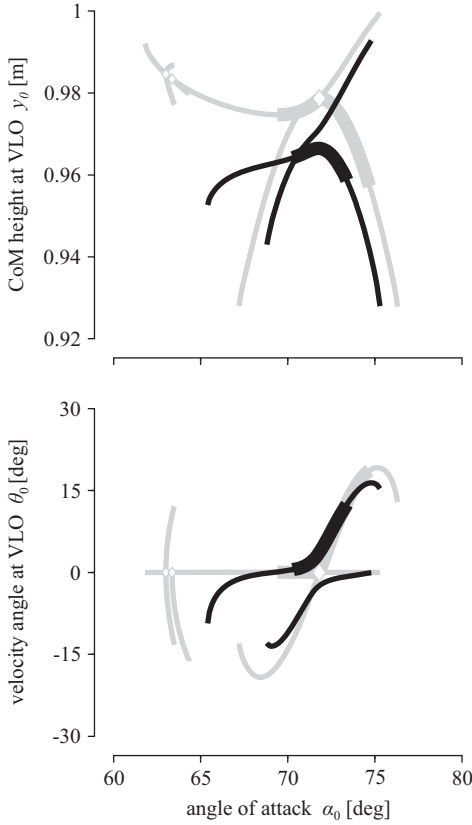
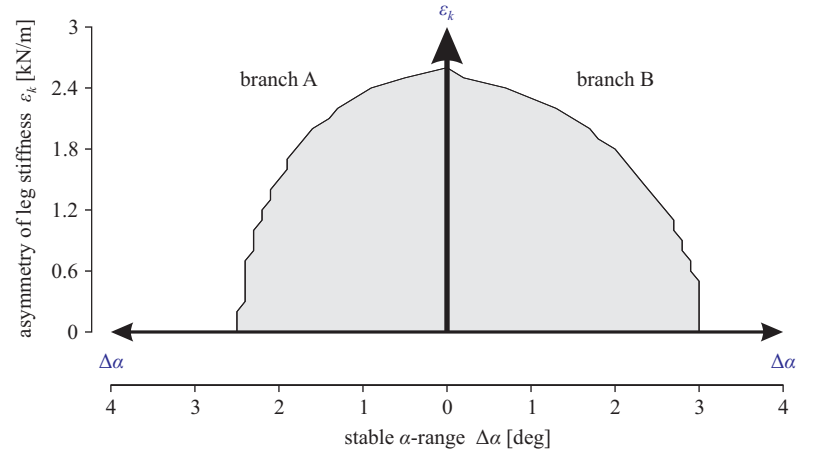
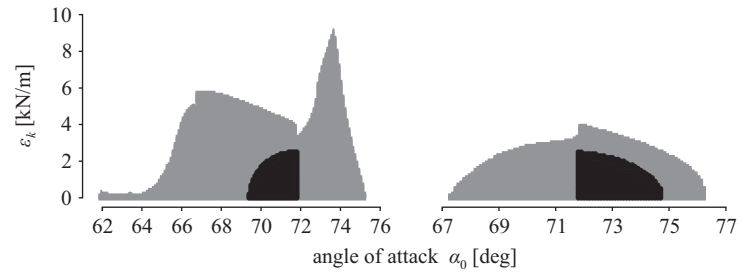


**Figure 2.12.** Initial VLO conditions depending on the angle of attack  $\alpha_0$  for  $\varepsilon_k = 2$  kN/m. The upper figure shows the height  $y_0$  of CoM at VLO. In the lower figure the velocity angle  $\theta_0$  at VLO is represented. The grey curves are the initial conditions of the reference periodic gait patterns (Figure 2.6). The thick lines indicate stable solutions.



(a)



(b)

**Figure 2.13.** (a) Development of the  $\alpha$ -range  $\Delta\alpha$  with increasing asymmetry  $\varepsilon_k$ .

(b) Development of periodic solutions of branches A (left) and B (right) (Figure 2.7(a)) with increasing  $k$ -asymmetry. Gray and black regions show unstable and stable asymmetric patterns, respectively.

2004] show that vertical GRFs of the longer leg are larger than the GRFs of the shorter leg. This is in agreement with our model predictions (Figure 2.16). However, the analyzed walking model is very sensitive to the  $L$ -asymmetry. In the spring-mass model, the leg length  $L_0$  has not only influence on the leg dynamics during the stance. It affects also the instances of touch-down and of take-off.

The effects of  $\tilde{E}$ -asymmetry are similar. This could be due to the fact that  $\tilde{E}_0$  is directly affected by  $L_0$ . Additionally,  $\tilde{E}_0$  is also affected by  $k_0$ . Hence, the effects of  $\tilde{E}$ -asymmetry could further depend on the selected leg stiffness  $k_0$  or system energy  $E_0$ . This needs to be investigated in more detail.

In humans, even small deviations of the leg length can cause stress fractures, back pain and

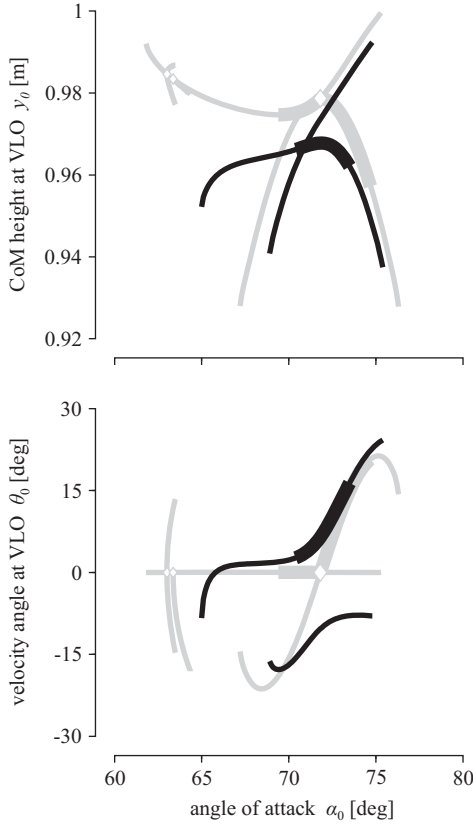


**Figure 2.14.** Initial VLO conditions depending on the angle of attack  $\alpha_0$  for  $\varepsilon_L = 7$  mm. The upper figure shows the height  $y_0$  of CoM at VLO. In the lower figure the velocity angle  $\theta_0$  at VLO is represented. The grey curves are the initial conditions of the reference periodic gait patterns (see Figure 2.6). The thick lines indicate stable solutions.

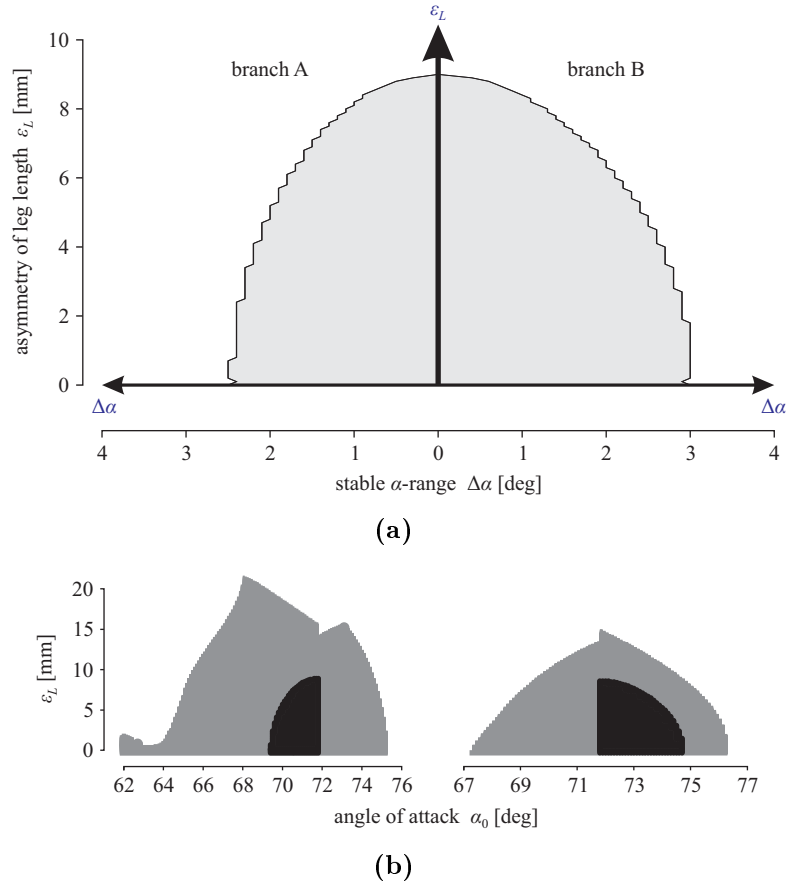


**Figure 2.15.** (a) Development of the  $\alpha$ -range  $\Delta\alpha$  with increasing asymmetry  $\varepsilon_L$ . (b) Development of periodic solutions of branches A (left) and B (right) (Figure 2.7(a)) with increasing  $L$ -asymmetry. Gray and black regions show unstable and stable asymmetric patterns, respectively.

osteoarthritis [McCaw & Bates, 1991]. However, because of the flexibility of human legs small leg length discrepancies are not expected to affect stability of walking in such a crucial way. We suppose the missing leg segmentation in the spring-mass model as one of the reasons for the high sensitivity with respect to  $L$ -asymmetry. Extending the spring-mass model by a knee joint [Rummel & Seyfarth, 2008] or by foot segment [Maykranz et al., 2009] could increase the range of stable solutions. Other possible ways to improve the stability behaviour of the system under influence of  $\varepsilon_L$  could be swing leg control as described by Herr et al. [2002]; Seyfarth et al. [2003] and Blum et al. [2010] or suitable combinations of  $L$ -asymmetry with asymmetry of  $\alpha_0$  or asymmetry of  $k_0$ .

Humans with asymmetric leg mechanics often walk shifting their body weight from one leg to

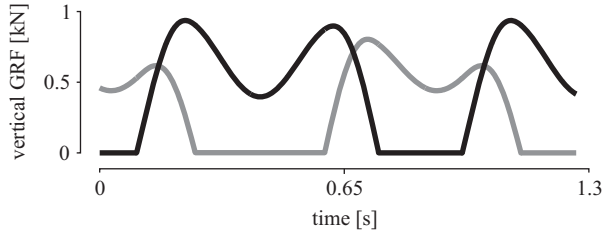


**Figure 2.16.** Vertical ground reaction force of an asymmetric pattern for  $\varepsilon_L = 10$  mm at  $\alpha_0 = 70^\circ$ . The black curve represents the GRF of the longer leg, the grey one shows the GRF of the shorter leg.

another in the lateral plane. For instance, the medial-lateral acceleration of the center of mass at touch-down is greater for the short leg, indicating a faster transfer of the mass to the shorter extremity [Song et al., 1997]. For this, an extension of the spring-mass model into the lateral plane could predict appropriate methods to manage the disadvantages of asymmetric walking. Since humans avoid narrow step widths, because they are less stable [Donelan et al., 2004], a suitable lateral foot placement could additionally stabilize asymmetric gaits. First three-dimensional symmetrical models for running [Peucker & Seyfarth, 2010; Seipel & Holmes, 2005] and walking [Adolfsson et al., 2001] already exist.

Except for the  $\alpha$ -asymmetry  $\varepsilon_\alpha$ , all stable solutions of the asymmetric system for one set of parameters lie between two Hopf bifurcation points (Figures 2.12 and 2.14). In case of  $\varepsilon_\alpha$ , a part of the region of stable solutions is cut off (Figure 2.11). Here, larger left-right deviations of  $\varepsilon_\alpha$  lead to the flight phases caused by take-offs during single support. The resulting gaits are skipping, i.e. gaits which contain double-support phases along with flight phases [Farley, 1998; Minetti, 1998]. Hence, allowing short flight phases in walking patterns of a robot with asymmetric leg configuration could enlarge its range of stable gaits.

Despite the tolerance and increasing stability of the system towards  $\alpha$ -asymmetry, there is one important disadvantage of asymmetric gaits. As it shown in Srinivasan [2010], asymmetric walking is more energy consuming than the symmetric gait. However, it is still not clear, in which way asymmetries of  $\alpha_0$ ,  $k_0$ ,  $L_0$  and  $\tilde{E}_0$  affect the energetic costs of periodic walking patterns. Although the model is conservative, the mechanical work of the legs during contact can be calculated and used as an estimation of energetic efficiency [Rummel et al., 2010b]. This reflects the situation that legs are not just passive springs but need to be actuated with muscles or motors. Hence, only part of the work predicted by the spring-mass model can be done completely passively by springs. The actual percentage of passive vs. active work during walking will depend on the way how actuators and springs are arranged and operated during locomotion. This would require to extend the model, which was not envisioned in this study. Additionally, by changes either of the leg stiffness [Kalveram & Seyfarth, 2009] or of the leg length [Schmitt & Clark, 2009] during ground contact an additional energy input can be simulated. Such an actuated asymmetric model could be an important tool for investigations of asymmetric energy supply in the contralateral legs. For example, the exact point of actuation short before take-off could significantly improve performance of active prostheses [Eilenberg et al., 2010; Hitt et al., 2010; Sup et al., 2009].

In our study the model is assumed to be deterministic, i.e. all parameters and states are precisely defined. However, this contradicts the nature of human gait where leg parameters and system states do change over time. In order to estimate the "global" stability, like indicated by a risk of falling, it would be required to take the uncertainties of the system into account. This could be done based on stochastic models, e.g. by introducing metastability as suggested by [Byl & Tedrake \[2009\]](#).

The walking model used in our study is currently the best candidate for a template of human walking [[Biewener & Daley, 2007](#); [Blickhan et al., 2007](#); [Geyer et al., 2006](#)]. It is able to predict walking patterns which are periodic even with asymmetric leg configurations. Hence, humans could benefit from such solutions by appropriately adjusting leg parameters. However, the model is much too simple to indicate, *how* these patterns can be achieved in a neuro-muscular system.

Even though the model predicts stable walking solutions based on asymmetric compliant leg configurations, it needs to be proven in future studies whether such mechanically attractive behavior indicated by the template model has any practical advantage. In order to address these issues, experimental studies on asymmetric gait are required and need to be compared to biomechanical model of increased complexity taking neuronal and muscular mechanisms into account.

Gait asymmetries naturally occur in both, human walking and in technical walking systems (e.g. legged robots, prosthetic legs). The predictions of the model may help to estimate the tolerated range of asymmetries depending on the overall leg properties (e.g. leg stiffness, leg length) and the gait characteristics (e.g. walking speed, angle of attack). This could help to derive procedures to indicate when differences in leg function may threaten the overall gait stability.

As the leg angle is a leg parameter which is adjustable in the PogoWalker, we focused on analyzing the effects of different leg angles on walking stability with asymmetric legs. In future, similar considerations should also include changes in leg stiffness and leg length in order to calculate the corresponding  $k$ -range and  $L$ -range, representing the range of parameters resulting in stable walking. Future studies need to show how asymmetries affect stable  $k$ -range and  $L$ -range. Moreover, suitable combinations of leg asymmetries (e.g.  $\varepsilon_\alpha$ ,  $\varepsilon_k$ ,  $\varepsilon_L$  and  $\varepsilon_{\tilde{E}}$ ) could allow additional effects influencing the range of stable walking. Also, the proper selection of the control parameters ( $\alpha_0$ ,  $k_0$ ,  $L_0$ ,  $\tilde{E}_0$ ) could further enhance the tolerated range of asymmetries  $\varepsilon_\alpha$ ,  $\varepsilon_k$ ,  $\varepsilon_L$  and  $\varepsilon_{\tilde{E}}$ . These effects need to be studied in more detail.

## 3. Spring-mass model

### 3.1. Introduction

In this chapter, we give a detailed mathematical description of the planar spring-mass model, which is also called *spring loaded inverted pendulum* (SLIP, [Schwind, 1998]). Due to the complexity of the mechanics of human locomotion, its investigation often requires an extension of the model. Examples of its numerous modifications are: segmented leg [Rummel & Seyfarth, 2008], foot extension [Maykranz et al., 2009], swing leg control [Blum et al., 2011, 2010], trunk extension [Maus et al., 2010; Rummel & Seyfarth, 2010], asymmetric legs [Merker et al., 2011b], lateral extension [Peuker et al., 2012], non-conservative extension [Riese et al., 2013]. All these publications have one thing in common, namely improvement of stability of the locomotor system. Stable periodic solutions are robust against small perturbations, which reduces the risk to fall [Geyer et al., 2006; Seyfarth et al., 2002].

The growing complexity of the model often results in considerably increased computational effort. Therefore, a new approach is required to work efficiently with the model in future. One way to avoid expensive calculations is to reduce the computation of stability regions to the computation of their boundaries, i.e. bifurcations (see Chapter 4 for more details). For this, transformation of the model from a hybrid dynamical system [Alur et al., 1995], i.e. a sequence of initial value problems, into a two-point boundary value problem is necessary. However, this new implementation of the model has some useful properties on its own. For instance, a boundary value problem is then more numerically stable, i.e. a less accurate initial guess is often sufficient for its computation. Sensitive dependence on initial conditions may leave parts of the solution manifolds unexplored, unless very high accuracy is used.

We explain the idea of transition using the first single-support phase of the bipedal model as example (Section 2.3.1). A more detailed description can be found e.g. in Stoer & Bulirsch [1993]. First, we rewrite (2.1) as a system of four one-dimensional ordinary differential equations

$$\dot{y}(t) = f(t, y; \alpha_0), \quad y(t_0) = r_0, \quad (3.1)$$

where  $r_0$  is a vector of initial conditions. The phase starts at time  $t_0$  and ends at time  $t_1$ , when

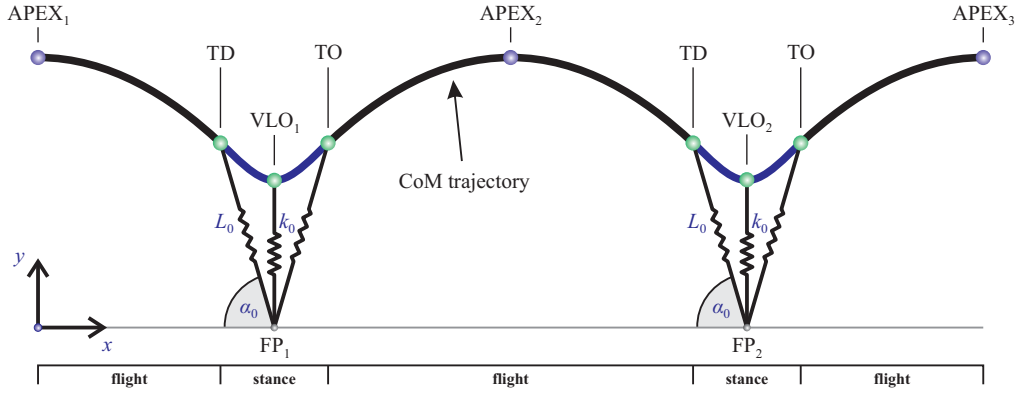


**Figure 3.1.** The spring-mass model for running. The green dots on the center of mass (CoM) trajectory show events of touch-down (TD), vertical leg orientation (VLO) and take-off (TO). The blue dots are events of apex (APEX). Black and blue parts of the CoM trajectory represent flight and stance phases, respectively.  $FP_i$  is the position of the  $i$ th foot point.

the touch-down condition  $y_3(t_1) = L_0 \sin(\alpha_0)$  is fulfilled. Since the transfer to the next phase is determined by an event, i.e. touch-down of the second leg,  $t_1$  is not known in advance. Thus, only one boundary abscissa  $t_0$  of the boundary value problem is prescribed. To determine  $t_1$ , the system has to be extended by an additional variable  $z_5 := (t_1 - t_0)/(\tau_1 - \tau_0)$ , which can also be considered as scaling parameter. Here,  $\tau_0$  and  $\tau_1$  denote the new boundary abscissas, which can be defined according to the requirements. The additional boundary condition reflects the touch-down condition. The resulting parametrized boundary value problem is

$$\begin{aligned} \dot{z}(\tau) &= z_5 f(\tau, z; \alpha_0) & z(\tau_0) &= r_0, \\ \dot{z}_5(\tau) &= 0 & z_3(\tau_1) &= L_0 \sin(\alpha_0). \end{aligned} \quad (3.2)$$

In this thesis, we set  $\tau_0 := 0$  and  $\tau_1 := 1$ .

The bipedal spring-mass model has a manifold of solutions (Chapter 2, see also [Geyer et al. \[2006\]](#); [Rummel et al. \[2010b\]](#)). However, only some of them are biologically relevant. A human walking gait is usually characterized by single- and double-support phases as well as by double-humped patterns of the vertical ground reaction force [[Alexander & Jayes, 1978](#); [Lipfert, 2010](#)]. For this, we consider solutions of the bipedal spring-mass model with double-humped force patterns only, and define walking as the locomotion gait with at least one leg always having ground contact. Furthermore, we do not consider walking patterns with appearance of negative horizontal velocity, i.e. the model is not allowed to walk backwards.

## 3.2. The model as a hybrid dynamical system

In this section, the general description of the spring-mass model is presented. The original implementation was realized in planar Cartesian coordinates. The description of the model in polar coordinates is given in [Martinez Salazar & Carbajal \[2011\]](#).

### 3.2.1. Running

The monopodal spring-mass model consists of the point mass  $m$  representing the center of mass of the human body and one massless leg spring with stiffness  $k_0$  and rest length  $L_0$  (Figure 3.1, [Blickhan, 1989](#)). Location and velocity of the center of mass in the real plane  $\mathbb{R}^2$  are given by  $(x, y)^T$  and  $(\dot{x}, \dot{y})^T$ , respectively. Any gait of the model is completely characterized by four fundamental system parameters (leg stiffness  $k_0$ , angle of attack  $\alpha_0$ , rest length  $L_0$ , system energy  $E_0$ ) and the four-dimensional vector of initial conditions  $r_0 = (x_0, \dot{x}_0, y_0, \dot{y}_0)^T$ .

One running step comprises a flight phase and a stance phase (also called the single-support phase, Figure 3.1), which can be split and arranged in a certain order according to the goal of the investigation. Events of touch-down and take-off are transitions between the phases. The trajectory of the center of mass in each phase is the solution of an initial value problem. The equations of the motion during flight are

$$\begin{aligned} m\ddot{x}(t) &= 0, \\ m\ddot{y}(t) &= -mg. \end{aligned} \tag{3.3}$$

The transition (touch-down) from the flight phase to the single-support phase happens, when the landing condition

$$y(t_1) = L_0 \sin(\alpha_0)$$

is fulfilled (Figure 3.1). The motion of center of mass during stance is then given by equations

$$\begin{aligned} m\ddot{x}(t) &= k_0 (L_0 - L_1(t)) \frac{x(t) - x_{\text{FP}_1}}{L_1(t)}, \\ m\ddot{y}(t) &= k_0 (L_0 - L_1(t)) \frac{y(t)}{L_1(t)} - mg, \end{aligned} \tag{3.4}$$

where  $L_1(t) := \sqrt{(x(t) - x_{\text{FP}_1})^2 + y^2(t)}$  is the length of the compressed leg spring during stance. The position of the footpoint  $\text{FP}_1$  is given by  $(x_{\text{FP}_1}, 0)$ . The transition (take-off) from the single-support phase to the flight phase occurs when the extending length  $L_1$  of the leg spring reaches the rest length  $L_0$ , i.e. when the take-off condition  $(x(t_2) - x_{\text{FP}_1})^2 + y^2(t_2) = L_0^2$  is fulfilled.

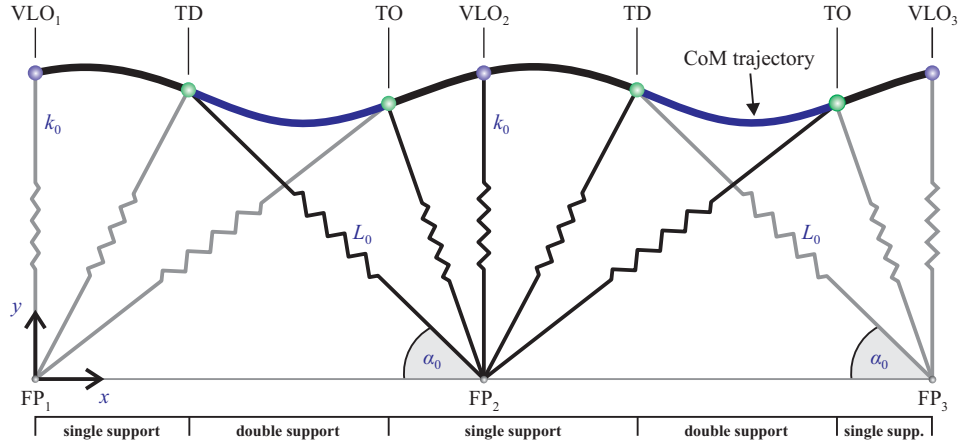


**Figure 3.2.** The bipedal spring-mass model for walking. The green dots on the center of mass (CoM) trajectory show events of touch-down (TD) and take-off (TO). The blue dots are events of vertical leg orientation (VLO). Black and blue parts of the CoM trajectory represent single- and double-support phases, respectively.  $FP_i$  is the position of the  $i$ th foot point.

In this thesis, the apex of the flight curve is usually selected as the beginning of the step. Here, the vertical velocity  $\dot{y}_0$  is zero (Figure 3.1). This choice allows to reduce the dimension of the return map (Section 3.3). The step is continued by the stance phase and the second flight phase. The step ends in the next apex, i.e. when  $\dot{y}(t_3) = 0$  is fulfilled. The initial values for the first initial value problem are  $(x_0, \dot{x}_0, y_0, \dot{y}_0)^T$ . The initial values of all subsequent phases are the last points of the corresponding previous phases. Times  $t_1$ ,  $t_2$  and  $t_3$  mark the ends of the corresponding phases, i.e. the times, when the events of touch-down, take-off and the second apex occur.

The system is energy-conservative, i.e. the system energy  $E_0$  remains constant during the whole step. During flight, the system energy is given by

$$E_0 = mgy + \frac{m(\dot{x}^2 + \dot{y}^2)}{2}. \quad (3.5)$$

During stance, the additional energy of the compressed leg spring must be considered:

$$E_0 = mgy + \frac{m(\dot{x}^2 + \dot{y}^2)}{2} + \frac{k_0}{2}(L_0 - L_1)^2, \quad (3.6)$$

where  $L_1$  is defined as above.

All calculations for running in this chapter are done with constant dimensional energy  $E_0 = 1800$  J corresponding to the average horizontal velocity  $v_x \approx 5$  m/s. The leg stiffness  $k_0 = 20$  kN/m and the leg length  $L_0 = 1$  m were derived from experimental data in Seyfarth et al. [2002]. Moreover, we set  $m = 80$  kg and  $g = 9.81$  m/s<sup>2</sup>.



### 3.2.2. Walking

The planar bipedal spring-mass model consists of two massless leg springs supporting the point mass  $m$ , which represents the center of mass of the human body (Figure 3.2, [Geyer et al., 2006]). Both leg springs have the same stiffness  $k_0$  and rest length  $L_0$ . Again, location and velocity of the center of mass in the real plane  $\mathbb{R}^2$  are given by  $(x, y)^T$  and  $(\dot{x}, \dot{y})^T$ , respectively. Like in the case of running, any bipedal gait is completely characterized by four fundamental system parameters (leg stiffness  $k_0$ , angle of attack  $\alpha_0$ , rest length  $L_0$ , system energy  $E_0$ ) and the four-dimensional vector of initial conditions  $(x_0, \dot{x}_0, y_0, \dot{y}_0)^T$ .

A walking step comprises a single-support phase and a double-support phase (Figure 3.2). Events of touch-down and take-off are transitions between the phases. Like in the case of running, the trajectory of the center of mass in each phase is the solution of an initial value problem. The initial values for the first initial value problem are  $(x_0, \dot{x}_0, y_0, \dot{y}_0)^T$ . The initial values of each subsequent phase is the last point of the corresponding previous phase. The motion of the center of mass during the single-support phase is described by the equations (3.4). The transition (touch-down) from single-support phase to double-support phase happens, when the landing condition

$$y(t_1) = L_0 \sin(\alpha_0)$$

is fulfilled (Figure 3.2). Here,  $t = t_1$  marks the time, when the touch-down occurs. The equations of the motion during the double-support phase are given by

$$\begin{aligned} m\ddot{x}(t) &= k_0 (L_0 - L_1(t)) \frac{x(t) - x_{\text{FP}_1}}{L_1(t)} + k_0 (L_0 - L_2(t)) \frac{x(t) - x_{\text{FP}_2}}{L_2(t)}, \\ m\ddot{y}(t) &= k_0 (L_0 - L_1(t)) \frac{y(t)}{L_1(t)} + k_0 (L_0 - L_2(t)) \frac{y(t)}{L_2(t)} - mg, \end{aligned} \quad (3.7)$$

where  $L_2(t) := \sqrt{(x(t) - x_{\text{FP}_2})^2 + y^2(t)}$  is the length of the second compressed leg spring (see blue parts of the center of mass trajectory in Figure 3.2). The positions of both footpoints  $\text{FP}_1$  and  $\text{FP}_2$  are given by  $(x_{\text{FP}_1}, 0)$  and  $(x_{\text{FP}_2}, 0)$ , respectively. The transition (take-off) from the double-support phase to the single-support phase occurs when the extending length  $L_1$  of the first leg spring reaches the rest length  $L_0$ , i.e. when the take-off condition

$$(x(t_2) - x_{\text{FP}_1})^2 + y^2(t_2) = L_0^2$$

is fulfilled. Here,  $t = t_2$  marks the time, when the take-off occurs.

Here, the trajectory of the center of mass is computed by three initial value problems. The calculation of a walking step starts at time  $t = t_0$  during the single-support phase at the instant of the vertical leg orientation (VLO, [Rummel et al., 2010a,b], Figure 3.2). Using VLO as the initial point of a step (i.e. as Poincaré section), allows to reduce the dimension of the return map

(Section 3.3). Here, the center of mass is located exactly over the foot point of the supporting leg spring. The first single-support phase is calculated using equations (3.4) and the vector  $(x_0, \dot{x}_0, y_0, \dot{y}_0)^T$  as initial values, followed by the double-support phase (system (3.7)) and by the second single-support phase (again (3.4)). The initial values of the latter two phases are the last points of the previous phases at  $t = t_1$  and  $t = t_2$ , respectively. The walking step ends at the next VLO at time  $t = t_3$ , when the condition  $x(t_3) = x_{\text{FP}_2}$  is fulfilled.

The system is energy-conservative, i.e. the system energy  $E_0$  remains constant during the whole step. During single-support phase, the system energy is given by relation (3.6). During double-support phase, the additional energy of the second leg spring must be considered:

$$E_0 = mgy + \frac{m(\dot{x}^2 + \dot{y}^2)}{2} + \frac{k_0}{2}(L_0 - L_1)^2 + \frac{k_0}{2}(L_0 - L_2)^2, \quad (3.8)$$

with  $L_1$  and  $L_2$  defined as above.

Unless otherwise mentioned, all calculations for walking in this chapter are done with constant dimensional energy  $E_0 = 820$  J corresponding to the average horizontal velocity  $v_x \approx 1.1$  m/s. Since the bipedal model is used for investigations of asymmetric locomotion (Chapter 2), the leg stiffness  $k_0$  is set to 16 kN/m corresponding to experimental data of PogoWalker (Section 2.3.1). Like in case of running, we set  $m = 80$  kg and  $g = 9.81$  m/s<sup>2</sup>.

### 3.3. Periodic solutions

Periodic running and walking solutions are found and analyzed using the well-known Poincaré return map  $\mathbf{F}$  [Poincaré, 1890]. Their stability is determined by the value of the corresponding Floquet multipliers [Floquet, 1883]. The detailed mathematical description can be found e.g. in Guckenheimer & Holmes [1983] or Marx & Vogt [2011]. Here, we give only its basic idea, which is simple and intuitive. First, select an event as Poincaré section. Here, a single (running or walking) step starts at the system state  $s_1 := (x_1, \dot{x}_1, y_1, \dot{y}_1)^T$ . After one full step, the next state of the system is  $s_2 := \mathbf{F}(s_1) = (x_2, \dot{x}_2, y_2, \dot{y}_2)^T$ . The length of the step is determined as  $x_2 - x_1$ . The step is periodic, if the conditions  $\dot{x}_1 = \dot{x}_2$ ,  $y_1 = y_2$  and  $\dot{y}_1 = \dot{y}_2$  are fulfilled. In general, the dimension of the Poincaré return map is three. However, with appropriate choice of the Poincaré section the dimension of  $\mathbf{F}$  can be reduced. Periodic solutions are computed as fixed points  $s^*$  of the Poincaré map  $\mathbf{F}$ , i.e. as zeros of the function

$$\mathbf{G}(s) = s - \mathbf{F}(s). \quad (3.9)$$

A periodic solution  $s^*$  is stable if the magnitude of all eigenvalues of the derivative  $\frac{\partial \mathbf{F}}{\partial s}(s^*)$ , i.e. the Floquet multipliers, are less than one [Guckenheimer & Holmes, 1983; Strogatz, 1994]. Since there are some significant differences between the implementations of the return map for running and walking, both cases are described in separate sections.

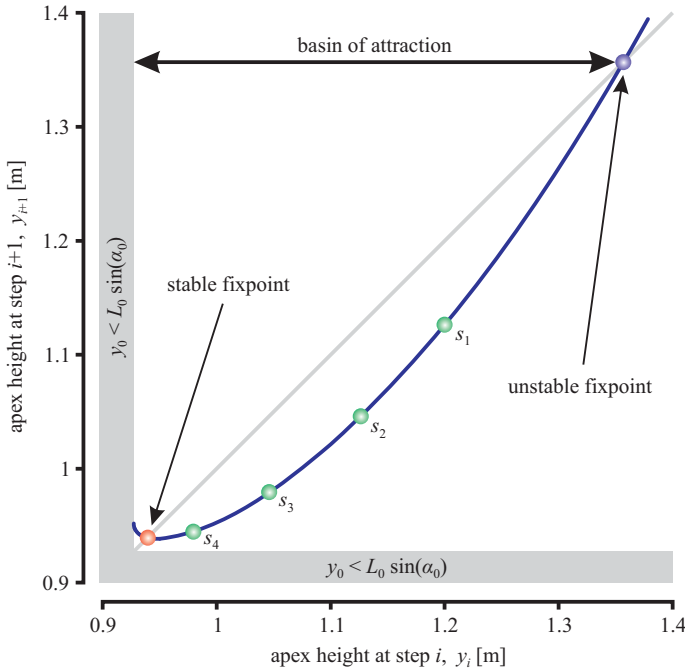


**Figure 3.3.** Example of the one-dimensional Poincaré return map (blue line) of the stable periodic solution at  $y_0 = 0.939$  (red dot) for the parameters  $\alpha_0 = 68^\circ$ ,  $k_0 = 20$  kN/m,  $E_0 = 1800$  J and the initial state  $s_1 = 1.2$ . The green dots show the first four steps of the return map. The blue dot indicates the unstable fixpoint at  $y_0 = 1.357$ .

### 3.3.1. Running

In case of running, the apex of the flight curve is usually chosen as Poincaré section. Here, vertical velocity  $\dot{y}$  is zero and system energy  $E_0$  is given by

$$E_0 = mgy_0 + \frac{m\dot{x}_0^2}{2}. \quad (3.10)$$

For this, the vector of initial conditions  $(x_0, \dot{x}_0, y_0, \dot{y}_0)^T$  depends on the initial apex height  $y_0$ , only. Hence, dimension of the return map is one and the state of the system at the beginning of the step is  $s_1 = y_1$ .

For a given set of parameters, the unstable periodic solution lies on the unstable manifold, which is the border of the basin of attraction of the corresponding stable solution [Guckenheimer & Holmes, 1983]. Since the dimension of the return map is one, the basin of attraction of a stable periodic running solution is also one-dimensional. In most cases, it is limited by the unstable periodic solution and the touch-down line  $y_{TD} = L_0 \sin(\alpha_0)$  (Figure 3.3).

To compare running to walking, the phases of the running step must be arranged differently. The calculation starts during stance phase at the instant of VLO, followed by the flight phase and the second stance phase. That means, the running step looks like the walking one with the flight phase replacing the double-support phase (compare Figure 3.1 and Figure 3.2). Since all period-1 running solutions are symmetric with respect to VLO, the vertical velocity  $\dot{y}_0$  in VLO is zero as well. Therefore, the return map with VLO as Poincaré section is also one-dimensional, i.e. a similar system analysis may be applied with slight changes only.

### 3.3.2. Walking

The system analysis of the bipedal model is more complex. In this case, the instant of VLO is chosen as Poincaré section. Here, system energy  $E_0$  is given by

$$E_0 = mgy_0 + \frac{m(\dot{x}_0^2 + \dot{y}_0^2)}{2} + \frac{k_0}{2}(L_0 - y_0)^2. \quad (3.11)$$

For this, the vector of initial conditions  $(x_0, \dot{x}_0, y_0, \dot{y}_0)^T$  depends only on the initial height  $y_0$  and the velocity angle

$$\theta_0 := \arctan\left(\frac{\dot{y}_0}{\dot{x}_0}\right)$$

with

$$\dot{x}_0 = \sqrt{\frac{2}{m} \left( E_0 - mgy_0 - \frac{k_0}{2}(L_0 - y_0)^2 \right)} \cos(\theta_0)$$

and

$$\dot{y}_0 = \sqrt{\frac{2}{m} \left( E_0 - mgy_0 - \frac{k_0}{2}(L_0 - y_0)^2 \right)} \sin(\theta_0)$$

(see inset in Figure 3.4). Therefore, the dimension of the Poincaré map is reduced to two.

Now, let  $s_i = (y_0^{(i)}, \theta_0^{(i)})$  be the state of the system in  $\text{VLO}_i$  (Figure 3.2). Then after one step, the state in  $\text{VLO}_{i+1}$  is  $s_{i+1} = \mathbf{F}(s_i)$ , where  $\mathbf{F}$  is the corresponding Poincaré map.

The basin of attraction of a stable periodic walking solution is also a two-dimensional set (Figure 3.4). If there exist an unstable fixpoint for the same set of parameters, then the basin can be determined by calculation of the unstable manifold through this unstable fixpoint. Otherwise, the common steps-to-fall method can be applied. The details of its computation can be found in Rummel et al. [2010b].

## 3.4. Transformation into a boundary value problem

To apply appropriate techniques for the calculation of bifurcations, it is beneficial to transform the model into a two-point boundary value problem

$$\begin{aligned} \dot{z}(\tau) &= f(z(\tau)), \quad \tau \in [0, 1], \\ r(z(0), z(1); \alpha_0) &= 0. \end{aligned} \quad (3.12)$$

The functions  $f : \mathbb{R}^n \rightarrow \mathbb{R}^n$  and  $r : \mathbb{R}^n \times \mathbb{R}^n \times \mathbb{R} \rightarrow \mathbb{R}^n$  are different for running and walking. To avoid discontinuities at the transition events touch-down (TD) and take-off (TO), we re-arrange the three phases of the step. Since the end of each phase of a running or walking step is defined

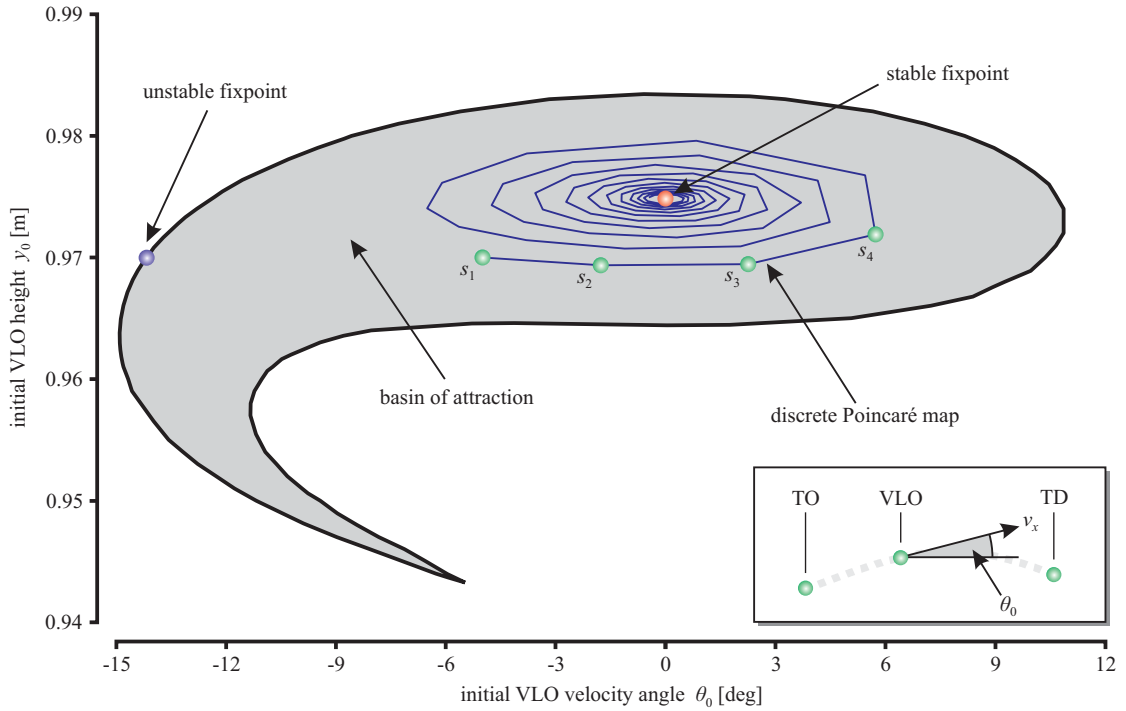


**Figure 3.4.** Example of the discrete two-dimensional Poincaré return map (blue line) of the stable periodic solution at  $(y_0, \theta_0) = (0.974, 0)$  (red dot) for the parameters  $\alpha_0 = 70^\circ$ ,  $k_0 = 16$  kN/m,  $E_0 = 820$  J and the initial state  $s_1 = (0.97, -5)$ . The green dots show the first four steps of the return map. The blue dot indicates the unstable fixpoint at  $(y_0, \theta_0) = (14.174, 0.970)$ .

by an event, the times  $t_1$ ,  $t_2$ , and  $t_3$  are not known in advance. Instead of solving the initial value problems consecutively, we scale each phase to the unit interval  $[0, 1]$ , e.g. Doedel et al. [2005]; Hermann [2004], and solve all three phases at once.

### 3.4.1. Running

The functions  $f : \mathbb{R}^n \rightarrow \mathbb{R}^n$  and  $r : \mathbb{R}^n \times \mathbb{R}^n \times \mathbb{R} \rightarrow \mathbb{R}^n$  for running are listed in Table 3.1. In the new system, the durations  $t_1 - t_0$ ,  $t_2 - t_1$  and  $t_3 - t_2$  of the three phases are transformed into the scaling parameters  $z_5, z_{10}$  and  $z_{16}$ . Equations  $f_1$  to  $f_4$ ,  $f_6$  to  $f_9$  and  $f_{12}$  to  $f_{15}$  describe the motion of the center of mass during the first flight phase (equations (3.3)), the stance phase (equations (3.4)) and the second flight phase (again (3.3)), respectively. Equation  $f_{11}$  together with the boundary condition  $r_{11} = 0$  determine the horizontal position  $x_{\text{FP}_1} = L_0 \cos(\alpha_0)$  of the foot point  $\text{FP}_1$  (Figure 3.1).

The boundary functions  $r_1 \dots r_4$  define initial location and velocity of the center of mass. The switches between the phases of the step are described by  $r_6 \dots r_9$  and  $r_{12} \dots r_{15}$ . Finally,  $r_5, r_{10}, r_{16}$  determine the events of touch-down, take-off and second apex.

To find a periodic running solution for a given set of parameters, the functions  $r_2$  and  $r_3$  have to be replaced by

$$\begin{aligned}\widehat{r}_2 &= E_0 - mgz_3(0) - \frac{mz_2(0)^2}{2}, \\ \widehat{r}_3 &= z_3(0) - z_{14}(1).\end{aligned}\tag{3.13}$$

The new boundary condition  $\widehat{r}_2 = 0$  describes the relationship (3.10) between the initial apex height  $z_3(0) = y_0$  and the initial horizontal velocity  $z_2(0) = \dot{x}_0$  with respect to the system energy  $E_0$ . The function  $\widehat{r}_3$  corresponds to the Poincaré return map (3.9) of the original model, i.e. it describes the periodic condition for the initial apex height  $y_0$  of the center of mass.

### 3.4.2. Walking

The functions  $f : \mathbb{R}^n \rightarrow \mathbb{R}^n$  and  $r : \mathbb{R}^n \times \mathbb{R}^n \times \mathbb{R} \rightarrow \mathbb{R}^n$  for walking are listed in Table 3.2. Like in case of running, the durations  $t_1 - t_0$ ,  $t_2 - t_1$  and  $t_3 - t_2$  of the three phases are transformed into the scaling parameters  $y_5$ ,  $y_{10}$  and  $y_{16}$ . Equations  $f_1$  to  $f_4$ ,  $f_6$  to  $f_9$  and  $f_{12}$  to  $f_{15}$  describe the motion of the center of mass during the first single-support phase (equations (3.4)), the double-

$f_1 = z_5 z_2$	$r_1 = z_1(0) - x_0$
$f_2 = 0$	$r_2 = z_2(0) - \sqrt{\frac{2}{m}(E_0 - mgy_0)}$
$f_3 = z_5 z_4$	$r_3 = z_3(0) - y_0$
$f_4 = -z_5 g$	$r_4 = z_4(0)$
$f_5 = 0$	$r_5 = z_3(1) - L_0 \sin(\alpha_0)$
$f_6 = z_{10} z_7$	$r_6 = z_6(0) - z_1(1)$
$f_7 = \frac{1}{m} z_{10} k_0 (L_0 - L_1) \frac{z_6 - z_{11}}{L_1}$	$r_7 = z_7(0) - z_2(1)$
$f_8 = z_{10} z_9$	$r_8 = z_8(0) - z_3(1)$
$f_9 = \frac{1}{m} z_{10} k_0 (L_0 - L_1) \frac{z_8}{L_{12}} - mg$	$r_9 = z_9(0) - z_4(1)$
$f_{10} = 0$	$r_{10} = (z_6(1) - z_{11}(0))^2 + z_8(1)^2 - L_0^2$
$f_{11} = 0$	$r_{11} = z_{11}(0) - z_6(0) - L_0 \cos(\alpha_0)$
$f_{12} = z_{16} z_{13}$	$r_{12} = z_{12}(0) - z_6(1)$
$f_{13} = 0$	$r_{13} = z_{13}(0) - z_7(1)$
$f_{14} = z_{16} z_{15}$	$r_{14} = z_{14}(0) - z_8(1)$
$f_{15} = -z_{16} g$	$r_{15} = z_{15}(0) - z_9(1)$
$f_{16} = 0$	$r_{16} = z_{15}(1)$

**Table 3.1.** The functions  $f$  and  $r$  for the boundary value problem (3.12) computing a single running step. Here,  $L_1 := \sqrt{(z_6 - z_{11})^2 + z_3^2}$  is the length of the compressed leg spring during stance phase.

support phase (equations (3.7)) and the second single-support phase (again (3.4)), respectively. Equation  $f_{11}$  together with the boundary condition  $r_{11} = 0$  determine the horizontal position  $x_{\text{FP}_2} = L_0 \cos(\alpha_0)$  of the second foot point  $\text{FP}_2$  (Figure 3.2).

The boundary functions  $r_1 \dots r_4$  define initial location and velocity of the center of mass. The switches between the phases of the step are described by  $r_6 \dots r_9$  and  $r_{12} \dots r_{15}$ . Finally,  $r_5, r_{10}, r_{16}$  determine the events of touch-down, take-off and second VLO.

To find a periodic solution for the given parameters  $\alpha_0, k_0, L_0$  and  $E_0$ , the functions  $r_2, r_3, r_4$  have

$f_1 = y_5 z_2$	$r_1 = z_1(0) - x_0$
$f_2 = \frac{1}{m} z_5 k_0 (L_0 - L_{11}) \frac{z_1 - x_0}{L_{11}}$	$r_2 = z_2(0) - v_0 \cos(\theta_0)$
$f_3 = z_5 z_4$	$r_3 = z_3(0) - y_0$
$f_4 = \frac{1}{m} z_5 \left( k_0 (L_0 - L_{11}) \frac{z_3}{L_{11}} - mg \right)$	$r_4 = z_4(0) - v_0 \sin(\theta_0)$
$f_5 = 0$	$r_5 = z_3(1) - L_0 \sin(\alpha_0)$
$f_6 = z_{10} z_7$	$r_6 = z_6(0) - z_1(1)$
$f_7 = \frac{1}{m} z_{10} \left( k_0 (L_0 - L_{12}) \frac{z_6 - x_0}{L_{12}} + k_0 (L_0 - L_{21}) \frac{z_6 - z_{11}}{L_{21}} \right)$	$r_7 = z_7(0) - z_2(1)$
$f_8 = z_{10} z_9$	$r_8 = z_8(0) - z_3(1)$
$f_9 = \frac{1}{m} z_{10} \left( k_0 (L_0 - L_{12}) \frac{z_8}{L_{12}} + k_0 (L_0 - L_{21}) \frac{z_8}{L_{21}} - mg \right)$	$r_9 = z_9(0) - z_4(1)$
$f_{10} = 0$	$r_{10} = (z_6(1) - x_0)^2 + z_8(1)^2 - L_0^2$
$f_{11} = 0$	$r_{11} = z_{11}(0) - z_6(0) - L_0 \cos(\alpha_0)$
$f_{12} = z_{16} z_{13}$	$r_{12} = z_{12}(0) - z_6(1)$
$f_{13} = \frac{1}{m} z_{16} k_0 (L_0 - L_{22}) \frac{z_{12} - z_{11}}{L_{22}}$	$r_{13} = z_{13}(0) - z_7(1)$
$f_{14} = z_{16} z_{15}$	$r_{14} = z_{14}(0) - z_8(1)$
$f_{15} = \frac{1}{m} z_{16} \left( k_0 (L_0 - L_{22}) \frac{z_{14}}{L_{22}} - mg \right)$	$r_{15} = z_{15}(0) - z_9(1)$
$f_{16} = 0$	$r_{16} = z_{12}(1) - z_{11}(1)$

**Table 3.2.** The functions  $f$  and  $r$  for the boundary value problem (3.12) computing a single walking step. Here,  $L_{11} := \sqrt{(z_1 - x_0)^2 + z_3^2}$  and  $L_{12} := \sqrt{(z_6 - x_0)^2 + z_8^2}$  are the lengths of the first compressed leg spring during different phases of the step. The lengths of the second compressed leg spring are given by  $L_{21} := \sqrt{(z_6 - z_{11})^2 + z_8^2}$  and  $L_{22} := \sqrt{(z_{12} - z_{11})^2 + z_{13}^2}$ . The general velocity of the system at the instant of VLO is given by  $v_0 := \sqrt{\frac{2}{m}(E_0 - mgy_0 - \frac{k_0}{2}(L_0 - y_0)^2)}$ .

to be replaced by

$$\begin{aligned}\widehat{r}_2 &= E_0 - mgz_3(0) - \frac{m(z_2(0)^2 + z_4(0)^2)}{2} - \frac{k_0}{2}(L_0 - z_3(0))^2, \\ \widehat{r}_3 &= z_3(0) - z_{14}(1), \\ \widehat{r}_4 &= \arctan\left(\frac{z_4(0)}{z_2(0)}\right) - \arctan\left(\frac{z_{15}(1)}{z_{13}(1)}\right).\end{aligned}\tag{3.14}$$

The new boundary condition  $\widehat{r}_2 = 0$  describes the relationship (3.11) between initial VLO height  $z_3(0) = y_0$ , initial horizontal velocity  $z_2(0) = \dot{x}_0$  and initial vertical velocity  $z_4(0) = \dot{y}_0$  of the center of mass with respect to the system energy  $E_0$  in the instant of VLO. The functions  $\widehat{r}_3$  and  $\widehat{r}_4$  correspond to the Poincaré return map (3.9) of the bipedal model, i.e. they describe the periodic conditions for VLO height  $y_0$  and VLO velocity angle  $\theta_0 = \arctan\left(\frac{z_4(0)}{z_2(0)}\right)$  of the center of mass.

### 3.4.3. Period-2 solutions

Period-2 solutions deserve special attention, since they are required for the study of the asymmetric spring-mass model (Chapters 2 and 5). Period-2 solutions of the symmetric model are often very unstable and thus difficult to compute. However, the numerical stability of the boundary value problem allows the computation of the complete manifold of period-2 solutions. The extension of the boundary value problem for the computation of a double step is intuitive. The functions  $f$  and  $r$  for (3.12) computing a double walking step are constructed in the following way (the boundary value problem for running looks similar).

The step starts with leg 1 on the ground (functions  $f_1$  to  $f_4$  and  $r_1$  to  $r_4$ ). The boundary condition  $r_5 = 0$  describes the touch-down of leg 2 and  $r_{11} = 0$  marks the horizontal position of the second foot point. The step continues with the double-support phase ( $f_6$  to  $f_9$ ), which ends with the take-off of the first leg ( $r_{10} = 0$ ). The second single-support phase lasts from take-off until touch-down of leg 1. It is described by functions  $f_{12}$  to  $f_{15}$ , followed by touch-down of the first leg ( $r_{16} = 0$ ).

	single	SP	double	SP	FP <sub>2</sub>	single	SP	double	SP	FP <sub>3</sub>	single	SP
$x$	$z_1$	$z_5$	$z_6$	$z_{10}$	$z_{11}$	$z_{12}$	$z_{16}$	$z_{17}$	$z_{21}$	$z_{22}$	$z_{23}$	$z_{27}$
$\dot{x}$	$z_2$		$z_7$			$z_{13}$		$z_{18}$			$z_{24}$	
$y$	$z_3$		$z_8$			$z_{14}$		$z_{19}$			$z_{25}$	
$\dot{y}$	$z_4$		$z_9$			$z_{15}$		$z_{20}$			$z_{26}$	

**Table 3.3.** Relationship of variables  $x, \dot{x}, y, \dot{y}$  of the original model to variables  $z_i$  of the transformed model for different phases of a double walking step (Figure 3.2). SP are scaling parameters of the corresponding phase. FP <sub>$i$</sub>  is the  $x$ -position of the footpoint  $i$ .



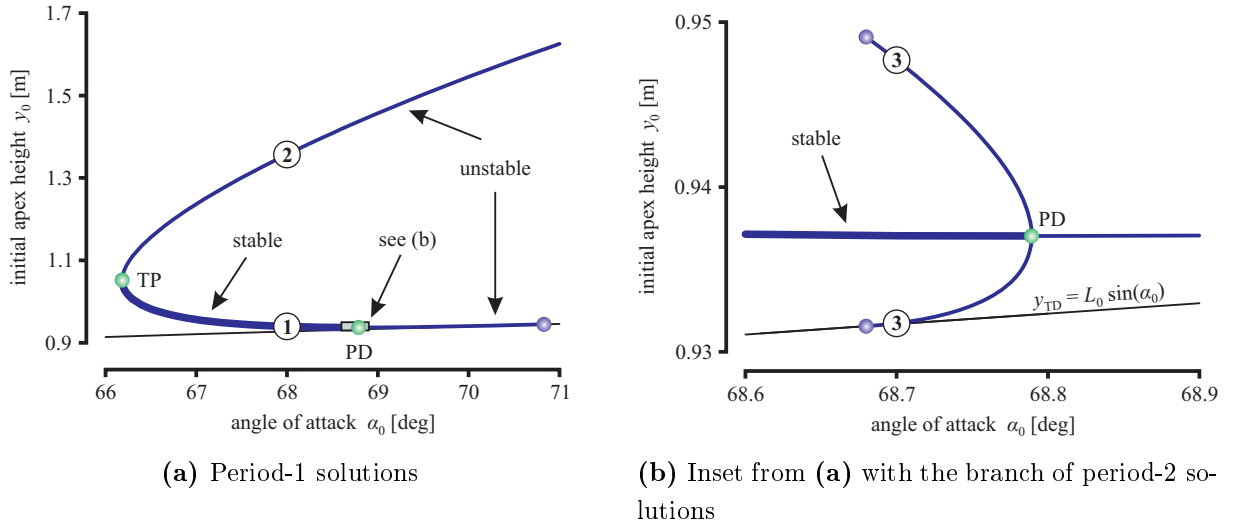


**Figure 3.5.** Initial apex height  $y_0$  of periodic running patterns dependent on the angle of attack  $\alpha_0$ . The green dots represent bifurcations: TP = simple turning point, PD = period-doubling bifurcation (Chapter 4). The blue dots are solutions on the touch-down line  $y_{TD} = L_0 \sin(\alpha_0)$ . Thick lines indicate stable solutions. The examples of the center of mass trajectories and ground-reaction forces corresponding to the white dots are shown in Figure 3.6.

The last two phases are again double-support and another single-support. The step ends in the VLO of leg 1. Hence, the dimension of the boundary value problem is  $n = 27$ .

There is a small difference in case of the monopedal model. Here, the middle flight phase is separated in two flight phases with the event of apex between them. This modification increases the dimension of the boundary value problem to  $n = 32$ . However, the strict separation of two steps is often required for computation of stability limits of asymmetric model (see the definition of touch-down and take-off points in Section 5.3).

## 3.5. Results

The new implementation of the model is a necessary intermediate step to calculate bifurcations. However, it has one useful property on its own, namely it can be used to compute even highly unstable periodic solutions of the spring-mass model. The details, which are different for walking and running, are given below.

### 3.5.1. Running

Stable running solutions are located between a simple turning point (TP) and a period-doubling bifurcation point (PD, Figure 3.5(a)). Periodic solutions exist between the touch-down line

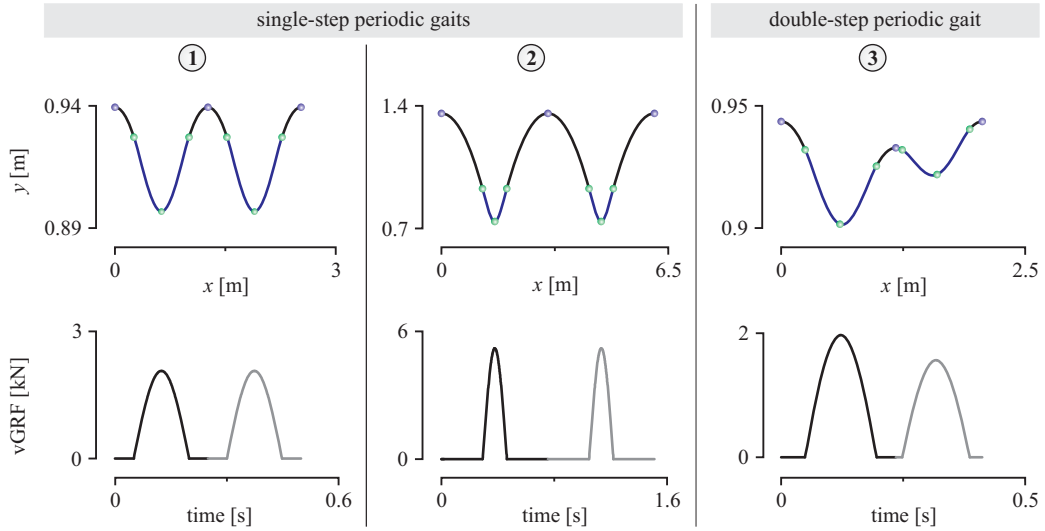


**Figure 3.6.** Examples of CoM trajectories (upper row) and vertical ground reaction forces (vGRF) of both legs (lower row) corresponding to the points in Figure 3.5. The blue points indicate events of apex, the green ones are events of touch-down (TD) and take-off (TO)

$y_{\text{TD}} = L_0 \sin(\alpha_0)$  and maximal hopping height  $y_{\text{max}} = E_0/mg$ . The branch of period-2 solutions is short, because the lower part is limited by the touch-down line (Figure 3.5(b)). Examples of periodic solutions for running are presented in Figure 3.6. In particular, example 3 shows that the branch of period-2 solutions exhibits a typical bilateral symmetry of a pitchfork bifurcation, namely both parts of the branch consist of the same periodic solutions with alternating apex heights.

The return map of the monopedal model is one-dimensional. The solutions around the turning point and the bifurcation point are either stable or just slightly unstable. For this, there are no difficulties computing period-1 solutions by the original implementation based on initial value problems. However, instability of the period-2 solutions grows rapidly. For instance, the Floquet multiplier of example 3 in Figure 3.6 is 3.6. Here, the angle of attack is  $\alpha_0 = 68.7^\circ$ . The Floquet multiplier of the periodic solution at  $\alpha_0 = 68.69^\circ$  is already 6.7. Thus, computation of these solutions with the original model requires very precise initial conditions. In order to compute them using the boundary value problem (3.12), it is sufficient to use any other point from this branch as initial guess.

Another problematic case could be the computation of periodic solutions around the transition point between walking and running for lower energies (Figure 3.7). Here, the running patterns are also highly unstable and almost impossible to compute with the original model. Again, the boundary value problem does not have any significant problems computing them. In particular, to compute all periodic solutions, it is sufficient to use the simple shooting method.

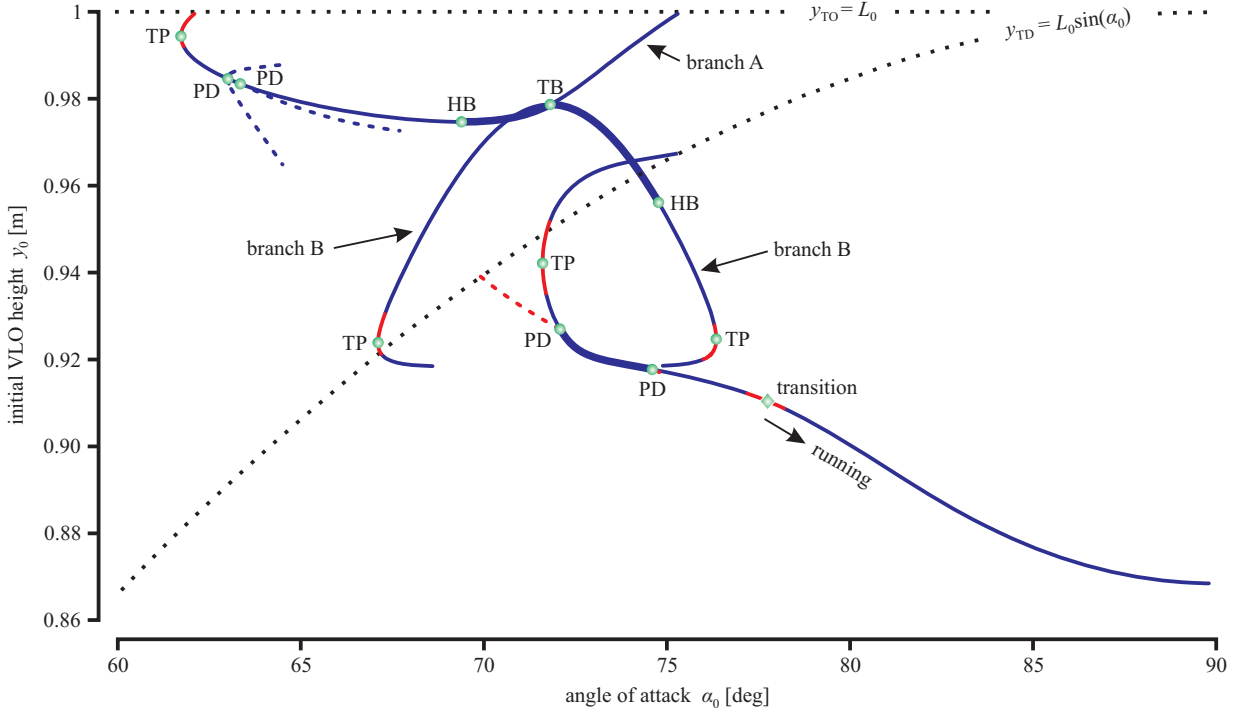


**Figure 3.7.** Initial VLO height  $y_0$  of periodic walking patterns dependent on the angle of attack  $\alpha_0$ . The dots represent bifurcations: TP = simple turning point, TB = transcritical bifurcation, HB = Hopf bifurcation, PD = period-doubling bifurcation (Chapter 4). Blue lines show periodic solutions computed with the original implementation of the model. The red ones are computed with the boundary value problem (3.12). Thick lines indicate stable solutions. For the examples of CoM trajectories and ground-reaction forces see Figures 2.6 and 2.8.

### 3.5.2. Walking

For  $E_0 = 820$  J, there are two regions of stable solutions (Figure 3.7). Stable walking solutions are located between two Hopf bifurcations on two branches connected by a transcritical bifurcation. Stable grounded running solutions are confined either between two period-doubling bifurcations ( $E_0 = 820$  J) or between a PD-bifurcation and a Hopf bifurcation ( $E_0 = 810$  J) (Figure 3.9). Grounded running is a type of bipedal locomotion, where the center of mass crosses the touchdown line  $y_{TD} = L_0 \sin(\alpha_0)$  from below (Figure 3.8, [Andrada et al., 2012; Martinez & Carbajal, 2011; Rummel et al., 2009]).

Examples of periodic solutions for walking are shown in Figure 2.8 and 3.10. The center of mass trajectory and the ground-reaction force of the patterns from branch B (examples  $b_1$  and  $b_2$ ) cannot be mirrored around VLO.<sup>1</sup> In this case, the velocity angle  $\theta_0$  at VLO is non-zero. All other branches in Figure 3.7 consist of walking patterns with  $\theta_0 = 0$ .<sup>2</sup> Examples of stable grounded

<sup>1</sup>These periodic solutions are often called *asymmetric* [Rummel et al., 2010b]. Since a great part of this thesis deals with the asymmetric spring-mass model, this notation would cause confusion. Thus, we only refer to solutions of the asymmetric model as *asymmetric* (Chapter 2).

<sup>2</sup>For obvious reasons, these patterns are also called *symmetric* [Rummel et al., 2010b].

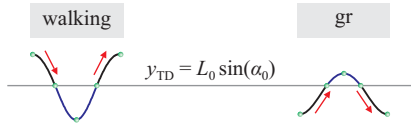


**Figure 3.8.** Motion of the center of mass in a walking (left) and a grounded running (right) pattern.

running patterns are shown in Figure 3.10.

Two branches of period-2 walking gaits are located around  $\alpha_0 = 70^\circ$ . Another two branches consist of period-2 grounded running patterns.

Periodic solutions in the area of the simple turning points (TP in Figure 3.7) are highly unstable. Moreover, the locomotion gaits around the transition from walking to running (diamond in Figure 3.7) are also hard to find. In contrast, the implementation of the model as a boundary value problem together with the simple shooting method does not have any significant difficulties to compute these solutions.

Since we consider biologically relevant walking patterns only, a part of periodic solutions calculated by the new model is omitted. In particular, no solutions above the take-off line at  $y_{\text{TO}} = L_0$  are shown, since all of them contain a flight phase (Figure 3.7). Similarly, we neglect part of the solutions below the touch-down line  $y_{\text{TD}} = L_0 \sin(\alpha_0)$ . Here, several patterns contain backward walking, jump-offs, or some other actions, which contradict our definition of walking.

To compute all periodic solutions, it is sufficient to use the simple shooting method to solve the boundary value problem (3.12). Even in the nearest neighborhood of the turning points or around the transition to running (diamond in Figure 3.7), where the periodic solutions are highly unstable, the application of multiple shooting is not necessary to reach the desired precision. However it was observed, that for fast convergence the initial guess of the scaling parameters  $z_5$ ,  $z_{10}$  and  $z_{16}$  should be as precise as possible.

## 3.6. Discussion

The most important result of this chapter is the new implementation of the model as a two-point boundary value problem. Now, it is possible to calculate even highly unstable solutions in the neighborhood of simple turning points and around the transition point from walking to running. This is due to the high numerical stability of the shooting method compared to the classical approaches (like various Runge-Kutta methods) for solving initial value problems [Hermann, 2004; Stoer & Bulirsch, 1993].

The application of the simple shooting method is sufficient for the computation of periodic solutions. The hybrid dynamical system described in Section 3.2 consists of three initial value problems

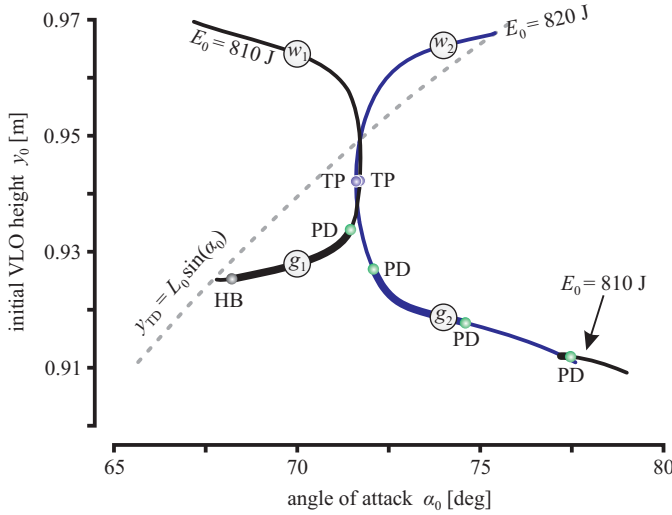


**Figure 3.9.** Initial VLO height of grounded running patterns dependent on the angle of attack  $\alpha_0$ . Green points are period-doubling bifurcations (PD), blue points are simple turning points (TP) and the gray point is a Hopf bifurcation (HB). Thick lines indicate stable solutions. Examples of CoM trajectories and vertical ground reaction forces corresponding to the points  $g_1$ ,  $g_2$  (stable grounded running),  $w_1$  and  $w_2$  (walking) are shown in Figure 3.10.

with 12 differential equations. Additionally, three event functions for touch-down, take-off and the second VLO must be evaluated. The boundary value problem (3.12) for a single walking or running step has the dimension 16. Some additional time may be needed for the scaling of the original equations to the unit interval  $[0, 1]$ . Both cases require the computation of zeros of a non-linear function. Thus, the computation time of both approaches is comparable, while the second one provides the advantage to be more robust against numerical perturbations.

With the new model, it is possible to find periodic solutions at the touch-down line. The touch-down line  $y_{TD} = L_0 \sin(\alpha_0)$  occurs in the original model as an event of the hybrid dynamical system. To trigger the event of touch-down, the hyper plane must be hit by the flow transversely, which means, that solutions on this line and in the nearest neighborhood are almost impossible to compute. In the boundary value problem, the events of touch-down and take-off are described by the boundary functions. Hence, there are no restrictions for calculations anymore and the desired accuracy of these periodic solutions can be achieved with no significant problems (Figure 3.7). Moreover, it is possible to find the exact value of the angle of attack  $\alpha_0$ , where an event occurs. Since it is required for computation of the stability boundaries of the asymmetric running model, a detailed description of this technique is given in Chapter 5.

Sometimes it is not sufficient to know the position of a periodic solution. It may be necessary to study the shape of the center of mass trajectory or the ground reaction force corresponding to this solution. In this case, the multiple shooting method could be applied to solve the boundary value problem (3.12). However, with the growing number of shooting points, the complexity of the calculation - and therefore the computation time - increases considerably. Moreover, the choice of the appropriate initial guess may be troublesome. Here, the more efficient strategy is to solve the boundary value problem using the simple shooting method. Afterwards, one could use this periodic solution as the initial condition for the original model, which could be solved with the required precision.

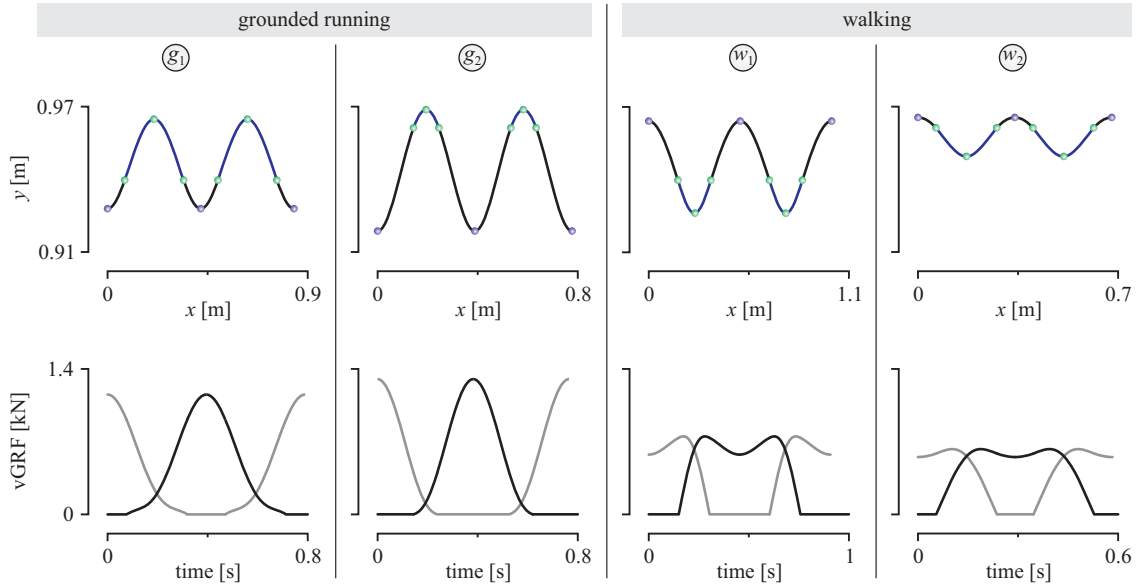


**Figure 3.10.** Examples of CoM trajectories (upper row) and vertical ground reaction forces (vGRF) of both legs (lower row) corresponding to the points  $g_1$ ,  $g_2$  (stable grounded running),  $w_1$  and  $w_2$  (walking) in Figure 3.9. The blue points indicate events of vertical leg orientation (VLO), the green ones are events of touch-down (TD) and take-off (TO) (Figure 3.2).

The spring-mass model is a useful tool for the development of artificial locomotion systems like legged robots or rehabilitation devices [Renjewski et al., 2008; Renjewski & Seyfarth, 2012; Seyfarth et al., 2012]. With the approach presented in this work, suitable robot leg parameters can be checked for feasibility and implemented in a technical device much faster and efficiently than before. On the other hand, robot and human locomotion data are often used to validate and verify predictions made by models. To compare measured data to the results of the basic spring-mass model with only three leg parameters  $\alpha_0$ ,  $k_0$  and  $L_0$ , common optimization approaches like the least squares method may be completely sufficient [Lipfert et al., 2012]. However, even such a simple extension of the model like leg asymmetry already doubles the number of leg parameters (Chapter 2). Enhancing the model by a leg segmentation [Maykranz et al., 2009; Rummel & Seyfarth, 2008] or by a trunk [Maus et al., 2010], considerably increases the number of degrees of freedom. One possible way to deal with the growing complexity is to define the optimization problem as a boundary value problem as described in this work, transform it into a finite dimensional non-linear programming problem, and solve it using an appropriate optimization method [Betts, 2010; Bock & Plitt, 1984; Diehl et al., 2006].

Gait transitions from walking to running and from running to walking are an important research field in biomechanics, e.g. Martinez & Carbajal [2011]; Minetti et al. [1994]; Segers et al. [2007b]. For instance, it is still not fully clear, how the transition is triggered mechanically. This is one reason, why most legged robots are built either for walking or for running. In the spring-mass model, these both locomotion gaits exist side-by-side (Figure 3.7). However, applications of the

model for the investigation of gait transitions were limited so far, since it is difficult to find periodic solutions around the transition point. Here, the return map of the walking model becomes one-dimensional. Therefore, its Jacobian matrix is nearly singular. Furthermore, periodic running solutions near the transition point are highly unstable. In both cases, any precise computation around the transition point is nearly impossible. Hence, there is a gap between walking and running solutions, as shown in [Rummel et al. \[2009\]](#) for all values of system energy  $E_0$ . The boundary value problem presented in this work closes this gap and allows more effective usage of the spring-mass model for studies of this biomechanical issue.

# 4. Numerical bifurcation analysis of the spring-mass model

## 4.1. Introduction

In the previous chapter, we presented the transformation of the spring-mass model into a parametrized two-point boundary value problem of the form

$$\dot{y}(t) = f(t, y; \lambda), \quad r(y(0), y(1); \lambda) = 0. \quad (4.1)$$

In the neighbourhood of an *isolated* solution  $(\bar{y}, \bar{\lambda})$  of this problem, i.e. where the Fréchet-derivative of the corresponding operator is invertible, the implicit function theorem guarantees the existence of a unique solution curve  $\{(y(\lambda), \lambda)\}$ . Thus, an appropriate numerical continuation can now be used to compute the branch of solutions around this point, e.g. [Hermann & Ullrich \[1992\]](#); [Keller \[1978\]](#); [Seydel \[1984\]](#). However, there often exist *nonisolated* solutions  $(y_0, \lambda_0)$  of the boundary value problem, where the Fréchet-derivative is *not* invertible. If the solution curve  $\{(y(\lambda), \lambda)\}$  is not unique in the neighbourhood of the nonisolated solution, then  $(y_0, \lambda_0)$  is a singular point (*turning point* or *bifurcation point*). Bifurcations are events, where qualitative and topological changes in the dynamics of the system occur, like vanishing stability or changing shape of the phase portrait. Singular points are determined by parameter values  $\lambda_0$ , at which these events happen [[Marx & Vogt, 2011](#); [Strogatz, 1994](#)].

As mentioned above, bifurcation points are singularities in a given system, and thus they cannot be found by standard numerical techniques. Therefore, the computation of bifurcation points requires a special approach. One popular method to treat bifurcation problems arising from (4.1) is to transform them into a system of parametrized nonlinear algebraic equations [[Gavrilyuk et al., 2010](#); [Hermann, 2004](#); [Makarov et al., 2004](#)]. However, with the discretization an approximation error is introduced into the system. The consequence is that so-called ghost solutions of the finite dimensional problem often occur, which have nothing to do with the solutions of the original infinite dimensional problem [[Brezzi et al., 1984](#); [Seydel, 2010](#)]. Moreover, to achieve the prescribed accuracy, the interval  $[0, 1]$  has to be subdivided into very small segments resulting in a high-dimensional nonlinear algebraic problem [[Stoer & Bulirsch, 1993](#)]. Therefore, we avoid this



discretization and work with functions in infinite dimensional Banach spaces, which are adjusted to the given problem.

Here, we use an approach based on the so-called *Lyapunov-Schmidt reduction* [Lyapunov, 1906; Schmidt, 1908]. Here, the original problem is embedded into a higher dimensional boundary value problem. Then, the isolated solutions of this modified problem can be determined with numerical standard techniques like shooting methods. Some of the computed isolated solutions represent the nonisolated of the given problem (4.1). This approach can further be modified e.g. for the computation of simple turning points [Keener & Keller, 1973; Moore & Spence, 1980] and transcritical bifurcation points [Moore, 1980; Weber, 1979, 1981]. The required starting values can efficiently be obtained using the appropriate numerical continuation [Hermann & Milde, 2009].

The type of a bifurcation point can be determined by the so-called *bifurcations coefficients*. However, their calculation requires a symbolic computation of the second and third partial derivatives of the corresponding operator. For a boundary value problem with non-linear boundary conditions, this means that also the partial derivatives of the boundary function  $r$  have to be determined. Thus, their computation can become a time-consuming task, especially for the high-dimensional problems, which occur in our study. Therefore, in this thesis the type of bifurcation points are determined by the shape of the generated bifurcation diagram and the stability behaviour of periodic solutions in the neighbourhood [Ikeda & Murota, 2002].

In our spring-mass model, bifurcation points connect curves of periodic solutions and also confine the regions of stable locomotion (Chapter 2 and 3, see also Rummel et al. [2010b]). In the bipedal model, all common kinds of bifurcations like simple turning points, secondary bifurcation points or Hopf bifurcations occur. In the monopedal model, only simple turning points and period-doubling bifurcation points have been observed.

## 4.2. Some topics of the analytical bifurcation theory

In this section, a short introduction to bifurcation theory is presented. Using the boundary value problem from the previous chapter, it is not difficult to build extended systems for computation of different kinds of singular points. A more detailed description of the bifurcation theory can be found e.g. in Wallisch & Hermann [1987] or Zeidler [1998].

### 4.2.1. Definitions and important theorems

Let

$$\begin{aligned} \dot{y}(t) &= f(t, y; \lambda), \quad a \leq t \leq b, \\ r(y(a), y(b); \lambda) &= 0 \end{aligned} \tag{4.2}$$

be a parameter dependent two-point boundary value problem with

$$\begin{aligned} y &\in \mathbf{C}^1([a, b], \mathbb{R}^n), \quad \lambda \in \mathbb{R}, \\ f &: \mathfrak{D}_f \rightarrow \mathbb{R}^n, \quad \mathfrak{D}_f \subset [a, b] \times \mathbb{R}^n \times \mathbb{R}, \\ r &: \mathfrak{D}_r \rightarrow \mathbb{R}^n, \quad \mathfrak{D}_r \subset \mathbb{R}^n \times \mathbb{R}^n \times \mathbb{R}. \end{aligned}$$

Consider the equation

$$T(y, \lambda) = 0 \tag{4.3}$$

with  $T : \mathbb{X} \times \mathbb{R} \rightarrow \mathbb{Y}$  given by

$$T(y, \lambda) := \begin{pmatrix} \dot{y} - f(\cdot, y; \lambda) \\ r(y(a), y(b); \lambda) \end{pmatrix}. \tag{4.4}$$

The Banach spaces  $\mathbb{X} := \mathbf{C}^1([a, b], \mathbb{R}^n)$  and  $\mathbb{Y} := \mathbf{C}([a, b], \mathbb{R}^n) \times \mathbb{R}^n$  are given with corresponding norms

$$\|x\|_{\mathbb{X}} := \sup_{[a, b]} \{|x(t)| + |\dot{x}(t)|\}, \tag{4.5}$$

$$\|y\|_{\mathbb{Y}} := \sup_{[a, b]} \{|g(t)|\} + \|v\|, \tag{4.6}$$

where  $y := (g, v) \in \mathbb{Y}$ ,  $|x| := (x^T x)^{\frac{1}{2}}$  and  $\|\cdot\|$  is any norm of  $\mathbb{R}^n$ . In the following, we set  $\mathbb{Z} := \mathbb{X} \times \mathbb{R}$ .

The *Fréchet-derivative*  $T_y$  of the operator  $T$  with respect to  $y$  is given by

$$T_y(y, \lambda)v := \begin{pmatrix} \dot{v} - f_y(\cdot, y; \lambda)v \\ B_a v(a) + B_b v(b) \end{pmatrix} \tag{4.7}$$

with  $B_a := r_{y(a)}(y(a), y(b); \lambda)$  and  $B_b := r_{y(b)}(y(a), y(b); \lambda)$ .

**Definition 4.1:** Let  $X$  and  $Y$  be Banach spaces. An operator  $T \in \mathcal{L}(X, Y)$  is a *Fredholm operator* iff the dimension of the null space  $\mathcal{N}(T)$  of  $T$  and the codimension of the range  $\mathcal{R}(T)$  of  $T$  are finite numbers and the range  $\mathcal{R}(T)$  is closed in  $Y$ . The number

$$\text{ind}(T) := \dim(\mathcal{N}(T)) - \text{codim}(\mathcal{R}(T))$$

is called *index* of  $T$ .

**Definition 4.2:** For an operator  $T \in \mathcal{L}(X, Y)$ , the *dual operator*  $T^* : Y^* \rightarrow X^*$  is given by

$$(T^*y^*)(x) := y^*(Tx) \quad (4.8)$$

for all  $y^* \in Y^*$  and  $x \in X$ .

For further discussion on the operator  $T_y^*$ , which is dual to the operator  $T_y$  from (4.7), see [Middelmann \[1998\]](#).

**Definition 4.3:** Let  $X$  be a Banach space. Let  $\emptyset \neq M \subset X$  and  $\emptyset \neq N \subset X^*$  be two subsets. Then, the *annihilators* of  $M$  and  $N$  are defined by

$$M^\perp := \{x^* \in X^* \mid \forall x \in M : x^*(x) = 0\}$$

and

$$N_\perp := \{x \in X \mid \forall x^* \in N : x^*(x) = 0\}.$$

**Theorem 4.4** (Banach's closed range theorem [[Banach, 1932](#)]): Let  $X$  and  $Y$  be Banach spaces and  $T \in \mathcal{L}(X, Y)$ . Then, the following statements are equivalent:

1.  $\mathcal{R}(T)$  is closed in  $Y$ .
2.  $\mathcal{R}(T) = \mathcal{N}(T^*)_\perp$ .
3.  $\mathcal{R}(T^*)$  is closed in  $X^*$ .
4.  $\mathcal{R}(T^*) = \mathcal{N}(T)^\perp$ .

*Proof.* See [Yosida \[1980\]](#). □

**Theorem 4.5:**  $T_y$  as it given in (4.7) is a Fredholm operator with  $\text{ind}(T) = 0$ .

*Proof.* See [Hermann et al. \[1998\]](#). □

**Theorem 4.6** (Implicit Function Theorem): Let  $X, Y, Z$  be Banach spaces,  $U \subset X, V \subset Y$  be open subsets and  $T \in \mathbf{C}^p(U \times V, Z)$ ,  $p \geq 1$ . Moreover, let  $z_0 := (x_0, y_0) \in U \times V$  be such that  $T(z_0) = 0$  and let  $T_x(z_0)$  be a linear homeomorphism from  $X$  to  $Z$ . Then, there exist a neighborhood  $U_1 \times V_1 \subset U \times V$  of  $z_0$  and a function  $g \in \mathbf{C}^p(V_1, X)$  with  $g(y_0) = x_0$  and  $T(x, y) = 0$  for  $(x, y) \in U_1 \times V_1$  iff  $x = g(y)$ .

*Proof.* See [Zeidler \[1998\]](#). □

### 4.2.2. Lyapunov-Schmidt reduction

The Lyapunov-Schmidt reduction transforms the problem from the infinite-dimensional Banach space to the finite many solutions with real variables.

**Definition 4.7:** A solution  $(y_0, \lambda_0) \in \mathbb{X} \times \mathbb{R}$  of (4.3) is *simple*, if the derivative  $T'(y_0, \lambda_0) := (T_y^0 \ T_\lambda^0) \in \mathcal{L}(\mathbb{Z}, \mathbb{Y})$  fulfills the conditions

$$\dim(\mathcal{N}(T'(y_0, \lambda_0))) = 1 \text{ and } \mathcal{R}(T'(y_0, \lambda_0)) = \mathbb{Y}. \quad (4.9)$$

Consider the following

$$\begin{aligned} \begin{pmatrix} T_y^0 & T_\lambda^0 \end{pmatrix} \begin{pmatrix} w \\ \mu \end{pmatrix} = 0 &\implies T_y^0 w + T_\lambda^0 \mu = 0 \\ &\implies T_y^0 w = -T_\lambda^0 \mu. \end{aligned}$$

Thus,  $(y_0, \lambda_0) \in \mathbb{X} \times \mathbb{R}$  is a simple solution of (4.3) iff one of two possible situations, that exclude each other, occur:

1.  $T_\lambda^0 \in \mathcal{R}(T_y^0)$  "isolated solutions"

$$\begin{aligned} \implies T_y^0 w_1 &= -T_\lambda^0 \quad \text{with } \begin{pmatrix} w_1 \\ 1 \end{pmatrix} := \begin{pmatrix} w \\ \mu \end{pmatrix} \\ \implies \mathcal{N}(T_y^0) &= \{0\}. \end{aligned}$$

2.  $T_\lambda^0 \notin \mathcal{R}(T_y^0)$  "nonisolated solutions"

$$\begin{aligned} \implies \mu &= 0 \\ \implies \begin{pmatrix} w \\ \mu \end{pmatrix} &= \begin{pmatrix} w_2 \\ 0 \end{pmatrix} \quad \text{with } T_y^0 w_2 = 0 \\ \implies \mathcal{N}(T_y^0) &= \text{span}\{\varphi\}, \quad 0 \neq \varphi \in \mathbb{X}. \end{aligned}$$

In the first case, the Implicit Function Theorem 4.6 guarantees the existence of a unique solution curve  $\{y(\lambda), \lambda\}$  in the neighborhood of the isolated solutions.

A similar statement is true for nonisolated solutions. Let the null space  $\mathcal{N}(T_y^0)$  be spanned by a normalized function  $\varphi_0 \in \mathbb{X}_1$ ,  $\|\varphi_0\| = 1$ :

$$\mathcal{N}(T_y^0) = \text{span}\{\varphi_0\}. \quad (4.10)$$

Since  $\text{ind}(T_y^0) = 0$ , the dimension of the null space of the dual operator  $T_y^{0*} : \mathbb{Y}^* \rightarrow \mathbb{X}^*$  is also one:

$$\mathcal{N}(T_y^{0*}) = \text{span}(\psi_0^*), \quad (4.11)$$

where  $\psi_0^* \in \mathbb{Y}^*$ ,  $\|\psi_0^*\| = 1$ . From a corollary of the Hahn-Banach Theorem [Zeidler, 1998], we obtain

$$\exists \varphi_0^* \in \mathbb{X}^*, \psi_0 \in \mathbb{Y} \text{ with } \varphi_0^* \varphi_0 = 1 \text{ and } \psi_0^* \psi_0 = 1. \quad (4.12)$$

There exist the following decompositions of the spaces  $\mathbb{X}$  and  $\mathbb{Y}$ :

$$\begin{aligned} \mathbb{X} &= \text{span}\{\varphi_0\} \oplus \mathbb{X}_1 \\ &\text{with } \mathbb{X}_1 := \{y \in \mathbb{X} \mid \varphi_0^* y = 0\}. \end{aligned} \quad (4.13)$$

$$\begin{aligned} \mathbb{Y} &= \text{span}\{\psi_0\} \oplus \mathbb{Y}_1 \\ &\text{with } \mathbb{Y}_1 := \{z \in \mathbb{Y} \mid \psi_0^* z = 0\}. \end{aligned}$$

Additionally, the Fredholms Alternative applies:

$$\mathbb{Y}_1 = \mathcal{R}(T_y^0).$$

With this decomposition of the Banach spaces  $\mathbb{X}$  and  $\mathbb{Y}$ , the well-known Lyapunov-Schmidt reduction can be applied to the operator equation (4.3). The result can be used in the so called extended systems for computing turning points and bifurcation points. These techniques are described in the following sections.

Another important result of the Lyapunov-Schmidt reduction are certain coefficients, which characterize the type of bifurcations. The first one,  $c := \psi_0^* T_\lambda^0$ , is called the *characteristic coefficient*. It determines, whether the singularity is a turning point or a bifurcation point. In this thesis, the following bifurcations occur:

**Definition 4.8:** Let  $c \neq 0$ .

- A non-isolated solution  $(y_0, \lambda_0) \in \mathbb{X} \times \mathbb{R}$  of (4.3) is a *simple turning point* iff  $a_2 := \psi_0^* T_{yy}^0 \varphi_0^2 \neq 0$ .
- A non-isolated solution  $(y_0, \lambda_0) \in \mathbb{X} \times \mathbb{R}$  of (4.3) is a *double turning point* iff  $a_2 = 0$  and  $a_3 := \psi_0^* (6T_{yy}^0 \varphi_0 w_0 + T_{yyy}^0 \varphi_0^3) \neq 0$ , where  $w_0 \in \mathbb{X}_1$  such that  $T_y^0 w_0 = -\frac{1}{2} T_{yy}^0 \varphi_0^2$ .

**Definition 4.9:** Let  $c = 0$ .

- A non-isolated solution  $(y_0, \lambda_0) \in \mathbb{X} \times \mathbb{R}$  of (4.3) is *transcritical (asymmetric) bifurcation point* iff  $a_2 \neq 0$ .
- A non-isolated solution  $(y_0, \lambda_0) \in \mathbb{X} \times \mathbb{R}$  of (4.3) is *pitchfork (symmetric) bifurcation point* iff  $a_2 = 0$  and  $a_3 \neq 0$ .

A general classification of singular points can be found e.g. in Ikeda & Murota [2002].

### 4.2.3. Simple turning points

The computation of simple turning points is based on the following extension  $\tilde{T}$  of the operator  $T : \mathbb{X} \times \mathbb{R} \rightarrow \mathbb{Y}$ :

$$\tilde{T} : \begin{cases} \tilde{\mathbb{Z}} := \mathbb{X} \times \mathbb{R} \times \mathbb{X} \rightarrow \tilde{\mathbb{Y}} := \mathbb{Y} \times \mathbb{Y} \times \mathbb{R} \\ \tilde{z} := (z, \varphi_0) := (y, \lambda, \varphi_0) \mapsto \begin{bmatrix} T(y, \lambda) \\ T_y(y, \lambda) \cdot \varphi_0 \\ \varphi_0^* \varphi_0 - 1 \end{bmatrix} \end{cases} \quad (4.14)$$

This extended operator can be transformed into a boundary value problem in several ways. The classical approach has the dimension of  $2n + 1$ , e.g. Keener & Keller [1973]; Moore & Spence [1980]; Wallisch & Hermann [1987]:

$$\begin{aligned} \dot{y} &= f(t, y; \lambda) & r(y(a), y(b); \lambda) &= 0, \\ \dot{\varphi}_0 &= f_y(t, y; \lambda) \varphi_0 & \mathcal{B}_a \varphi_0(a) + \mathcal{B}_b \varphi_0(b) &= 0, \\ \dot{\lambda} &= 0 & \varphi_0(a)^T \varphi_0(a) &= 1, \end{aligned} \quad (4.15)$$

where  $\mathcal{B}_a := r_{y(a)}(y(a), y(b); \lambda)$  and  $\mathcal{B}_b := r_{y(b)}(y(a), y(b); \lambda)$  are the derivatives of the boundary condition vector  $r$ .

### 4.2.4. Double turning points

Double turning points can only occur in the two-parameter systems:

$$\begin{aligned} \tilde{T}(y, \lambda, \tau) &= 0, \\ \tilde{T} : \mathbb{X} \times \mathbb{R} \times \mathbb{R} &\rightarrow \mathbb{Y}. \end{aligned} \quad (4.16)$$

For the computation of double turning points, the operator  $\tilde{T}$  must be extended in the following way [Roose & Piessens, 1985]:

$$\widehat{T} : \left\{ \begin{array}{l} \widehat{\mathbb{Z}} := \mathbb{X} \times \mathbb{R} \times \mathbb{R} \times \mathbb{R} \times \mathbb{X} \times \mathbb{Y}^* \rightarrow \widehat{\mathbb{Y}} := \mathbb{Y} \times \mathbb{Y} \times \mathbb{X}^* \times \mathbb{R} \times \mathbb{R} \times \mathbb{R} \\ \widehat{z} := (y, \lambda, \tau, \mu, \varphi_0, \psi_0^*) \mapsto \begin{bmatrix} \tilde{T}(y, \lambda, \tau) \\ \tilde{T}_y(y, \lambda, \tau)\varphi_0 \\ \tilde{T}_y^*(y, \mu, \tau)\psi_0^* \\ \varphi_0^*\varphi_0 - 1 \\ \psi_0^*\psi_0 - 1 \\ \psi_0^*\tilde{T}_{yy}(y, \lambda, \tau)\varphi_0^2 \end{bmatrix} \end{array} \right. \quad (4.17)$$

The resulting boundary value problem has dimension  $3n + 4$ :

$$\begin{aligned} \dot{y} &= f(t, y; \lambda, \tau) & r(y(a), y(b); \lambda, \tau) &= 0, \\ \dot{\varphi}_0 &= f_y(t, y; \lambda, \tau)\varphi_0 & \mathcal{B}_a(\lambda)\varphi_0(a) + \mathcal{B}_b(\lambda)\varphi_0(b) &= 0, \\ \dot{\psi}_0 &= -(f_y(t, y; \mu, \tau))^T \psi_0 & \mathcal{B}_a^*(\mu)\psi_0(a) + \mathcal{B}_b^*(\mu)\psi_0(b) &= 0, \\ \dot{\xi}_0 &= \psi_0^T (f_{yy}(t, y; \lambda, \tau)\varphi_0^2) & \psi_0(a)^T (\mathcal{B}_{aa}(\lambda)\varphi_0^2(a) + 2\mathcal{B}_{ab}(\lambda)\varphi_0(a)\varphi_0(b) + \mathcal{B}_{bb}(\lambda)\varphi_0^2(b)) &= 0, \\ \dot{\lambda} &= 0 & \xi_0(a)^T \xi_0(a) &= 0, \\ \dot{\mu} &= 0 & \varphi_0(a)^T \varphi_0(a) &= 1, \\ \dot{\tau} &= 0 & \psi_0(a)^T \psi_0(a) &= 1. \end{aligned} \quad (4.18)$$

The matrices  $\mathcal{B}_a(\lambda) := r_{y(a)}(y(a), y(b); \lambda)$  and  $\mathcal{B}_b(\lambda) := r_{y(b)}(y(a), y(b); \lambda)$  are derivatives of the boundary function  $r$ . The matrices  $\mathcal{B}_a^*(\mu)$  and  $\mathcal{B}_b^*(\mu)$  are adjoint to the derivatives  $\mathcal{B}_a(\mu) := r_{y(a)}(y(a), y(b); \mu)$ ,  $\mathcal{B}_b(\mu) := r_{y(b)}(y(a), y(b); \mu)$ , i.e. they must fulfill relation (4.25). The matrices  $\mathcal{B}_{aa}$ ,  $\mathcal{B}_{ab}$  and  $\mathcal{B}_{bb}$  are the corresponding second derivatives of  $r$ .

#### 4.2.5. Secondary bifurcation points

In this thesis, we describe two general approaches for the computation of secondary bifurcation points. Both are based on the theorem of Crandall & Rabinowitz [1971]. The approach of Weber [1979, 1981] has larger dimension, whereas the approach of Moore [1980] requires the computation of adjointed matrices.

**Definition 4.10:** [Beyn, 1980]  $(y_0, \lambda_0) \in \mathbb{X} \times \mathbb{R}$  is a *hyperbolic point* of the operator  $T$  iff:

- (i)  $T(y_0, \lambda_0) = 0$ ,
- (ii)  $\dim(\mathcal{N}(T'(y_0, \lambda_0))) = 2$ ,  $\text{codim}(\mathcal{R}(T'(y_0, \lambda_0))) = 1$ ,
- (iii)  $\tau := \alpha\gamma - \beta^2 < 0$ .

Here,  $\alpha, \beta, \gamma \in \mathbb{R}$  are defined by

$$\begin{aligned}\alpha &:= \psi_0^* T'''(y_0, \lambda_0) p^2, \\ \beta &:= \psi_0^* T''(y_0, \lambda_0) p q, \\ \gamma &:= \psi_0^* T''(y_0, \lambda_0) q^2\end{aligned}$$

with  $p, q \in \mathbb{X}$  such that

$$\text{span}\{p, q\} = \mathcal{N}(T'(y_0, \lambda_0))$$

and  $\psi_0^* \in \mathbb{Y}^*$  such that

$$\mathcal{N}(\psi_0^*) = \mathcal{R}(T'(y_0, \lambda_0)).$$

### Approach of Weber

Let  $(y_0, \lambda_0) \in \mathbb{X} \times \mathbb{R}$  be a hyperbolic point. Additionally, let

$$T_\lambda(y_0, \lambda_0) \in \mathcal{R}(T_y(y_0, \lambda_0)). \quad (4.19)$$

For the null space of  $T'(y_0, \lambda_0)$ , the following is true

$$\mathcal{N}(T'(y_0, \lambda_0)) = \text{span}\{p, q\}, \quad p, q \in \mathbb{Z},$$

with  $p = (p_1, p_2)^T$ ,  $q = (q_1, q_2)^T$ , such that  $p_1, q_1 \in \mathbb{X}$ ,  $p_2, q_2 \in \mathbb{R}$ . If  $\varphi_0^* \in \mathbb{X}^*$  is a suitable linear functional, then  $p$  and  $q$  are unique (up to the sign) with  $p = (\varphi_0, 0)$ ,  $q = (s_0, 1)$  such that  $\varphi_0, s_0 \in \mathbb{X}$ ,  $\varphi_0^* \varphi_0 = 1$  and  $\varphi_0^* s_0 = 0$ . Moreover, let  $0 \neq \psi_0 \in \mathbb{Y}$  be such that

$$\psi_0^* \psi_0 \neq 0. \quad (4.20)$$

The operator  $T$  can now be extended in the following way:

$$\tilde{T} : \begin{cases} \tilde{\mathbb{Z}} := \mathbb{X} \times \mathbb{R} \times \mathbb{X} \times \mathbb{X} \times \mathbb{R} \rightarrow \tilde{\mathbb{Y}} := \mathbb{Y} \times \mathbb{Y} \times \mathbb{Y} \times \mathbb{R} \times \mathbb{R} \\ \tilde{z} := (y, \lambda, \varphi_0, s, \mu) \mapsto \begin{bmatrix} T(y, \lambda) + \mu \psi_0 \\ T_y(y, \lambda) \varphi_0 \\ T_y(y, \lambda) s + T_\lambda(y, \lambda) \\ \varphi_0^* \varphi_0 - 1 \\ \varphi_0^* s \end{bmatrix} \end{cases} \quad (4.21)$$

with the functional  $\varphi_0^* \in \mathbb{X}^*$  such that  $\varphi_0^* \varphi_0 = 1$ . The corresponding boundary value problem has dimension  $3n + 2$ :

$$\begin{aligned}\dot{y} &= f(t, y; \lambda) - \mu \psi_0 & \mathcal{B}_a y(a) + \mathcal{B}_b y(b) &= 0, \\ \dot{\varphi}_0 &= f_y(t, y; \lambda) \varphi_0 & \mathcal{B}_a \varphi_0(a) + \mathcal{B}_b \varphi_0(b) &= 0, \\ \dot{s} &= f_y(t, y; \mu) s + f_\lambda(t, y; \lambda) & \mathcal{B}_a s(a) + \mathcal{B}_b s(b) + \mathcal{B}_\lambda &= 0, \\ \dot{\lambda} &= 0 & \varphi_0(0)^T \varphi_0(0) &= 1, \\ \dot{\mu} &= 0 & \varphi_0(0)^T s(0) &= 0,\end{aligned} \quad (4.22)$$



where  $\mathcal{B}_\lambda$  is the derivative  $r_{\lambda(a)}(y(a), y(b); \lambda)$ . Since the boundary value problem (4.22) is self-adjoint, the functional  $\psi_0$  can be chosen as  $\psi_0 := \varphi_0$  as suggested in Wallisch & Hermann [1987].

### Approach of Moore

This technique is a modification of the approach of Weber. It has dimension  $2n + 2$ , which is smaller, but it requires the computation of adjointed matrices, which could be expensive for high-dimensional systems. The extended operator  $\widehat{T}$  of  $T$  is then

$$\widehat{T} : \begin{cases} \widehat{\mathbb{Z}} := \mathbb{X} \times \mathbb{R} \times \mathbb{Y}^* \times \mathbb{R} \rightarrow \widehat{\mathbb{Y}} := \mathbb{Y} \times \mathbb{X}^* \times \mathbb{R} \times \mathbb{R} \\ \widehat{z} := (y, \lambda, \psi_0^*, \mu) \mapsto \begin{bmatrix} T(y, \lambda) + \mu\psi_0 \\ T_y^*(y, \lambda)\psi_0^* \\ \psi_0^* T_\lambda(y, \lambda) \\ \psi_0^* \psi_0 - 1 \end{bmatrix} \end{cases} \quad (4.23)$$

The corresponding boundary value problem is then:

$$\begin{aligned} \dot{y} &= f(t, y; \lambda) - \mu\psi_0 & \mathcal{B}_a y(a) + \mathcal{B}_b y(b) &= 0, \\ \dot{\psi}_0^* &= -f_y^T(t, y; \lambda)\psi_0^* & \mathcal{B}_a^* \psi_0^*(a) + \mathcal{B}_b^* \psi_0^*(b) &= 0, \\ \xi_0 &= -\psi_0^* f_\lambda(t, y; \lambda) & \xi_0^T(a)\xi_0(b) &= 1 \\ \dot{\lambda} &= 0 & \psi_0^*(a)^T \mathcal{B}_\lambda &= 0, \\ \dot{\mu} &= 0 & \psi_0^*(a)^T \psi_0^*(a) &= 1. \end{aligned} \quad (4.24)$$

The matrices  $\mathcal{B}_a^*$  and  $\mathcal{B}_b^*$  are adjoint to the derivatives  $\mathcal{B}_a$  and  $\mathcal{B}_b$ , i.e. they must fulfill the relation

$$\mathcal{B}_a^* \mathcal{B}_a^T - \mathcal{B}_b^* \mathcal{B}_b^T = 0, \quad \text{rank}[\mathcal{B}_a^* \ \mathcal{B}_b^*] = n. \quad (4.25)$$

### 4.2.6. Continuation

Numerical continuation (or path following) is a technique to trace solution curves of parametrized systems of equations. Combined with a boundary value problem solver, the path following is a powerful tool for investigation of dynamical systems from different fields of science. The probably most prominent example is the pseudo-arclength continuation by Keller [1978], which also allows the path following past a turning point. In this thesis, the simple and efficient predictor-corrector continuation from Seydel [1984] is used, which is implemented in the RWPM package [Hermann & Ullrich, 1992]. The predictor step is realized as the secant to the solution branch. The corrector consists of the application of the shooting method to a transformed boundary value problem as described in Hermann & Ullrich [1992].

### 4.3. Bifurcations in the spring-mass model

The following techniques of handling bifurcations are based on the well-known Lyapunov-Schmidt reduction [Marx & Vogt, 2011; Wallisch & Hermann, 1987; Zeidler, 1998]. Consider the equation

$$T(z, \lambda) = \begin{pmatrix} \dot{z} - f(z(\tau)) \\ r(z(0), z(1); \lambda) \end{pmatrix} = 0,$$

where  $T : \mathbb{R}^n \times \mathbb{R} \rightarrow \mathbb{R}^n \times \mathbb{R}^n$  is a twice continuously differentiable operator and  $\tau \in [0, 1]$ . The functions  $f : \mathbb{R}^n \rightarrow \mathbb{R}^n$  and  $r : \mathbb{R}^n \times \mathbb{R}^n \times \mathbb{R} \rightarrow \mathbb{R}^n$  are defined in Table 3.1 for running and in Table 3.2 for walking. The Fréchet derivative  $T_z(z, \lambda)$  of the operator  $T$  is a Fredholm operator of index zero. Furthermore, let us assume that the one-dimensional null space  $\mathcal{N}(T_z)$  of  $T_z$  is spanned by the function  $\varphi_0$  with  $\|\varphi_0\| = 1$  and let the null space  $\mathcal{N}(T_z^*)$  of the adjointed operator  $T_z^*$  be spanned by  $\psi_0$  with  $\|\psi_0\| = 1$ .

In the following, the angle of attack  $\alpha_0$  is considered as the control (or bifurcation) parameter, i.e. we set  $\lambda := \alpha_0$ . Note that  $\alpha_0$  does not appear in the definition of the function  $f$ .

#### 4.3.1. Simple turning point

To find a simple turning point, we use the classical approach, as described by several authors, e.g. Keener & Keller [1973]; Moore & Spence [1980]; Wallisch & Hermann [1987]. It requires the extension of the original system by linearization of the function  $f$ . Keeping in mind, that the bifurcation parameter  $\alpha_0$  does not occur in  $f$ , the extended system (4.15) then is

$$\begin{aligned} \dot{z} &= f(z) & r(z(0), z(1); \alpha_0) &= 0, \\ \dot{\varphi}_0 &= f_z(z)\varphi_0 & B_0\varphi_0(0) + B_1\varphi_0(1) &= 0, \\ \dot{\alpha}_0 &= 0 & \varphi_0(0)^T \varphi_0(0) &= 1, \end{aligned} \tag{4.26}$$

where  $B_0 := r_{z(0)}(z(0), z(1); \alpha_0)$  and  $B_1 := r_{z(1)}(z(0), z(1); \alpha_0)$  are the derivatives of the vector  $r$ . The resulting extended boundary value problem has dimension  $2n + 1$ .

### 4.3.2. Transcritical bifurcation

Using the approach of Weber (Section 4.2.5), we obtain the following boundary value problem with dimension  $3n + 4$ :

$$\begin{aligned}
\dot{z} &= f(z) + \mu\psi_0 & r(z(0), z(1); \alpha_0) + \mu\varphi_0(0) &= 0, \\
\dot{\varphi}_0 &= f_z(z)\varphi_0 & B_0\varphi_0(0) + B_1\varphi_0(1) &= 0, \\
\dot{s} &= f_z(z)s & B_0s(0) + B_1s(1) + B_\alpha &= 0, \\
\dot{\mu} &= 0 & \varphi_0(0)^T\varphi_0(0) &= 1, \\
\dot{\alpha}_0 &= 0 & \varphi_0(0)^T s(0) &= 0.
\end{aligned} \tag{4.27}$$

Again,  $B_0 := r_{z(0)}(z(0), z(1); \alpha_0)$ ,  $B_1 := r_{z(1)}(z(0), z(1); \alpha_0)$  and  $B_\alpha := r_{\alpha_0}(z(0), z(1); \alpha_0)$  are the derivatives of the vector  $r$ .

Using the approach of Moore (Section 4.2.5), the dimension of the extended boundary value problem is reduced to  $2n + 2$ , but additionally the adjointed matrices  $B_0^*$  and  $B_1^*$  have to be computed. This can be very time-consuming for high-dimensional systems. As mentioned above, the parameter  $\alpha_0$  only occurs in the boundary function  $r$  (Tables 3.1 and 3.2). The extended system in this case is

$$\begin{aligned}
\dot{z} &= f(z) + \mu\psi & r(z(0), z(1); \alpha_0) + \mu\psi(0) &= 0, \\
\dot{\psi} &= -f_z^T(z)\psi & B_0^*\psi(0) + B_1^*\psi(1) &= 0, \\
\dot{\mu} &= 0 & \psi(0)^T B_\alpha &= 0, \\
\dot{\alpha}_0 &= 0 & \psi(0)^T \psi(0) &= 1,
\end{aligned} \tag{4.28}$$

where  $B_\alpha$  is the derivative  $r_{\alpha_0(0)}(z(0), z(1); \alpha_0)$ . The matrices  $B_0^*$  and  $B_1^*$  are adjoint to the derivatives  $B_0$  and  $B_1$ , i.e. they must fulfill the relation

$$B_0^* B_0^T - B_1^* B_1^T = 0, \quad \text{rank}[B_0^* \ B_1^*] = n. \tag{4.29}$$

The matrices  $B_0^*$  and  $B_1^*$  are determined using the symbolic  $QR$  decomposition of the matrix  $[B_0 \ B_1]^T$  via Givens transformations [Hermann, 2011; Stoer & Bulirsch, 1993] and then inserted into the boundary value problem (4.28) (see Appendix A).

### 4.3.3. Period-doubling bifurcation

Period-doubling bifurcation points can be calculated indirectly, since they are invisible for period-one solutions. Here, exactly one of the two Floquet multipliers must be equal to -1. Therefore, the calculation of the bifurcation point can be reduced to the search of the point, where exactly one

Floquet multiplier equals -1. This approach can also be applied for investigation of the asymmetric model (see Discussion and Chapter 2). For example, one asymmetric double step may comprise two subsequent single steps with two different angles of attack  $\alpha_1 \neq \alpha_2$  (Chapter 2).

First, we have to modify the functions  $f$  and  $r$  in Section 3.4.3. The additional equations can easily be understood using Table 3.2 and Figure 3.7. To find periodic solutions, the boundary functions  $r_2, r_3$  and  $r_4$  have to be changed similar to equation (3.14):

$$\begin{aligned}\hat{r}_2 &= m(z_2(0)^2 + z_4(0)^2) - 2E_0 + 2mgz_3(0) + k_0(L_0 - z_3(0))^2, \\ \hat{r}_3 &= z_3(0) - z_{25}(1), \\ \hat{r}_4 &= \arctan\left(\frac{z_4(0)}{z_2(0)}\right) - \arctan\left(\frac{z_{26}(1)}{z_{24}(1)}\right).\end{aligned}\tag{4.30}$$

In this case, the dimension of the boundary value problem (3.12) is  $n = 27$ , and by using the method of Moore (Section 4.2.5, [Moore & Spence, 1980]), we get the desired bifurcation point.

#### 4.3.4. Hopf bifurcation

Hopf bifurcations [Hopf, 1942; Marsden & McCracken, 1976] can be found using the appropriate numerical continuation, e.g. Gross & Feudel [2004]. Here, we compute them indirectly, since they are not visible in the real plane. We use the original model (Section 3.2) and search for points with two complex-conjugate Floquet multipliers of magnitude one. Perturbations, like leg asymmetry, have no destroying effect on Hopf bifurcations (Chapter 2).

#### 4.3.5. Double turning point

In this thesis, double turning points are computed using the secant-predictor continuation (Section 4.2.6, [Jepson & Spence, 1985]). However, it is also possible to find these points directly using the modified extended system (4.18). The resulting boundary value problem has the dimen-

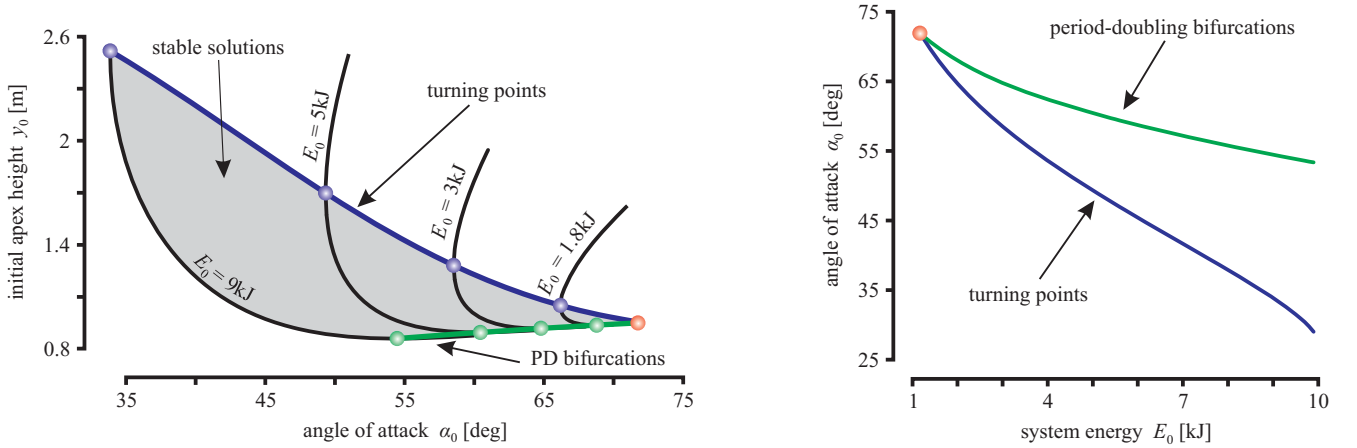
sion  $3n + 4$ :

$$\begin{aligned}
\dot{z} &= f(z; \tau) & r(z(0), z(1); \alpha_0, \tau) &= 0, \\
\dot{\varphi}_0 &= f_z(z; \tau)\varphi_0 & B_0(\alpha_0)\varphi_0(0) + B_1(\alpha_0)\varphi_0(1) &= 0, \\
\dot{\psi}_0 &= -f_z^T(z; \tau)\psi_0 & B_0^*(\mu)\psi_0(0) + B_1^*(\mu)\psi_0(1) &= 0, \\
\dot{\xi}_0 &= \psi_0^T (f_{zz}(z; \tau)\varphi_0^2) & \psi_0(0)^T (B_{00}(\alpha_0)\varphi_0^2(0) + 2B_{01}(\alpha_0)\varphi_0(0)\varphi_0(1) + B_{11}(\alpha_0)\varphi_0^2(1)) &= 0, \\
\dot{\alpha}_0 &= 0 & \xi_0(0)^T \xi_0(1) &= 0, \\
\dot{\mu} &= 0 & \varphi_0(0)^T \varphi_0(0) &= 1, \\
\dot{\tau} &= 0 & \psi_0(0)^T \psi_0(0) &= 1.
\end{aligned} \tag{4.31}$$

Like in previous cases, the first bifurcation parameter is the angle of attack  $\alpha_0$ . Depending on the bifurcation problem, the second bifurcation parameter  $\tau$  is either system energy  $E_0$  (Figure 4.2) or an asymmetry parameter (figures 5.6 and 5.7). The matrices  $B_0(\alpha_0) := r_{z(0)}(z(0), z(1); \alpha_0)$  and  $B_1(\alpha_0) := r_{z(1)}(z(0), z(1); \alpha_0)$  are defined as above. The matrices  $B_0^*$  and  $B_1^*$  are adjoint to the derivatives  $B_0(\mu) := r_{z(0)}(z(0), z(1); \mu)$ ,  $B_1(\mu) := r_{z(1)}(z(0), z(1); \mu)$ , i.e. they must fulfill relation (4.29).

### 4.3.6. Implementation

Both, the original and transformed spring-mass model are implemented in MATLAB (version R2011a, The MathWorks Inc., Natick, MA, USA). All boundary value problems in this study are solved using the latest version of the boundary value problem solver RWPM [Hermann & Kaiser, 1993]. This package uses standard simple and multiple shooting methods for the computation of boundary value problems [Hermann, 2004; Stoer & Bulirsch, 1993]. The associated initial value problems are solved using the MATLAB solver ode45 [Shampine & Reichelt, 1997]. The MATLAB function `fsolve` from the Optimization Toolbox is then applied to find the zeros of the system of non-linear equations. All these calculations are done with an absolute and relative tolerance of  $10^{-8}$ . All periodic solutions and extended systems are calculated using the simple shooting method. All required derivatives of the functions  $f$  and  $r$ , as well as the  $QR$  decomposition to compute the adjointed matrices (Appendix A) are calculated using the Symbolic Math Toolbox of MATLAB.



(a) Initial apex height  $y_0$  of periodic running solutions dependent on the angle of attack  $\alpha_0$  for different values of the system energy  $E_0$ . The grey region represents stable periodic solutions. The blue line consists of simple turning points. The green one is the curve of period-doubling bifurcations.

(b) Projection of the curve of simple turning points (blue) and the curve of period-doubling bifurcations (green) from (a) onto the plane  $(E_0, \alpha_0)$ . The red dot is the intersection of both curves at  $E_0 = 1.14\text{kJ}$ .

**Figure 4.1.** Manifold of stable solutions of the spring-mass model for running

## 4.4. Results

### 4.4.1. Running

As shown in the previous chapter, the region of symmetric stable solutions is located between a simple turning point and a period-doubling bifurcation point (Figure 3.5). Using the extended systems (4.26) and (4.30), it is now possible to compute the complete manifold of stable periodic solutions of the spring-mass model (Figure 4.1(a)). It is confined between the curve of the turning points and the curve of the period-doubling bifurcations. Periodic stable solutions exist for the system energy between  $E_0 = 1100\text{J}$  and  $9900\text{J}$  (Figure 4.1(b)). Both curves are computed using the secant-predictor continuation [Hermann & Ullrich, 1992; Seydel, 1984] with system energy  $E_0$  as the second bifurcation parameter.

In Chapter 5, we investigate the size of the region where locomotion is stable. Like in Chapter 2, we define the continuous range of stable solutions  $\Delta\alpha = \alpha_{\max} - \alpha_{\min}$  and call it the  $\alpha$ -range. The symmetric model exhibits an  $\alpha$ -range of  $\Delta\alpha = 2.7^\circ$ , which provides a reference for investigations of the asymmetric model in Chapter 5.

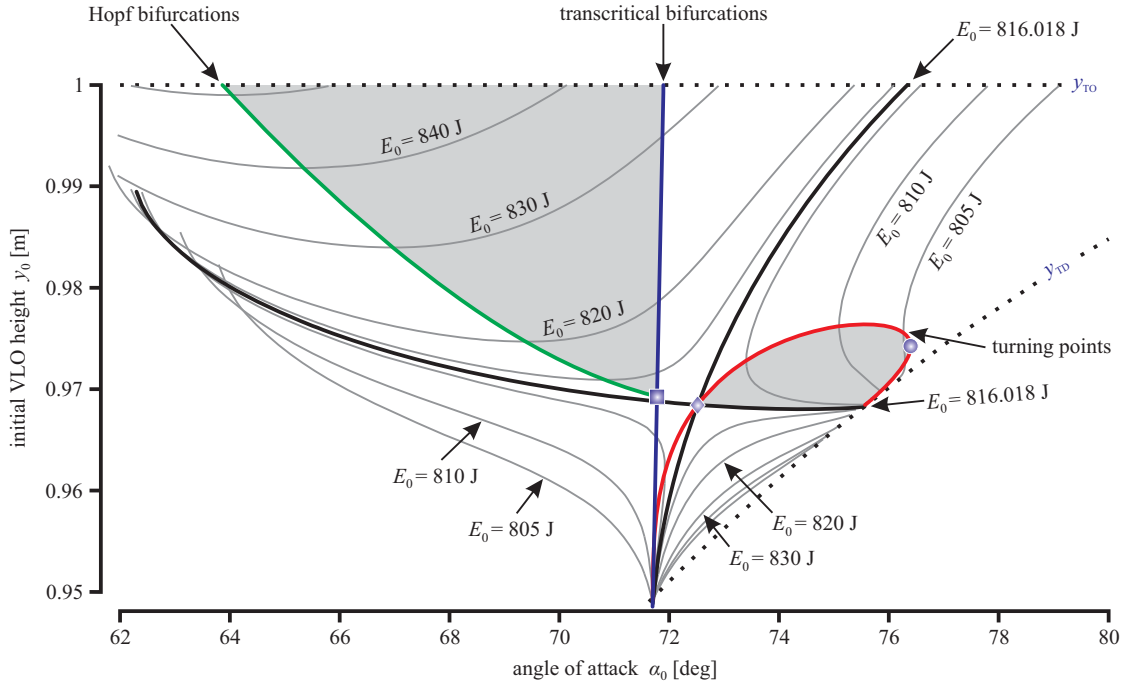


**Figure 4.2.** Initial VLO height  $y_0$  of periodic walking patterns dependent on the angle of attack  $\alpha_0$  for different values of the system energy  $E_0$  (grey lines). For reasons of clarity, patterns with  $\theta_0 \neq 0$ , e.g. Branch B in Figure 3.7, are omitted. The solid black curves represent periodic solutions for  $E_0 = 816.018$  J, i.e. for the value of the system energy where a unique two-parameter bifurcation occurs (diamond). The green line is the curve of Hopf bifurcations, the blue one is the curve of transcritical bifurcations, and the red one is the curve of simple turning points. The intersection of the curves of transcritical and Hopf bifurcations at  $E_0 = 815.963$  J and  $\alpha_0 = 71.824^\circ$  is marked by the square. The circle at  $E_0 = 804.295$  J and  $\alpha_0 = 76.397^\circ$  is the double turning point. The grey areas indicate regions of stable periodic solutions. See also Figure 4.3.

## 4.4.2. Walking

### Simple turning points and transcritical bifurcations

Figure 4.2 shows curves of simple turning points and transcritical bifurcations computed for different values of system energy  $E_0$  using the extended systems (4.26) and (4.28). For reasons of clarity, the curves of walking patterns with non-zero velocity angle  $\theta_0$  at VLO, e.g. branch B in Figure 3.7, are not displayed. These branches are extensively described and discussed in Rummel et al. [2010b]. We also refer to Section 2.4.1 and Figure 2.6.

Simple turning points are common in the bipedal spring-mass model (Figure 3.7). For values of  $E_0$  between 804.295 J and 816.018 J, they enclose the area of stable solutions (Figure 4.2).

Transcritical bifurcation points connect branches with two different kinds of periodic patterns (Figure 3.7). Moreover, for the system energy  $E_0$  larger than 815.983 J, the regions of stable walking gaits are located between the curve of Hopf bifurcations and the curve of transcritical

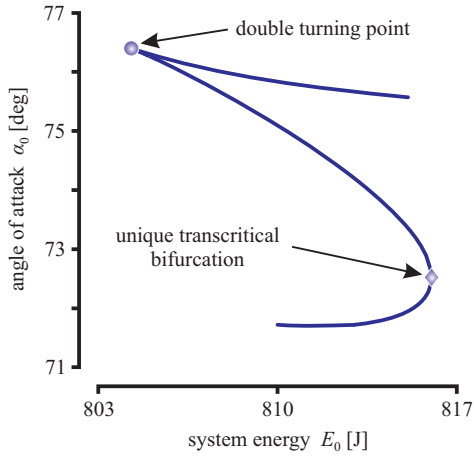


**Figure 4.3.** Projection of the curve of simple turning points from Figure 4.2 onto the plane  $(E_0, \alpha_0)$ . Here and in Figure 4.2, the diamond at  $E_0 = 816.018$  J and  $\alpha_0 = 72.520^\circ$  represents the unique two-parameter transcritical bifurcation point. The circle at  $E_0 = 804.295$  J and  $\alpha_0 = 76.397^\circ$  is the cusp point corresponding to the double turning point in Figure 4.2.

bifurcations (grey areas in Figure 4.2).

Additionally to the angle of attack  $\alpha_0$ , we consider the system energy  $E_0$  as the second bifurcation parameter. Using the secant-predictor continuation [Hermann & Ullrich, 1992; Seydel, 1984] for the system of equations (4.26), we obtain the curve of simple turning points and two two-parameter bifurcation points: a unique transcritical bifurcation at  $E_0 = 816.018$  J and  $\alpha_0 = 72.520^\circ$  (diamonds in Figure 4.2 and Figure 4.3) and the double turning point at  $E_0 = 804.295$  J and  $\alpha_0 = 76.397^\circ$  (circles in Figure 4.2 and Figure 4.3).

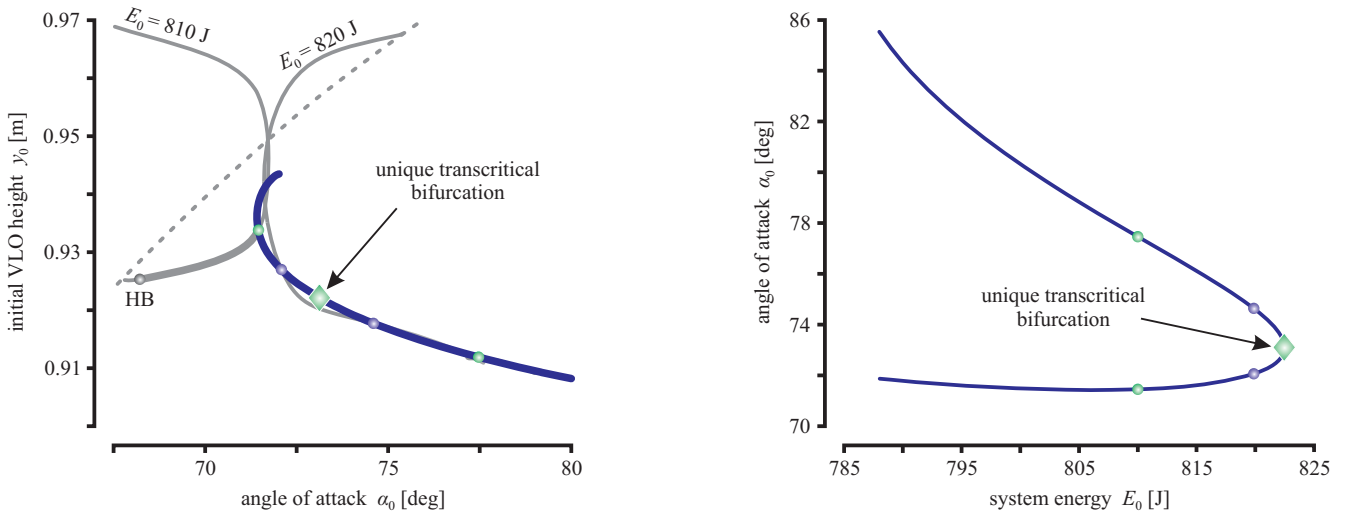
### Period-doubling bifurcations

The first group of two period-doubling bifurcation points is located between  $\alpha_0 = 60^\circ$  and  $63^\circ$  (Figure 3.7). Since they are located away from the region of stable solutions, any further discussion of these points is omitted.

The solution diagram under the touch-down line  $y_{TD} = L_0 \sin(\alpha_0)$ , where another two period-doubling bifurcation points are found, is very complex. As shown above, the curvature at turning points is changed at  $E_0 = 816.018$  J (Figure 4.2). Moreover, the continuous curve of periodic solutions splits in two distinct curves for  $E_0 < 819.2$  J. To avoid confusion, we present only two examples with period-doubling bifurcation points limiting the region of stable periodic solutions (Figure 3.9) and the curve of period-doubling bifurcations (Figure 4.4).

For the system energy  $E_0 = 820$  J, the stable region is confined between the period-doubling bifurcations at  $\alpha_0 = 72.081^\circ$  and  $\alpha_0 = 74.595^\circ$  (Figure 4.4(a)). For  $E_0 = 810$  J, there exist two distinct curves of periodic solutions. In this case, stable solutions lie between the period-doubling bifurcation at  $\alpha_0 = 71.454^\circ$  and the Hopf bifurcation at  $\alpha_0 = 68.209^\circ$ . Stable solutions exist until two period-doubling bifurcations merge (Figure 4.4(b)). Using the continuation, we obtain the unique transcritical bifurcation point at  $E_0 = 822.483$  J and  $\alpha_0 = 73.091^\circ$ .





(a) Period-doubling bifurcations (blue curve) connecting branches of periodic grounded running solutions. Solid grey lines are initial VLO height of grounded running solutions for  $E_0 = 810$  J and  $E_0 = 820$  J (compare Figure 3.9). The grey dot is a Hopf bifurcation. The diamond at  $E_0 = 822.483$  J and  $\alpha_0 = 73.091^\circ$  is a unique transcritical bifurcation point.

(b) Projection of the curve of period-doubling bifurcations onto the plain  $(E_0, \alpha_0)$ . The diamond at  $E_0 = 822.483$  J and  $\alpha_0 = 73.091^\circ$  represents the unique two-parameter transcritical bifurcation point. The green and blue points represent period-doubling bifurcations for  $E_0 = 810$  J and  $E_0 = 820$  J, respectively.

Figure 4.4. Grounded running

## 4.5. Discussion

In this chapter, we have presented a new computational approach for studying bifurcations in the bipedal spring-mass model. We used the technique of extended systems to find simple turning points and secondary bifurcation points. We have demonstrated that the investigation of the region of the stable solutions can be reduced to the calculation of its boundaries. Omitting the calculation of the periodic solutions between the bifurcations results in considerable benefits for computation time.

Using the technique of extended systems, it was possible to compute the complete manifold of periodic running solutions (Figure 4.1). Here, all stable solutions are located between the curve of simple turning points and the curve of period-doubling bifurcations. In Chapter 5, this approach will be extended for the analysis of the stability regions of the asymmetric spring-mass model.

The diagram of stable solutions of the bipedal model is much more complex. Here, we have presented only part of the solution manifold, which has some biological relevance (Figure 4.2). In this chapter, we have also presented stable grounded running solutions limited by period-doubling bifurcations (Figure 4.4). Grounded running may be considered as running without flight phases

[Andrada et al., 2012]. It is often observed in avian locomotion and may also correspond to human jogging. Since grounded running also serves as an intermediate step between walking and running [Martínez & Carbajal, 2011; Rummel et al., 2009], the calculation of these period-doubling bifurcations is helpful for investigations of gait transitions.

Like in case of periodic solutions, the simple shooting method is sufficient for the computation of all bifurcations. We use the periodic solution next to the bifurcation as the initial guess for the first  $n$  equations of an extended system and a suitable approximation of the desired parameter value. For all remaining equations in these three systems, it is adequate to use some trivial initial values like a vector filled with ones.

The approaches for calculation of bifurcations in the asymmetric model or period-doubling bifurcations in the symmetric one may lead to large systems of equations. For instance,  $2n + 2$  equations are required for the computation of a secondary bifurcation point by the boundary value problem (4.28), where  $n$  is the dimension of the vector-function  $f$ . Using the functions  $f$  and  $r$  for the period-2 solutions with asymmetric leg parameters, we would obtain an extended system of dimension 56, similar to the case of period-doubling bifurcations. To reduce the number of equations, the techniques of minimal systems may be applied [Allgower & Schwetlick, 1997]. Using minimal systems, the number of equations can be reduced to  $n + 2$ , which would provide a significant benefit regarding computation time. A similar approach also exists for the calculation of simple turning points [Pönisch & Schwetlick, 1981]. Here, the dimension of the extended boundary value problem is  $n + 1$ .

# 5. Stable running with asymmetric legs

## 5.1. Introduction

An approach towards describing asymmetric walking based on a minimalistic gait model was presented in Chapter 2. In particular, it is shown that considerable discrepancies between contralateral leg angles can be tolerated and may even stabilize unstable solutions of the symmetric model. While some general descriptions and features can be directly transferred to running, there are also some differences. During walking, unilateral amputees use the intact leg more extensively [Schaarschmidt et al., 2012]. Thus, the contact phases of the prosthetic limb are shorter. This happens because the amputees do not fully trust in the leg functionality of the artificial legs. During running, the existence of flight phases requires a greater reliability of the prosthesis, which must endure the full load of impact, when the touch-down happens. While the asymmetry in walking gaits is most visible for lower speeds [Goble et al., 2003; Nolan et al., 2003], there are reports that the gait asymmetry in running gaits increases with the growing speed [Burkett et al., 2003; Prince et al., 1992]. However, the development of new technologies and materials supports the design of new prostheses (e.g. carbon fibre prostheses) with improved running capabilities [Scholz et al., 2011].

Most of the scientific publications about the modeling of asymmetric gaits are about the so called *limb dominance* [Gregg et al., 2012, 2011; Moon & Spong, 2011]. It is developed by humans with a preferred leg, which executes a manipulative or mobilizing action while the other one provides stabilizing support [Gabbard & Hart, 1996]. Moreover, Martinez Salazar & Carbajal [2011] describe the importance of asymmetric patterns for the simulation of gait transitions. In particular, they confirm the role of skipping gait patterns [Farley, 1998] as the intermediate locomotion gait between walking and running.

Here, we investigate, to what extent contralateral leg asymmetry may challenge or even support stability of running. Therefore, we transform the model into a boundary value problem (BVP) as it shown in Merker et al. [2013], compute the stability region of the symmetric model and use it as reference for the analysis of the asymmetric model. Afterwards, we introduce the leg asymmetry parameters into the model and study their effects on the stability of running.

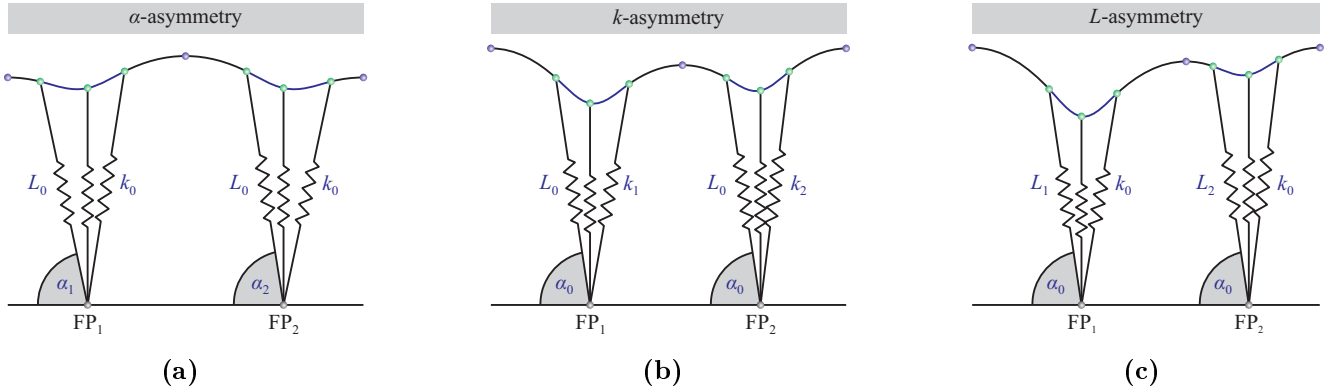


**Figure 5.1.** The asymmetric spring-mass model for running: **(a)**  $\alpha_1 \neq \alpha_2$ , **(b)**  $k_1 \neq k_2$ , **(c)**  $L_1 \neq L_2$ . The dots on the center of mass (CoM) trajectory show events of apex, touch-down, vertical leg orientation, and take-off.

Like in Chapter 2, to what extent contralateral leg asymmetry may challenge or even support stability of running. We use the transformed symmetric model and the results from Chapter 3 as references for our study. Therefore, we modify the functions  $f$  and  $r$  from Table 3.1 for the computation of two subsequent steps and introduce asymmetry parameters  $\varepsilon_\alpha$ ,  $\varepsilon_k$  and  $\varepsilon_L$  from (2.4) and (2.5) into the symmetric model. The influence of the asymmetry of the dimensionless energy  $\varepsilon_{\tilde{E}}$  on the stability of running is not discussed, since it exhibits the same behaviour as in case of the  $L$ -asymmetry (see Section 2.4.5). The resulting boundary value problem can now be applied to compute solutions of the asymmetric model. It can also be extended for the computation of singular points, which limit regions of stable asymmetric running. One type of boundaries of the region of stable symmetric solutions are simple turning points (Chapter 3). Another limit of stability are period-doubling bifurcation points. Hence, the goals of this chapter result in the following questions. Do the bifurcations of the asymmetric model still limit the regions of stable running? If it is correct, then how do the asymmetry parameters affect the bifurcations of the symmetric model? If it is not applicable, what are the new boundaries?

## 5.2. The asymmetric spring-mass model for running

The symmetric spring-mass model is described in Section 3.2.1. Again, we consider the full stride comprising two subsequent steps. Like for the bipedal model (Chapter 2), we define three positive asymmetry parameters  $\varepsilon_\alpha$ ,  $\varepsilon_k$  and  $\varepsilon_L$  of the angle of attack  $\alpha_0$  (Figure 5.1(a)), the leg stiffness  $k_0$  (Figure 5.1(b)) and the rest length  $L_0$  (Figure 5.1(c)), respectively. During the first step of a stride, these asymmetry parameters are subtracted from the corresponding reference parameters:

$$\alpha_1 = \alpha_0 - \varepsilon_\alpha, k_1 = k_0 - \varepsilon_k, L_1 = L_0 - \varepsilon_L. \quad (5.1)$$

During the subsequent step, they are added:

$$\alpha_2 = \alpha_0 + \varepsilon_\alpha, k_2 = k_0 + \varepsilon_k, L_2 = L_0 + \varepsilon_L. \quad (5.2)$$

All calculations in this investigation are done with constant dimensional energy  $E_0 = 1800$  J corresponding to the average initial horizontal velocity  $\dot{x}_0 = 5$  m/s (see relation (3.5)). The reference leg stiffness  $k_0 = 20$  kN/m is taken from Seyfarth et al. [2002] and [Lipfert et al., 2012]. Moreover, we set  $L_0 = 1$  m and  $m = 80$  kg.

### 5.3. Transformation into a boundary value problem

To compute a single step of the asymmetric spring-mass model for running, we use the modified boundary value for computation of a period-2 solution (Section 3.4.3). The modified functions  $f$  and  $r$  computing a periodic solution of the asymmetric model are listed in Table 5.1. In case of  $\alpha$ -asymmetry, we set  $\alpha_1 \neq \alpha_2$ . Similarly, for the asymmetry of stiffness and the leg length, we set  $k_1 \neq k_2$  and  $L_1 \neq L_2$ . The dimension  $n$  of the boundary value problem is 32. The modified problem (3.12) can now be used to find singular points as described in Chapter 4.

The computation of the points on the touch-down line  $y_{\text{TD}} = L_i \sin(\alpha_i)$  (left inset in Figure 5.3) or on the take-off line  $L_i = L_0$  (right inset in Figure 5.3) is required, since they occur as boundaries of stability regions in the asymmetric model. To find these points, we replace all  $\alpha_i$ 's in the modified functions  $f$  and  $r$  by the new variable  $z_{33}$ . Then, we add one more equation and, consequently, one more boundary condition to the boundary value problem (3.12):

$$f_{33} = 0 \quad r_{33} = z_5(0)z_{16}(0)z_{21}(0)z_{32}(0). \quad (5.3)$$

In case of  $z_5 = 0$  or  $z_{16} = 0$ , the first or the second step of the stride begins right with stance phase (touch-down point), i.e. the first apex and the first touch-down of the stride occur at the same time. In case of  $z_{21} = 0$  or  $z_{32} = 0$ , the corresponding step has no second flight phase (take-off point).

## 5.4. Results

### 5.4.1. Asymmetry of angle of attack

Examples of stable periodic solutions with  $\alpha$ -asymmetry are shown in Figure 5.2. They exist for  $\varepsilon_\alpha < 18.2^\circ$ , i.e. as long as the simple turning points exist (Figure 5.3). For  $\varepsilon_\alpha < 1.1^\circ$ , they are

$f_1 = z_5 z_2$	$r_1 = z_1(0) - x_0$
$f_2 = 0$	$r_2 = z_2(0) - \sqrt{\frac{2}{m}(E_0 - mgy_0)}$
$f_3 = z_5 z_4$	$r_3 = z_3(0) - z_{30}(1)$
$f_4 = -z_5 g$	$r_4 = z_4(0)$
$f_5 = 0$	$r_5 = z_3(1) - L_1 \sin(\alpha_1)$
$f_6 = z_{10} z_7$	$r_6 = z_6(0) - z_1(1)$
$f_7 = \frac{1}{m} z_{10} k_1 (L_1 - L_{11}) \frac{z_6 - z_{11}}{L_{11}}$	$r_7 = z_7(0) - z_2(1)$
$f_8 = z_{10} z_9$	$r_8 = z_8(0) - z_3(1)$
$f_9 = \frac{1}{m} z_{10} k_1 (L_1 - L_{11}) \frac{z_8}{L_{12}} - mg$	$r_9 = z_9(0) - z_4(1)$
$f_{10} = 0$	$r_{10} = (z_6(1) - z_{11}(0))^2 + z_8(1)^2 - L_1^2$
$f_{11} = 0$	$r_{11} = z_{11}(0) - z_6(0) - L_1 \cos(\alpha_1)$
$f_{12} = z_{16} z_{13}$	$r_{12} = z_{12}(0) - z_6(1)$
$f_{13} = 0$	$r_{13} = z_{13}(0) - z_7(1)$
$f_{14} = z_{16} z_{15}$	$r_{14} = z_{14}(0) - z_8(1)$
$f_{15} = -z_{16} g$	$r_{15} = z_{15}(0) - z_9(1)$
$f_{16} = 0$	$r_{16} = z_{15}(1)$
$f_{17} = z_{21} z_{18}$	$r_{17} = z_{17}(0) - z_{12}(1)$
$f_{18} = 0$	$r_{18} = z_{18}(0) - z_{13}(1)$
$f_{19} = z_{21} z_{20}$	$r_{19} = z_{19}(0) - z_{14}(1)$
$f_{20} = -z_{21} g$	$r_{20} = z_{20}(0) - z_{15}(1)$
$f_{21} = 0$	$r_{21} = z_{19}(1) - L_2 \sin(\alpha_2)$
$f_{22} = z_{26} z_{23}$	$r_{22} = z_{22}(0) - z_{17}(1)$
$f_{23} = \frac{1}{m} z_{26} k_2 (L_2 - L_{22}) \frac{z_{22} - z_{27}}{L_{22}}$	$r_{23} = z_{23}(0) - z_{18}(1)$
$f_{24} = z_{26} z_{25}$	$r_{24} = z_{24}(0) - z_{19}(1)$
$f_{25} = \frac{1}{m} z_{26} k_2 (L_2 - L_{22}) \frac{z_{24}}{L_{22}} - mg$	$r_{25} = z_{25}(0) - z_{20}(1)$
$f_{26} = 0$	$r_{26} = (z_{22}(1) - z_{27}(0))^2 + z_{24}(1)^2 - L_2^2$
$f_{27} = 0$	$r_{27} = z_{27}(0) - z_{22}(0) - L_2 \cos(\alpha_2)$
$f_{28} = z_{32} z_{29}$	$r_{28} = z_{28}(0) - z_{22}(1)$
$f_{29} = 0$	$r_{29} = z_{29}(0) - z_{23}(1)$
$f_{30} = z_{32} z_{31}$	$r_{30} = z_{30}(0) - z_{24}(1)$
$f_{31} = -z_{32} g$	$r_{31} = z_{31}(0) - z_{25}(1)$
$f_{32} = 0$	$r_{32} = z_{31}(1)$

**Table 5.1.** The functions  $f$  and  $r$  for the boundary value problem (3.12) computing a periodic solution of the asymmetric spring-mass model for running. Here, the lengths of both compressed leg springs during the first and the second stance phase are given by  $L_{11} := \sqrt{(z_6 - z_{11})^2 + z_8^2}$  and  $L_{22} := \sqrt{(z_{22} - z_{27})^2 + z_{24}^2}$ , respectively.

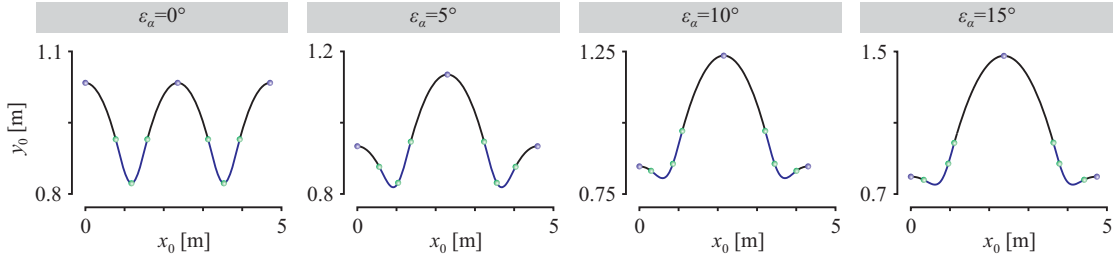


**Figure 5.2.** Development of the CoM-trajectory of a periodic stable solution for  $\alpha_0 = 66.2^\circ$  under the influence of different values of the asymmetry parameter  $\varepsilon_\alpha$ .

located between two turning points (Figure 5.4(a)). For  $1.2^\circ < \varepsilon_\alpha < 4.2^\circ$ , the right boundary of the stability area is a take-off point. At about  $\varepsilon_\alpha = 4.2^\circ$ , the transcritical bifurcation vanishes. From here until  $\varepsilon_\alpha = 18.2^\circ$ , the right limit of the stability area is the corresponding point on the touch-down line  $y_{TD} = L_0 \sin(\alpha_0)$ .

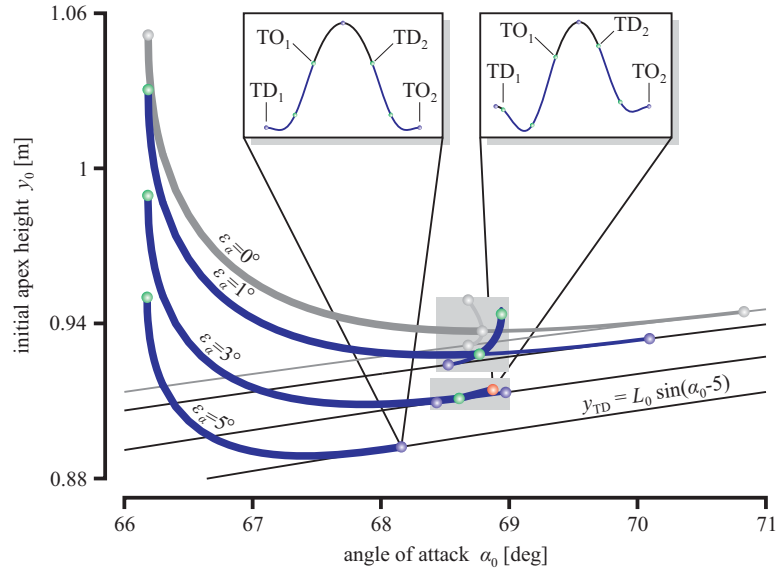
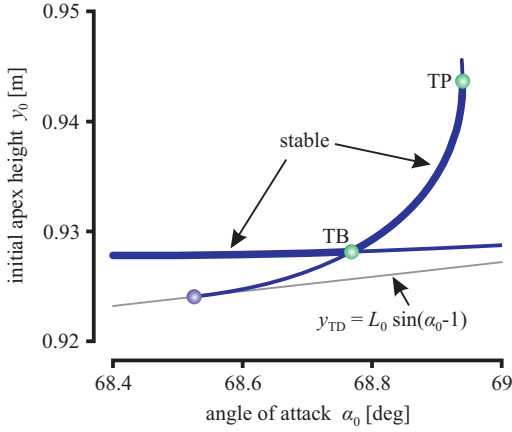
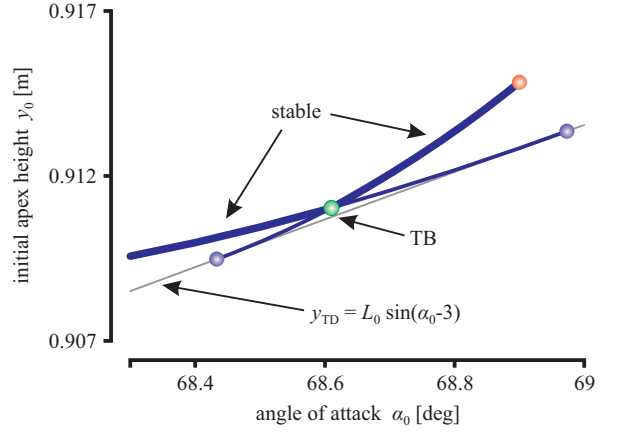
The maximum value of the  $\alpha$ -range  $\Delta\alpha = 3^\circ$  was found at  $\varepsilon_\alpha = 1.7^\circ$  (Figure 5.4(b)). Here, the left boundary of the region of stable solutions is the turning point at  $\alpha_{\min} = 66.2^\circ$ . The right one is the take-off point at  $\alpha_{\max} = 69.2^\circ$ . For  $\varepsilon_\alpha > 1.7^\circ$ , the  $\alpha$ -range monotonically decreases. Compared to the symmetric case with  $\Delta\alpha = 2.7^\circ$ , we observe an increase of the  $\alpha$ -range by 8%.

### 5.4.2. Asymmetry of leg stiffness

The asymmetry of leg stiffness  $\varepsilon_k$  is a bifurcation destroying perturbation (Figure 5.5, [Shearer, 1980]). Similar to the results of Chapter 2, no gain of the  $\alpha$ -range was observed in this case. However, stable solutions exist for values of  $\varepsilon_k < 6.3$  kN/m, where the double turning point occurs. Hence, the difference of 12.5 kN/m between the contralateral legs, which is 63% of the reference symmetric stiffness  $k_0 = 20$  kN/m, allows stable running. Stable solutions are located either between the simple turning point and a touch-down point ( $\varepsilon_k < 3.6$ ) or between two simple turning points ( $3.7 < \varepsilon_k < 6.3$ ).

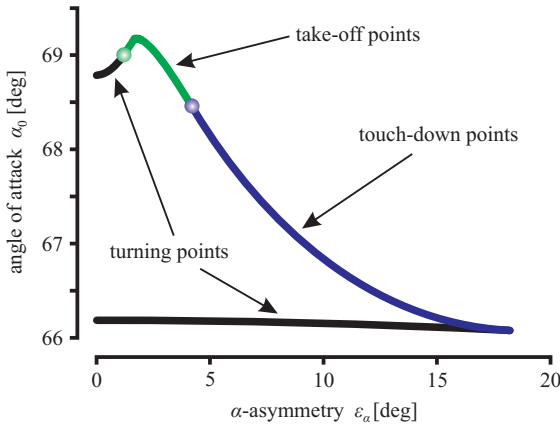
### 5.4.3. Asymmetry of rest length

Like above, the asymmetry parameter  $\varepsilon_L$  is a bifurcation destroying perturbation. Similar to the bipedal model, the monopedal model is very sensitive to  $\varepsilon_L$ . Again, with increasing  $\varepsilon_L$  the  $\alpha$ -range decreases rapidly (Figure 5.6). Stable solutions are located either between a simple turning point and a touch-down point ( $\varepsilon_L < 0.0063$ ) or between two simple turning points. Stable solutions exist up to  $\varepsilon_L = 0.0074$  m, where the double turning point occurs. For  $\varepsilon_L = 0.008$  m no stable solutions were found anymore. That means, stable running is possible with the total deviation

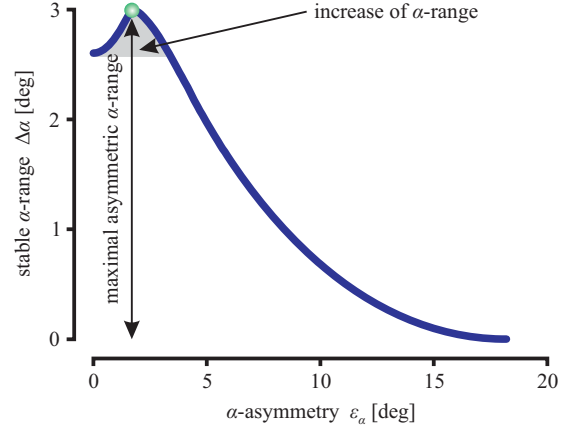
(a)  $\alpha$ -asymmetry(b)  $\varepsilon_\alpha = 1^\circ$ (c)  $\varepsilon_\alpha = 3^\circ$ 

**Figure 5.3.** Initial apex height  $y_0$  of asymmetric periodic patterns dependent on the reference angle of attack  $\alpha_0$  for  $\varepsilon_\alpha = 1^\circ, 3^\circ$  and  $5^\circ$ . The grey curves are the initial apex height of the reference periodic gait patterns (Figure 3.5). Thick parts indicate stable solutions. Blue dots are touch-down points, red dot is a take-off point. The green dots are bifurcations: TP = simple turning point, TB = transcritical bifurcation. Insets in (a) show the CoM trajectory of a touch-down point (left) and a take-off point (right). Plots (b) and (c) are the enlarged grey areas from (a) for  $\varepsilon_\alpha = 1^\circ$  and  $\varepsilon_\alpha = 3^\circ$ , respectively.





(a) Boundaries of the region of stable solutions dependent on the asymmetry parameter  $\varepsilon_\alpha$ . Black lines represent simple turning points. The green line consists of take-off points, the blue one consists of touch-down points.



(b) Stable  $\alpha$ -range  $\Delta\alpha$  dependent on the asymmetry parameter  $\varepsilon_\alpha$ . The green dot marks the maximal  $\alpha$ -range of  $\Delta\alpha = 3.0^\circ$  for  $\varepsilon_\alpha = 1.7^\circ$ .

**Figure 5.4.** Asymmetry of angle of attack  $\varepsilon_\alpha$ .

between the two leg lengths of 0.016 m, which is 1.6% of the symmetric leg length  $L_0 = 1$  m.

## 5.5. Discussion

In this chapter, we have shown that the boundary value problem approach from Chapter 4 can be extended for the study of the asymmetric spring-mass model. Moreover, a simple extension of the boundary value problem allows the computation of the points on the event hyperplanes, i.e the touch-down and the take-off lines. Like for the symmetric model, the approach described in this chapter is stable to numerical perturbations. The single shooting method is sufficient for solving of the occurring boundary value problems. The maximal value of  $\varepsilon_\alpha$ , where stable solutions exist, is given by the intersection of a curve of simple turning points and a curve of the touch-down points (Figure 5.4(a)). For the  $k$ - and  $L$ -asymmetry, these values can be determined by computation of double turning points (Figures 5.6 and 5.7).

Using the new technique, we have demonstrated that, like in walking, the asymmetric leg function does not necessarily reduce the region of stable running. The  $\alpha$ -asymmetry is not only tolerated during running but it may also provide some advantages, as demonstrated by the increased  $\alpha$ -range. With increasing asymmetry of leg stiffness  $\varepsilon_k$  and of leg length  $\varepsilon_l$  the  $\alpha$ -range  $\Delta\alpha$  diminishes continuously. Both, running and walking asymmetric models are very sensitive to the asymmetry of the leg length  $\varepsilon_L$ . We explain this sensitivity by the importance of the parameter  $L_0$  for the control of the motion of the center of mass. Like in the bipedal model, it influences not only the

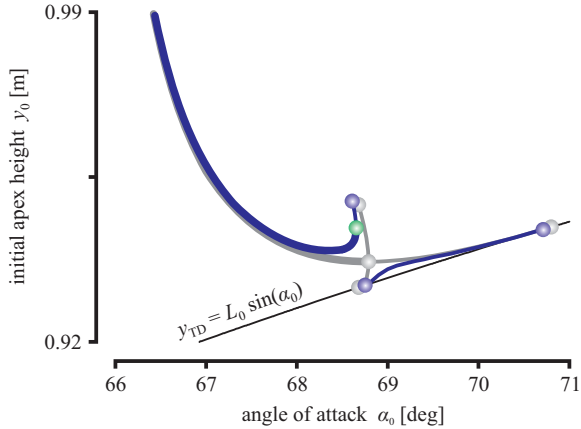


**Figure 5.5.** Example of a perturbed transcritical bifurcation. The blue curves represent asymmetric periodic solutions for  $\varepsilon_k = 0.1$  kN/m. The grey curves are the symmetric periodic solutions (Figure 3.5(b)). Thick parts indicate stable solutions. The green dot is a simple turning point.

leg dynamics during stance but also affects the instances of touch-down and take-off. Hence, a suitable leg retraction, e.g. Blum et al. [2010], or a suitable control of leg dynamics during stance, e.g. Riese & Seyfarth [2012], may help to increase the range of tolerated  $\varepsilon_L$  values.

Both asymmetric spring-mass models can stabilize symmetric gaits. In the bipedal model, the gain is achieved by the shift of both Hopf bifurcations, which serve as boundaries of stable patterns (Figure 2.12). In case of running, the asymmetry of angle of attack stabilizes a part of period-2 solutions. In the symmetric monopedal model, the right boundary of the stability region is a pitchfork bifurcation, which has the property to be a limit of stable solutions [Ikeda & Murota, 2002]. The introduction of  $\varepsilon_\alpha$  into the model changes the type of this bifurcation into a transcritical one making possible the increase of the  $\alpha$ -range (Figure 5.3).

The asymmetry parameters  $\varepsilon_\alpha$ ,  $\varepsilon_k$  and  $\varepsilon_L$  may be treated as perturbation parameters [Keener & Keller, 1973]. Thereby, the asymmetries of leg stiffness  $\varepsilon_k$  and leg length  $\varepsilon_L$  are bifurcation destroying perturbations [Shearer, 1980]. The influence of the asymmetry of angle of attack  $\varepsilon_\alpha$  is different, namely it only changes the type of bifurcation. The perturbed bifurcation problems can be solved using the so-called transformation technique [Wallisch & Hermann, 1987]. However, to reach acceptable precision, it is usually required to compute higher order derivatives of the functions  $f$  and  $r$  for the boundary value problem (3.12), which would cause a much higher computational effort.

During walking, amputees usually use the intact leg more often than the prosthetic one, since they trust more in the reliability of the natural limb than of the artificial one. Moreover, always having at least one leg on the ground provides them with more security [Schaarschmidt et al., 2012]. The existence of flight phases during running makes it difficult to run, because people are afraid to land on the prosthetic limb. The results of this study show similar behaviour: the walking model (maximal  $\alpha$ -range  $\Delta\alpha = 6.9^\circ$ ) provides more flexibility than the running model (maximal  $\alpha$ -range  $\Delta\alpha = 3^\circ$ ).

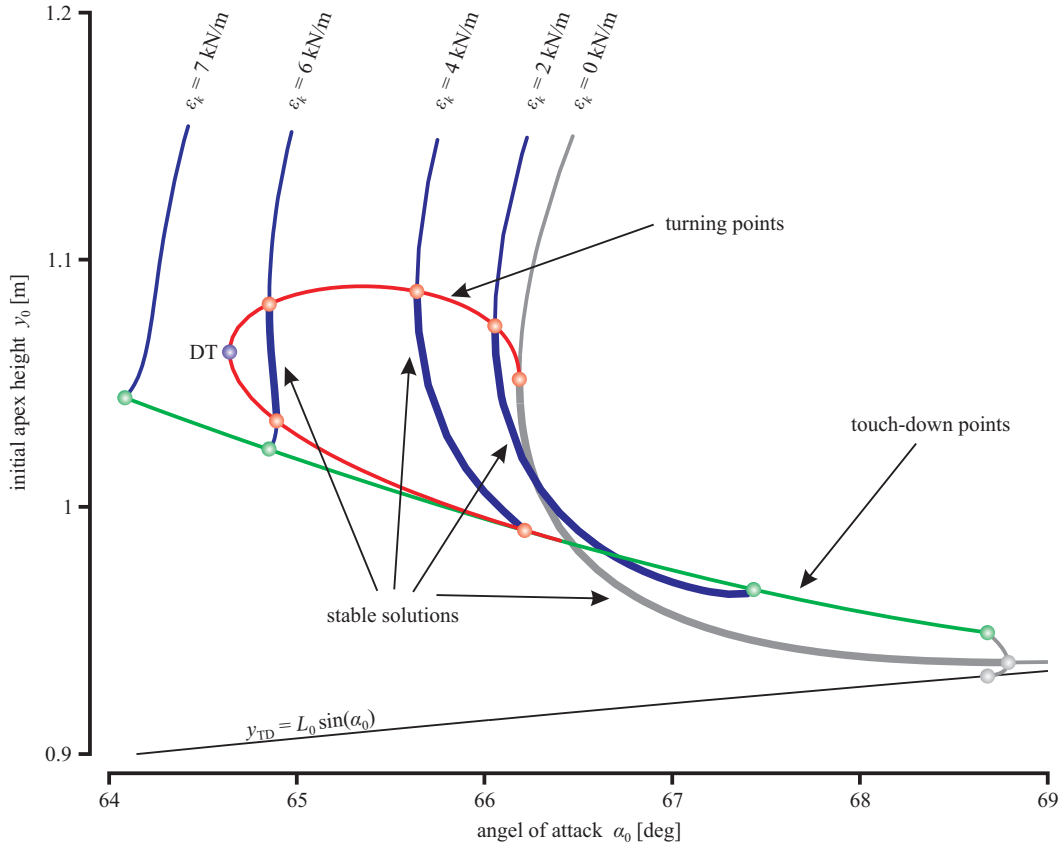


**Figure 5.6.** Initial apex height  $y_0$  of stable  $k$ -asymmetric solutions dependent on the angle of attack  $\alpha_0$  for  $\varepsilon_k = 2$  kN/m, 4 kN/m, 6 kN/m and 7 kN/m. The gray curves represent the initial conditions of the reference symmetric gait patterns (Figure 3.5). Thick parts indicate stable solutions. The green curve consists of touch-down points; the red one consists of simple turning points. The blue dot is a double turning point (DT).

Human locomotion is a result of complex interaction of bones, muscles and tendons. Thus, an asymmetric gait cannot be described by one single asymmetry parameter. Therefore, the further investigations should be extended on the effect of combinations of asymmetry parameters  $\varepsilon_\alpha$ ,  $\varepsilon_k$  and  $\varepsilon_L$  on the stability regions of walking and running. The reduction of the analysis of the region of stable solutions to the calculation of its boundaries provides a considerable benefit of computation time. For instance, this would allow a more realistic comparison of measured data to the results of the asymmetric spring-mass model.

Asymmetry is identified as one of the characteristics of gait transitions from walking to running and from running to walking [Segers et al., 2007b]. It disappeared from the locomotor system when the transition was completed. These experimental results were confirmed in a recent study [Martinez Salazar & Carbajal, 2011]. Using the spring-mass model, sequences of  $\alpha$ -asymmetric steps, which lead from walking to running, were investigated. Thereby, it was allowed, that a sequence contains an unstable intermediate step, as long as the sequence itself remains stable. The results show e.g. the appearance of skipping gaits (called *hopping gaits* in that paper) between walking and running, which is consistent with our results from Chapter 2. Moreover, this suggests

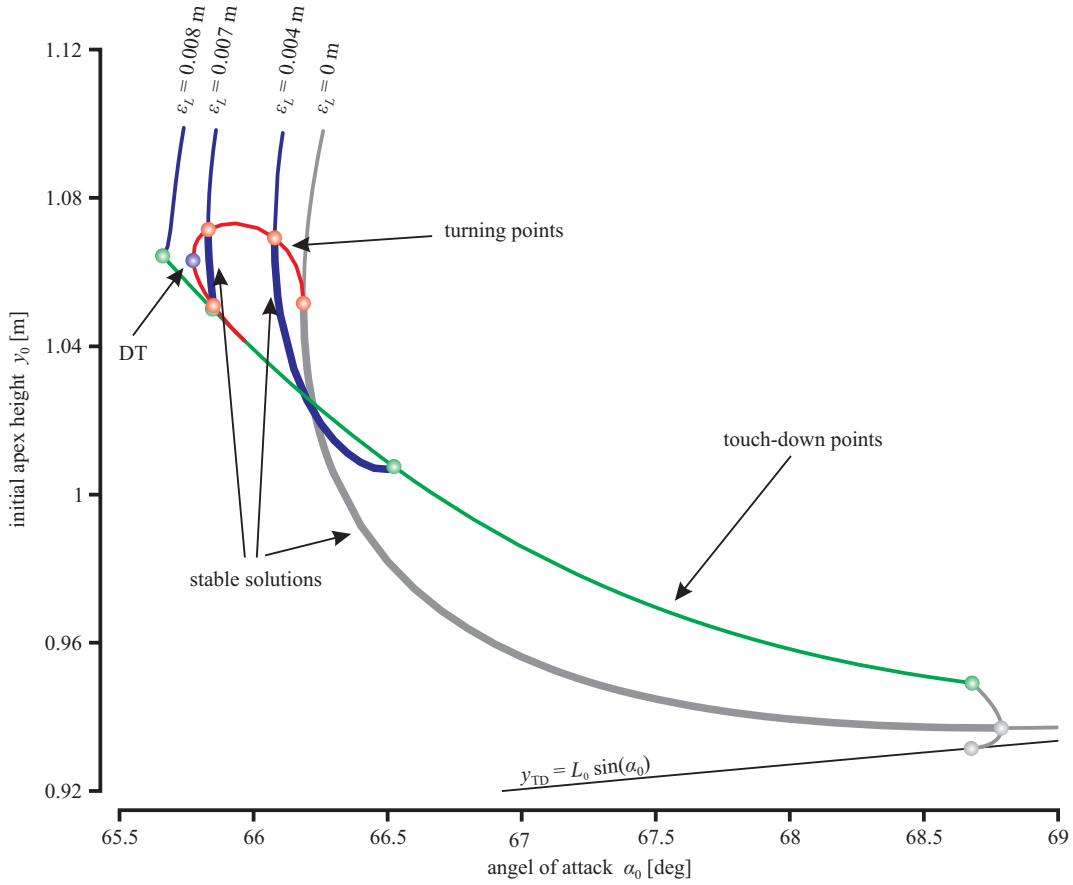


**Figure 5.7.** Initial apex height  $y_0$  of stable  $L$ -asymmetric solutions dependent on the angle of attack  $\alpha_0$  for  $\varepsilon_L = 0.004$  m,  $0.007$  m and  $0.008$  m. The gray curves represent the initial conditions of the reference symmetric gait patterns (Figure 3.5). Thick parts indicate stable solutions. The green curve consists of touch-down points; the red one consists of simple turning points. The blue dot is a double turning point (DT).

that the system tries to avoid the highly unstable solutions around the transition point and uses instead more stable asymmetric patterns. Since we are now able to find highly unstable patterns and the transition point itself, the next task could be to find out, how much asymmetry is absolutely necessary for a transition at a constant energy level.

The concept presented here can be easily applied to the asymmetric bipedal model. All computations in Chapter 2 were done with the implementation based on the sequence of initial value problems, i.e. using the heuristic approach. The bifurcation diagram of the bipedal symmetric model is much more complex than the diagram of the spring-mass model for running (compare Figures 4.1 and 4.2). Therefore, the calculations for Chapter 2 took a lot of computational effort. Using the proposed techniques, the comparable calculations for Chapter 5 could be done much faster. Thus, the boundary value problem approach provides a great benefit for the computational time, when we extend our study to the combination of asymmetry parameters. It promises fast and effective research in future.

# 6. General conclusions

## 6.1. Summary

In Chapter 2, we developed the asymmetric spring-mass model for walking. With its help, we investigated the behaviour of stable periodic solutions under the influence of increasing leg asymmetry. For the first time, we showed that the asymmetry of angle of attack does not necessarily reduce the region of stable walking. The leg asymmetry may also stabilize unstable symmetric solutions. However, we also showed that the asymmetric spring-mass model is unsuitable for the investigations of the asymmetry of the leg length. The model is very sensitive to this kind of deviations, which contradicts experimental observations. Thus, some modification of this model is required in future.

In Chapter 3, we successfully transformed the spring-mass model into a boundary value problem. It is robust to numerical perturbations and therefore can be applied for the computation of highly unstable periodic solutions. The resulting boundary value problem could be solved using the single shooting method. Thus, the new approach does not require more computational effort than the realization based on the sequence of initial value problems. Moreover, we showed for the first time that there exist stable grounded running solutions.

In Chapter 4, for the boundary value problem from the previous chapter we have developed appropriate extended systems for the computation of different types of bifurcation points. Using the extended systems for simple turning points and period-doubling bifurcation points, we computed the complete stable manifold of the spring-mass model for running. Moreover, we computed the biologically relevant parts of the stable manifold of the bipedal model.

In Chapter 5, we showed that the boundary value problem from Chapter 3 can be modified for the study of the asymmetric spring-mass model for running. We calculated the boundaries of the stability regions, which consist of bifurcation points and event points. We showed that the spring-mass model for running has a similar behaviour under the influence of asymmetric parameters, namely we achieved a gain of stability for the  $\alpha$ -asymmetry and a high sensitivity to the  $L$ -asymmetry. We also demonstrated that the numerical calculation of bifurcation points is

more efficient than the heuristic approach from Chapter 2.

## 6.2. Outlook

The asymmetric model is only one of many different extensions of the spring-mass model. For instance, the boundary value problem approach can also be applied to the other types of variability. Since all of these extensions lead to similar dynamical systems, the role of bifurcations is the same, namely they indicate a switch of stability or a change of the shape of patterns.

The first example is the non-conservative extension of the model. In our study, we considered leg stiffness and rest length as constant parameters during the whole stance phase. However, the human leg is not a perfect linear spring. Thus, in simulations the constant leg stiffness  $k_0$  and leg length  $L_0$  may be replaced by the time-dependent functions  $k_0(t)$  and  $L_0(t)$ . As it is shown in [Riese & Seyfarth \[2012\]](#), the application of the appropriate functions  $k_0(t)$  and  $L_0(t)$  provides a further improvement of the stability behaviour of the spring-mass model. Furthermore, this concept can be extended to the asymmetric parameters  $\varepsilon_k$  and  $\varepsilon_L$ . That means, that the asymmetric parameters  $k_1 \neq k_2$  and  $L_1 \neq L_2$  from Tab. 5.1 are replaced by the asymmetric functions  $k_i(t) = k_0 \pm \varepsilon_k(t)$  and  $L_i(t) = L_0 \pm \varepsilon_L(t)$ . Using techniques from this thesis, the stability behaviour of the modified model can be determined fast and effectively. For instance, the modified boundary value problem can be used for investigations of gait transitions at increasing speed [[Segers et al., 2007a,b](#)].

Another prominent example is the swing leg control for running, e.g. [Blum et al. \[2010\]](#); [Vejdani et al. \[2013\]](#). Here, all three constant parameters  $\alpha_0$ ,  $k_0$  and  $L_0$  are considered as time-dependent functions  $\alpha_0(t)$ ,  $k_0(t)$  and  $L_0(t)$  during flight phase. For stance phase, the parameters are constant. In this case, the functions  $f$  and  $r$  for the boundary value problem may be modified as above. The combination of an appropriate asymmetric swing leg control with suitable asymmetric functions  $\varepsilon_\alpha(t)$ ,  $\varepsilon_k(t)$  and  $\varepsilon_L(t)$  during stance may help to increase the range of tolerated  $\varepsilon_L$  values.

In the last example the concept of periodicity, which is common for many studies of human locomotion, is not used. In [Ludwig et al. \[2012\]](#), the apex heights were extracted from experimental data. Afterwards, the control parameters  $\alpha_0$ ,  $k_0$  and  $L_0$  were calculated to reproduce the exact sequence of steps, using the energy conservative and a non-conservative spring-mass model, respectively. This approach is predestined for the application of a boundary value problem: the initial and the final apex heights are parts of the boundary conditions and the trajectory of the center of mass between them is the solution of the corresponding boundary value problem. To improve the outcome, the measured data could be distinguished between the left and right leg. Additionally, the simulation may be repeated using the boundary value problem for the asymmetric spring-mass model.

## A. Computation of adjointed matrices

The adjointed matrices  $B_0^*$  and  $B_1^*$ , which are required in the equations (4.28) and (4.31), must fulfill the relations (4.29). For their computation, we determine the symbolic  $QR$  decomposition of the rectangular matrix  $[B_0 \ B_1]^T$  via Givens transformation [Hermann, 2011; Stoer & Bulirsch, 1993]:

$$\begin{bmatrix} B_0^T \\ B_1^T \end{bmatrix} = Q \begin{bmatrix} R \\ 0 \end{bmatrix} = \begin{bmatrix} Q_{11}Q_{12} \\ Q_{21}Q_{22} \end{bmatrix} \begin{bmatrix} R \\ 0 \end{bmatrix}.$$

Since  $Q$  is a quadratic orthonormal matrix, i.e.  $Q^{-1} = Q^T$ , we get

$$Q^T \begin{bmatrix} B_0^T \\ B_1^T \end{bmatrix} = \begin{bmatrix} Q_{11}^T Q_{21}^T \\ Q_{12}^T Q_{22}^T \end{bmatrix} \begin{bmatrix} B_0^T \\ B_1^T \end{bmatrix} = \begin{bmatrix} R \\ 0 \end{bmatrix}.$$

The desired adjointed matrices  $B_0^* := Q_{12}^T$  and  $B_1^* := -Q_{22}^T$  can now be inserted into the boundary value problem (4.28) and (4.31).





# Bibliography

- Adolfsson J, Dankowicz H, Nordmark A (2001)** 3d passive walkers: Finding periodic gaits in the presence of discontinuities. *Nonlinear Dynamics*, **24**:205–229. DOI:10.1023/A:1008300821973.
- Alexander RM, Jayes AS (1978)** Vertical movements in walking and running. *Journal of Zoology*, **185**(1):27–40. DOI:10.1111/j.1469-7998.1978.tb03311.x.
- Allgower EL, Schwetlick H (1997)** A general view of minimally extended systems for simple bifurcation points. *ZAMM - Journal of Applied Mathematics and Mechanics / Zeitschrift für Angewandte Mathematik und Mechanik*, **77**(2):83–97. DOI:10.1002/zamm.19970770203.
- Alur R, Courcoubetis C, Halbwachs N, Henzinger T, Ho PH, Nicollin X, Olivero A, Sifakis J, Yovine S (1995)** The algorithmic analysis of hybrid systems. *Theoretical Computer Science*, **138**(1):3–34. DOI:10.1016/0304-3975(94)00202-T.
- Andrada E, Nyakatura J, Müller R, Rode C, Blickhan R (2012)** Grounded running: An overlooked strategy for robots. **Levi P, Zweigle O, Häußermann K, Eckstein B**, eds., *Autonomous Mobile Systems*, Informatik aktuell, 79–87. Springer. DOI:10.1007/978-3-642-32217-4\_9.
- Banach S (1932)** *Théorie des opérations linéaires*. Monografie Matematyczne, Warszawa.
- Betts JT (2010)** *Practical methods for optimal control and estimation using nonlinear programming*. Advances in Design and Control. SIAM, second edn. ISBN:978-0-898716-88-7.
- Beyn WJ (1980)** *On discretizations of bifurcation problems*, 46–73. Bifurcation problems and their numerical solution: Workshop on Bifurcation Problems and Their Numerical Solution. Birkhäuser, Dortmund. ISBN:3-7643-1204-1.
- Bhave A, Paley D, Herzenberg JE (1999)** Improvement in gait parameters after lengthening for the treatment of limb-length discrepancy. *The Journal of Bone and Joint Surgery*, **81**(4):529–534.

- Biewener AA, Daley MA (2007)** Unsteady locomotion: integrating muscle function with whole body dynamics and neuromuscular control. *Journal of Experimental Biology*, **210(17)**:2949–2960. DOI:10.1242/jeb.005801.
- Blickhan R (1989)** The spring-mass model for running and hopping. *Journal of Biomechanics*, **22(11-12)**:1217–1227. DOI:10.1016/0021-9290(89)90224-8.
- Blickhan R, Seyfarth A, Geyer H, Grimmer S, Wagner H, Guenther M (2007)** Intelligence by mechanics. *Philosophical Transactions of the Royal Society A: Mathematical, Physical and Engineering Sciences*, **365(1850)**:199–220. DOI:10.1098/rsta.2006.1911.
- Blum Y, Birn-Jeffery A, Daley MA, Seyfarth A (2011)** Does a crouched leg posture enhance running stability and robustness? *Journal of Theoretical Biology*, **281(1)**:97–106. DOI:10.1016/j.jtbi.2011.04.029.
- Blum Y, Lipfert SW, Rummel J, Seyfarth A (2010)** Swing leg control in human running. *Bioinspiration & Biomimetics*, **5(2)**:026006 (11pp). DOI:10.1088/1748-3182/5/2/026006.
- Bock HG, Plitt KJ (1984)** A multiple shooting algorithm for direct solution of optimal control problems. *Proceedings of 9th IFAC World Congress*, 243–247. Pergamon Press, Budapest.
- Brezzi F, Ushiki S, Fujii H (1984)** “Real” and “Ghost” bifurcation dynamics in difference schemes for ODEs. **Küpper T, Mittelman H, Weber H**, eds., *Numerical Methods for Bifurcation Problems*, vol. 70 of *International Series of Numerical Mathematics*, 79–104. Birkhäuser. DOI:10.1007/978-3-0348-6256-1\_6.
- Bruijn SM (2010)** *Is stability an unstable concept? Quantifying dynamic stability of human locomotion*. Ph.d.thesis, Vrije Universiteit. ISBN:9789-0865-9455-9.
- Burkett B, Smeathers J, Barker T (2003)** Walking and running inter-limb asymmetry for paralympic trans-femoral amputees, a biomechanical analysis. *Prosthetics and Orthotics International*, **27(1)**:36–47. DOI:10.3109/03093640309167975.
- Byl K, Tedrake R (2009)** Metastable walking machines. *The International Journal of Robotics Research*, **28(8)**:1040–1064. DOI:10.1177/0278364909340446.
- Cavagna GA, Kaneko M (1977)** Mechanical work and efficiency in level walking and running. *The Journal of Physiology*, **268(2)**:467–481.
- Crandall MG, Rabinowitz PH (1971)** Bifurcation from simple eigenvalues. *Journal of Functional Analysis*, **8(2)**:321–340. DOI:10.1016/0022-1236(71)90015-2.
- Diehl M, Bock H, Diedam H, Wieber PB (2006)** Fast direct multiple shooting algorithms for optimal robot control. *Fast Motions in Biomechanics and Robotics*, vol. 340 of *Lecture*

*Notes in Control and Information Sciences*, 65–93. Springer.

DOI:10.1007/978-3-540-36119-0\_4.

**Dingwell JB, Cusumano JP (2010)** Re-interpreting detrended fluctuation analyses of stride-to-stride variability in human walking. *Gait & Posture*, **32(3)**:348–353. DOI: 10.1016/j.gaitpost.2010.06.004.

**Dingwell JB, John J, Cusumano JP (2010)** Do humans optimally exploit redundancy to control step variability in walking? *PLoS Computational Biology*, **6(7)**:e1000856.

DOI:10.1371/journal.pcbi.1000856.

**Doedel E, Govaerts W, Kuznetsov Y, Dhooge A (2005)** Numerical continuation of branch points of equilibria and periodic orbits. *International Journal of Bifurcation Chaos in Applied Sciences and Engineering*, **15(3)**:841–860. DOI:10.1142/S0218127405012491.

**Donelan JM, Shipman DW, Kram R, Kuo AD (2004)** Mechanical and metabolic requirements for active lateral stabilization in human walking. *Journal of Biomechanics*, **37(6)**:827–835. DOI:10.1016/j.jbiomech.2003.06.002.

**Eilenberg MF, Geyer H, Herr H (2010)** Control of a powered ankle-foot prosthesis based on a neuromuscular model. *IEEE Transactions on Neural Systems and Rehabilitation Engineering*, **18(2)**:164–173. DOI:10.1109/TNSRE.2009.2039620.

**Faber F, Behnke S (2007)** Stochastic optimization of bipedal walking using gyro feedback and phase resetting. *Proceedings of International Conference on Humanoid Robots (ICHR)*, 203–209. IEEE-RAS, Pittsburgh, Pennsylvania. DOI:10.1109/ICHR.2007.4813869.

**Farley CT (1998)** Locomotion: Just skip it. *Nature*, **394(6695)**:721–723. DOI:10.1038/29395.

**Floquet G (1883)** Sur les équations différentielles linéaires à coefficients périodiques. *Annales scientifiques de l'École Normale Supérieure*, **12**:47–88.

**Full RJ, Koditschek DE (1999)** Templates and anchors: neuromechanical hypotheses of legged locomotion on land. *Journal of Experimental Biology*, **202(23)**:3325–3332.

**Gabbard C, Hart S (1996)** A question of foot dominance. *The Journal of General Psychology*, **123(4)**:289–296. DOI:10.1080/00221309.1996.9921281.

**Gavrilyuk I, Hermann M, Kutniv M, Makarov V (2010)** Two-point difference schemes of an arbitrary given order of accuracy for nonlinear bvps. *Applied Mathematics Letters*, **23(5)**:585–590. DOI:10.1016/j.aml.2010.01.016.

**Geyer H, Seyfarth A, Blickhan R (2006)** Compliant leg behaviour explains basic dynamics of walking and running. *Proceedings of the Royal Society B: Biological Sciences*, **273(1603)**:2861–2867. DOI:10.1098/rspb.2006.3637.

- Goble DJ, Marino GW, Potvin JR (2003)** The influence of horizontal velocity on interlimb symmetry in normal walking. *Human Movement Science*, **22(3)**:271–283. DOI:10.1016/S0167-9457(03)00047-2.
- Gottlieb D, Orszag SA (1977)** *Numerical Analysis of Spectral Methods*, vol. 26 of *CBMS-NSF Regional Conference Series in Applied Mathematics*. Society for Industrial and Applied Mathematics. ISBN:978-0-898-71023-6.
- Gregg R, Dhaher Y, Degani A, Lynch K (2012)** On the mechanics of functional asymmetry in bipedal walking. *IEEE Transactions on Biomedical Engineering*, **59(5)**:1310–1318. DOI:10.1109/TBME.2012.2186808.
- Gregg RD, Degani A, Dhaher Y, Lynch K (2011)** The basic mechanics of bipedal walking lead to asymmetric behavior. *Proceedings of International Conference on Rehabilitation Robotics (ICORR)*, 1–6. IEEE, Zurich, Switzerland. DOI:10.1109/ICORR.2011.5975459.
- Grimmer M, Seyfarth A (2011a)** Stiffness adjustment of a series elastic actuator in a knee prosthesis for walking and running: The trade-off between energy and peak power optimization. *Intelligent Robots and Systems (IROS), 2011 IEEE/RSJ International Conference on*, 1811–1816. DOI:10.1109/IROS.2011.6094467.
- Grimmer M, Seyfarth A (2011b)** Stiffness adjustment of a series elastic actuator in an ankle-foot prosthesis for walking and running: The trade-off between energy and peak power optimization. *Robotics and Automation (ICRA), 2011 IEEE International Conference on*, 1439–1444. DOI:10.1109/ICRA.2011.5980183.
- Grimmer S, Ernst M, Gunther M, Blickhan R (2008)** Running on uneven ground: leg adjustment to vertical steps and self-stability. *Journal of Experimental Biology*, **211(18)**:2989–3000. DOI:10.1242/jeb.014357.
- Gross T, Feudel U (2004)** Analytical search for bifurcation surfaces in parameter space. *Physica D: Nonlinear Phenomena*, **195(3-4)**:292–302. DOI:10.1016/j.physd.2004.03.019.
- Guckenheimer J, Holmes P (1983)** *Nonlinear Oscillations, Dynamical Systems, and Bifurcations of Vector Fields*, vol. 42 of *Applied Mathematical Sciences*. Springer. ISBN:978-0-387-90819-9.
- Gurney B (2002)** Leg length discrepancy. *Gait & Posture*, **15(2)**:195–206. DOI:10.1016/S0966-6362(01)00148-5.
- Hausdorff JM (2007)** Gait dynamics, fractals and falls: Finding meaning in the stride-to-stride fluctuations of human walking. *Human Movement Science*, **26(4)**:555–589. DOI:10.1016/j.humov.2007.05.003.

- Hermann M (2004)** *Numerik gewöhnlicher Differentialgleichungen: Anfangs- und Randwertprobleme*. Oldenbourg. ISBN:978-3-4862-7606-0.
- Hermann M (2011)** *Numerische Mathematik*. Oldenbourg, 3. edn. ISBN:978-3-4867-0820-2.
- Hermann M, Kaiser D (1993)** RWPM: a software package of shooting methods for nonlinear two-point boundary value problems. *Applied Numerical Mathematics*, **13(1-3)**:103–108. DOI:10.1016/0168-9274(93)90134-D.
- Hermann M, Kaiser D, Schröder M (1999)** Theoretical and numerical studies of nonlinear shell equations. *Physica D: Nonlinear Phenomena*, **132(1-2)**:19–39. DOI:10.1016/S0167-2789(99)00032-9.
- Hermann M, Middelman W, Kunkel P (1998)** Augmented systems for the computation of singular points in banach space problems. *ZAMM - Journal of Applied Mathematics and Mechanics / Zeitschrift für Angewandte Mathematik und Mechanik*, **78(1)**:39–50. DOI:10.1002/(SICI)1521-4001(199801)78:1<39::AID-ZAMM39>3.0.CO;2-J.
- Hermann M, Milde T (2009)** Computing eigenfunctions of singular points in nonlinear parametrized two-point bvps. *Applied Numerical Mathematics*, **59(3-4)**:671–676. DOI:10.1016/j.apnum.2008.03.010.
- Hermann M, Saravi M (2014)** *A First Course in Ordinary Differential Equations. Analytical and Numerical Methods*. Springer. DOI: 10.1007/978-81-322-1835-7 ISBN: 978-81-322-1835-7.
- Hermann M, Timokha A (2005)** Modal modelling of the nonlinear resonant fluid sloshing in a rectangular tank I: a single-dominant model. *Mathematical Models and Methods in Applied Sciences*, **15(09)**:1431–1458. DOI:10.1142/S0218202505000777.
- Hermann M, Timokha A (2008)** Modal modelling of the nonlinear resonant fluid sloshing in a rectangular tank ii: Secondary resonance. *Mathematical Models and Methods in Applied Sciences*, **18(11)**:1845–1867. DOI:10.1142/S0218202508003212.
- Hermann M, Ullrich K (1992)** RWPKV: a software package for continuation and bifurcation problems in two-point boundary value problems. *Applied Mathematics Letters*, **5(2)**:57–61. DOI:10.1016/0893-9659(92)90112-M.
- Herr HM, Huang GT, McMahon TA (2002)** A model of scale effects in mammalian quadrupedal running. *Journal of Experimental Biology*, **205(7)**:959–967.
- Herzog W, Nigg BM, Read LJ, Olsson E (1989)** Asymmetries in ground reaction force patterns in normal human gait. *Medicine & Science in Sports & Exercise*, **21(1)**:110–114.

- Hitt JK, Sugar TG, Holgate M, Bellman R (2010)** An active foot-ankle prosthesis with biomechanical energy regeneration. *Journal of Medical Devices*, **4(1)**:011003. DOI:10.1115/1.4001139.
- Hof AL, van Bockel RM, Schoppen T, Postema K (2007)** Control of lateral balance in walking: Experimental findings in normal subjects and above-knee amputees. *Gait & Posture*, **25(2)**:250–258. DOI:10.1016/j.gaitpost.2006.04.013.
- Hopf E (1942)** Abzweigung einer periodischen Lösung von einer stationären Lösung eines Differentialsystems. *Berichten der Mathematisch-Physischen Klasse der Sächsischen Akademie der Wissenschaften zu Leipzig*, **94**:1–22.
- Hreljac A (2004)** Impact and overuse injuries in runners. *Medicine and Science in Sports and Exercise*, **36(5)**:845–849.
- Ikeda K, Murota K (2002)** *Imperfect bifurcation in structures and materials: Engineering use of group-theoretic bifurcation theory*, vol. 149 of *Applied Mathematical Sciences*. Springer. ISBN:978-0-387-95409-7.
- Jepson A, Spence A (1985)** Folds in solutions of two parameter systems and their calculation. Part I. *SIAM Journal on Numerical Analysis*, **22(2)**:347–368. DOI:10.1137/0722021.
- Jordan R (1990)** *The eye of the world*, vol. 1 of *The wheel of time*. Tor Books. ISBN:978-1-85723-076-5.
- Kalveram KT, Seyfarth A (2009)** Inverse biomimetics: How robots can help to verify concepts concerning sensorimotor control of human arm and leg movements. *Journal of Physiology - Paris*, **103(3-5)**:232–243. DOI:10.1016/j.jphysparis.2009.08.006.
- Kaufman KR, Miller LS, Sutherland DH (1996)** Gait asymmetry in patients with limb-length inequality. *Journal of Pediatric Orthopaedics*, **16(2)**:144–150.
- Keener JP, Keller HB (1973)** Perturbed bifurcation theory. *Archive for Rational Mechanics and Analysis*, **50**:159–175. DOI:10.1007/BF00703966.
- Keller HB (1978)** Numerical solution of bifurcation and nonlinear eigenvalue problems. **Rabinowitz PH**, ed., *Applications of bifurcation theory*, 359–384. Academic Press. ISBN:978-0-125-74250-4.
- Kohl N, Stone P (2004)** Policy gradient reinforcement learning for fast quadrupedal locomotion. *Proceedings of International Conference on Robotics and Automation (ICRA)*, vol. 3, 2619–2624. IEEE, New Orleans, LA. DOI:10.1109/ROBOT.2004.1307456.

- Lipfert SW (2010)** *Kinematic and dynamic similarities between walking and running*. Verlag Dr. Kovac. ISBN:978-3-8300-5030-8.
- Lipfert SW, Günther M, Renjewski D, Grimmer S, Seyfarth A (2012)** A model-experiment comparison of system dynamics for human walking and running. *Journal of Theoretical Biology*, **292(0)**:11–17. DOI:10.1016/j.jtbi.2011.09.021.
- Ludwig C, Grimmer S, Seyfarth A, Maus HM (2012)** Multiple-step model-experiment matching allows precise definition of dynamical leg parameters in human running. *Journal of Biomechanics*, **45(14)**:2472–2475. DOI:10.1016/j.jbiomech.2012.06.030.
- Lyapunov A (1906)** *Sur les figures d'équilibre peu différentes des ellipsoïdes d'une masse liquide homogène douée d'un mouvement de rotation*. Imprimerie de l'Acad. impériale des sciences.
- Makarov V, Gavrilyuk I, Kutniv M, Hermann M (2004)** A two-point difference scheme of an arbitrary order of accuracy for BVPs for systems of first order nonlinear ODEs. *Computational Methods in Applied Mathematics*, **4**:464–493. DOI:10.2478/cmam-2004-0026.
- Marsden JE, McCracken M (1976)** *The Hopf bifurcation and its applications*, vol. 19 of *Applied Mathematical Sciences*. Springer. ISBN:978-0-387-90200-5.
- Martinez HR, Carbajal JP (2011)** From walking to running: A natural transition in the SLIP model using the hopping gait. *Proceedings of International Conference on Robotics and Biomimetics (ROBIO)*, 2163–2168. IEEE, Phuket, Thailand. DOI:10.1109/ROBIO.2011.6181612.
- Martinez Salazar HR, Carbajal JP (2011)** Exploiting the passive dynamics of a compliant leg to develop gait transitions. *Physical Review E*, **83**:066707. DOI:10.1103/PhysRevE.83.066707.
- Marx B, Vogt W (2011)** *Dynamische Systeme - Theorie und Numerik*. Spektrum Akademischer Verlag. ISBN:978-3-8274-2447-1.
- Maurer C, von Tscharner V, Samsom M, Baltich J, Nigg BM (2013)** Extraction of basic movement from whole-body movement, based on gait variability. *Physiological Reports*, **1(3)**:00. DOI:10.1002/phy2.49.
- Maus HM (2012)** *Towards understanding human locomotion*. Universitätsverlag Ilmenau. ISBN:978-3-86360-054-9.
- Maus HM, Lipfert SW, Gross M, Rummel J, Seyfarth A (2010)** Upright human gait did not provide a major mechanical challenge for our ancestors. *Nat Commun*, **1(6)**:70. DOI:10.1038/ncomms1073.

- Maykranz D, Grimmer S, Lipfert SW, Seyfarth A (2009)** Foot function in spring mass running. *Autonome Mobile Systeme*, 81–88. Springer, Karlsruhe, Germany. DOI:10.1007/978-3-642-10284-4\_11.
- McCaw ST, Bates BT (1991)** Biomechanical implications of mild leg length inequality. *British Journal of Sports Medicine*, **25(1)**:10–13. DOI:10.1136/bjsm.25.1.10.
- McMahon TA, Cheng GC (1990)** The mechanics of running: how does stiffness couple with speed? *Journal of Biomechanics*, **23(Suppl. 1)**:65–78. DOI:10.1016/0021-9290(90)90042-2.
- Merker A, Kaiser D, Hermann M (2013)** Numerical bifurcation analysis of the bipedal spring-mass model. *Physica D: Nonlinear Phenomena*, (**submitted**).
- Merker A, Kaiser D, Hermann M (2014)** Numerical bifurcation analysis of the asymmetric spring-mass model. *Computer Methods in Biomechanics and Biomedical Engineering*, (**submitted**).
- Merker A, Riese S, Seyfarth A (2011a)** Influence of variable leg parameters on human locomotion. *Dynamic Walking*. Jena, July, 18–21. [http://www.dynamicwalking.uni-jena.de/sites/default/files/DynamicWalking2011\\_ExtendedAbstracts.pdf](http://www.dynamicwalking.uni-jena.de/sites/default/files/DynamicWalking2011_ExtendedAbstracts.pdf).
- Merker A, Rummel J, Seyfarth A (2011b)** Stable walking with asymmetric legs. *Bioinspiration & Biomimetics*, **6(4)**:045004. DOI:10.1088/1748-3182/6/4/045004.
- Middelmann W (1998)** *Konstruktion erweiterter Systeme für Bifurkationsphänomene mit Anwendung auf Randwertprobleme*. Ph.D. thesis, Friedrich-Schiller-Universität Jena, Germany.
- Minetti AE (1998)** The biomechanics of skipping gaits: a third locomotion paradigm? *Proceedings of the Royal Society B: Biological Sciences*, **265(1402)**:1227–1235. DOI:10.1098/rspb.1998.0424.
- Minetti AE, Ardigo LP, Saibene F (1994)** The transition between walking and running in humans: metabolic and mechanical aspects at different gradients. *Acta Physiologica Scandinavica*, **150(3)**:315–323. DOI:10.1111/j.1748-1716.1994.tb09692.x.
- Moon JS, Spong MW (2010)** Bifurcations and chaos in passive walking of a compass-gait biped with asymmetries. *Proceedings of International Conference on Robotics and Automation (ICRA)*, 1721–1726. IEEE, Anchorage, Alaska. DOI:10.1109/ROBOT.2010.5509856.
- Moon JS, Spong MW (2011)** Classification of periodic and chaotic passive limit cycles for a compass-gait biped with gait asymmetries. *Robotica*, **29**:967–974. DOI:10.1017/S0263574711000178.



- Moore G (1980)** The numerical treatment of non-trivial bifurcation points. *Numerical Functional Analysis and Optimization*, **2(6)**:441–472. DOI:10.1080/01630568008816070.
- Moore G, Spence A (1980)** The calculation of turning points of nonlinear equations. *SIAM Journal on Numerical Analysis*, **17(4)**:567–576. DOI:10.1137/0717048.
- Nolan L, Wit A, Dudzinski K, Lees A, Lake M, Wychowanski M (2003)** Adjustments in gait symmetry with walking speed in trans-femoral and trans-tibial amputees. *Gait & Posture*, **17(2)**:142–151. DOI:10.1016/S0966-6362(02)00066-8.
- Perttunen JR, Anttila E, Sodergard J, Merikanto J, Komi PV (2004)** Gait asymmetry in patients with limb length discrepancy. *Scandinavian Journal of Medicine & Science in Sports*, **14(1)**:49–56. DOI:10.1111/j.1600-0838.2003.00307.x.
- Peuker F, Maufroy C, Seyfarth A (2012)** Leg-adjustment strategies for stable running in three dimensions. *Bioinspiration & Biomimetics*, **7(3)**:036002. DOI:10.1088/1748-3182/7/3/036002.
- Peuker F, Seyfarth A (2010)** Adjusting legs for stable running in three dimensions. *6th World Congress of Biomechanics, Singapore*, vol. 31 of *IFMBE Proceedings*, 3–6. Springer. DOI:10.1007/978-3-642-14515-5\_1.
- Poincaré H (1890)** Sur le problème des trois corps et les équations de la dynamique. *Acta Mathematica*, **13(1)**:A3–A270. DOI:10.1007/BF02392506.
- Pönisch G, Schwetlick H (1981)** Computing turning points of curves implicitly defined by nonlinear equations depending on a parameter. *Computing*, **26**:107–121. DOI:10.1007/BF02241778.
- Prince F, Allard P, Therrien RG, McFadyen BJ (1992)** Running gait impulse asymmetries in below-knee amputees. *Prosthetics and Orthotics International*, **16(1)**:19–24. DOI:10.3109/03093649209164303.
- Renjewski D, Manoonpong P, Seyfarth A, Wörgötter F (2008)** From biomechanical concepts towards fast and robust robots. *Proceedings of the 11th International Conference on Climbing and Walking Robots (CLAWAR)*, 630–637. World Scientific, Coimbra, Portugal. DOI:10.1142/9789812835772\_0076.
- Renjewski D, Seyfarth A (2012)** Robots in human biomechanics - a study on ankle push-off in walking. *Bioinspiration & Biomimetics*, **7(3)**:036005. DOI:10.1088/1748-3182/7/3/036005.
- Riese S (2013)** *On the effects of variable leg-spring properties during hopping*. Ph.D. thesis, Friedrich-Schiller-Universität Jena, Germany.

- Riese S, Seyfarth A (2012)** Stance leg control: variation of leg parameters supports stable hopping. *Bioinspiration & Biomimetics*, **7(1)**:016006. DOI:10.1088/1748-3182/7/1/016006.
- Riese S, Seyfarth A, Grimmer S (2013)** Linear center-of-mass dynamics emerge from non-linear leg-spring properties in human hopping. *Journal of Biomechanics*, **46(13)**:2207–2212. DOI:10.1016/j.jbiomech.2013.06.019.
- Roose D, Piessens R (1985)** Numerical computation of nonsimple turning points and cusps. *Numerische Mathematik*, **46(2)**:189–211. DOI:10.1007/BF01390419.
- Rummel J, Blum Y, Maus HM, Rode C, Seyfarth A (2010a)** Stable and robust walking with compliant legs. *Proceedings of International Conference on Robotics and Automation (ICRA)*, 5250–5255. IEEE, Anchorage, Alaska. DOI:10.1109/ROBOT.2010.5509500.
- Rummel J, Blum Y, Seyfarth A (2009)** From walking to running. *Autonome Mobile Systeme*, 89–96. Springer, Karlsruhe, Germany. DOI:10.1007/978-3-642-10284-4\_12.
- Rummel J, Blum Y, Seyfarth A (2010b)** Robust and efficient walking with spring-like legs. *Bioinspiration & Biomimetics*, **5(4)**:046004 (13pp). DOI:10.1088/1748-3182/5/4/046004.
- Rummel J, Seyfarth A (2008)** Stable running with segmented legs. *The International Journal of Robotics Research*, **27(8)**:919–935. DOI:10.1177/0278364908095136.
- Rummel J, Seyfarth A (2010)** Passive stabilization of the trunk in walking. **Menegatti E**, ed., *Proceedings of the 2nd International Conference on Simulation, Modeling, and Programming for Autonomous Robots (SIMPAN)*, 127–136. Darmstadt, Germany. ISBN:978-3-00-032863-3.
- Sadeghi H, Allard P, Prince F, Labelle H (2000)** Symmetry and limb dominance in able-bodied gait: a review. *Gait & Posture*, **12(1)**:34–45. DOI:10.1016/S0966-6362(00)00070-9.
- Schaarschmidt M, Lipfert SW, Meier-Gratz C, Scholle HC, Seyfarth A (2012)** Functional gait asymmetry of unilateral transfemoral amputees. *Human Movement Science*, **31(4)**:907–917. DOI:10.1016/j.humov.2011.09.004.
- Schmidt E (1908)** Zur Theorie der linearen und nichtlinearen Integralgleichungen. Teil III. *Mathematische Annalen*, **65(3)**:370–399. DOI:10.1007/BF01456418.
- Schmitt J, Clark J (2009)** Modeling posture-dependent leg actuation in sagittal plane locomotion. *Bioinspiration & Biomimetics*, **4(4)**:046005 (17pp). DOI:10.1088/1748-3182/4/4/046005.

- Scholz MS, Blanchfield J, Bloom L, Coburn B, Elkington M, Fuller J, Gilbert M, Muflahi S, Pernice M, Rae S, Trevarthen J, White S, Weaver P, Bond I (2011)** The use of composite materials in modern orthopaedic medicine and prosthetic devices: A review. *Composites Science and Technology*, **71(16)**:1791–1803. DOI:10.1016/j.compscitech.2011.08.017.
- Schwind WJ (1998)** *Spring loaded inverted pendulum running: a plant model*. Ph.D. thesis, University of Michigan, Ann Arbor, MI, USA.
- Segers V, Aerts P, Lenoir M, De Clerq D (2007a)** Dynamics of the body centre of mass during actual acceleration across transition speed. *Journal of Experimental Biology*, **210(4)**:578–585. DOI:10.1242/jeb.02693.
- Segers V, Aerts P, Lenoir M, De Clerq D (2007b)** Kinematics of the transition between walking and running when gradually changing speed. *Gait & Posture*, **26(3)**:349–361. DOI:10.1016/j.gaitpost.2006.10.013.
- Seipel JE, Holmes P (2005)** Running in three dimensions: Analysis of a point-mass sprung-leg model. *The International Journal of Robotics Research*, **24(8)**:657–674. DOI:10.1177/0278364905056194.
- Seydel R (1984)** A continuation algorithm with step control. **Küpper T, Mittelman H, Weber H**, eds., *Numerical Methods for Bifurcation Problems*, vol. 70 of *International Series of Numerical Mathematics*, 480–494. Birkhäuser. DOI:10.1007/978-3-0348-6256-1\_33.
- Seydel R (2010)** *Practical bifurcation and stability analysis*, vol. 5. Springer. ISBN:978-1-4419-1739-3.
- Seyfarth A, Geyer H, Günther M, Blickhan R (2002)** A movement criterion for running. *Journal of Biomechanics*, **35(5)**:649–655. DOI:10.1016/S0021-9290(01)00245-7.
- Seyfarth A, Geyer H, Herr HM (2003)** Swing-leg retraction: a simple control model for stable running. *Journal of Experimental Biology*, **206(15)**:2547–2555. DOI:10.1242/jeb.00463.
- Seyfarth A, Grimmer S, Häufle D, Maus HM, Peuker F, Kalveram KT (2012)** Biomechanical and neuromechanical concepts for legged locomotion: Computer models and robot validation. *Routledge Handbook of Motor Control and Motor Learning*, chap. 5, 90–110. Routledge International Handbooks. ISBN:978-0-415-66960-3.
- Seyfarth A, Lipfert SW, Rummel J, Maus HM, Maykranz D (2013)** Walking and running: How leg compliance shapes the way we move. **Mombaur K, Berns K**, eds., *Modeling, Simulation and Optimization of Bipedal Walking*, vol. 18 of *Cognitive Systems Monographs*, 211–222. Springer. DOI:10.1007/978-3-642-36368-9\_17.

- Shampine L, Reichelt M (1997)** The MATLAB ODE suite. *SIAM Journal on Scientific Computing*, **18(1)**:1–22. DOI:10.1137/S1064827594276424.
- Shampine LF, Kierzenka J, Reichelt MW (2000)** *Solving boundary value problems for ordinary differential equations in MATLAB with bvp4c*.
- Shearer M (1980)** One-parameter perturbations of bifurcation from a simple eigenvalue. *Mathematical Proceedings of the Cambridge Philosophical Society*, **88(01)**:111–123. DOI:10.1017/S0305004100057388.
- Song KM, Halliday SE, Little DG (1997)** The effect of limb-length discrepancy on gait. *The Journal of Bone and Joint Surgery*, **79(11)**:1690–1698.
- Srinivasan M (2010)** Fifteen observations on the structure of energy-minimizing gaits in many simple biped models. *Journal of The Royal Society Interface*, **8(54)**:74–98. DOI:10.1098/rsif.2009.0544.
- Stoer J, Bulirsch R (1993)** *Introduction to Numerical Analysis*. Springer, second edn. ISBN:978-3-5409-7878-7.
- Strelkova N (2014)** Stochastic complexity analysis in synthetic biology. **Zelinka I, Sanayei A, Zenil H, Rössler OE**, eds., *How Nature Works*, vol. 5 of *Emergence, Complexity and Computation*, 161–194. Springer International Publishing. DOI:10.1007/978-3-319-00254-5\_8.
- Strogatz SH (1994)** *Nonlinear dynamics and chaos: With applications to physics, biology, chemistry, and engineering*. Westview Press. ISBN:978-0-2015-4344-5.
- Sup F, Varol HA, Mitchell J, Withrow TJ, Goldfarb M (2009)** Self-contained powered knee and ankle prosthesis: Initial evaluation on a transfemoral amputee. *Proceedings of International Conference on Rehabilitation Robotics (ICRR)*, 638–644. IEEE, Kyoto, Japan. DOI:10.1109/ICORR.2009.5209625.
- Thota P, Dankowicz H (2008)**  $\widehat{TC}$ : A novel toolbox for the continuation of periodic trajectories in hybrid dynamical systems. *SIAM Journal on Applied Dynamical Systems*, **7**:1283–1322. DOI:10.1137/070703028.
- Valderrabano V, Nigg BM, Hintermann B, Goepfert B, Dick W, Frank CB, Herzog W, Tschanner Vv (2007)** Muscular lower leg asymmetry in middle-aged people. *Foot & Ankle International*, **28(2)**:242–249. DOI:10.3113/FAI.2007.0242.
- Vejdani HR, Blum Y, Daley MA, Hurst JW (2013)** Bio-inspired swing leg control for spring-mass robots running on ground with unexpected height disturbance. *Bioinspiration & Biomimetics*, **8(4)**:046006. DOI:10.1088/1748-3182/8/4/046006.

- Wallisch W, Hermann M (1987)** *Numerische Behandlung von Fortsetzungs- und Bifurkationsproblemen bei Randwertaufgaben*, vol. 102 of *Teubner-Texte zur Mathematik*. Teubner. ISBN:978-3-3220-0431-4.
- Weber H (1979)** Numerische Behandlung von Verzweigungsproblemen bei gewöhnlichen Differentialgleichungen. *Numerische Mathematik*, **32**:17–29. DOI:10.1007/BF01397647.
- Weber H (1981)** On the numerical approximation of secondary bifurcation problems. *Numerical Solution of Nonlinear Equations*, vol. 878 of *Lecture Notes in Mathematics*, 407–425. Springer. DOI:10.1007/BFb0090690.
- Yosida K (1980)** *Functional Analysis*. Springer, sixth edn. ISBN:978-3-5401-0210-6.
- Zeidler E (1998)** *Nonlinear functional analysis and its applications I: Fixed-point theorems*. Springer. ISBN:978-0-3879-0914-1.

# Danksagung

Ich möchte mich sehr herzlich bei Prof. Dr. Martin Hermann und Prof. Dr. Andre Seyfarth bedanken, die mir die Welt der Bifurkationen und des Feder-Masse-Modells gezeigt haben.

Allen Kollegen aus dem Institut für (Angewandte) Mathematik und aus dem Lauflabor danke ich für nette Atmosphäre. Insbesondere bedanke ich mich bei Dr. Dieter Kaiser für alle Gespräche, die nichts mit Mathematik zu tun hatten, und bei Dr. Yvonne Blum, Dr. Frank Peuker, Dr. Sebastian Riese und Jürgen Rummel für ihre Hilfe bei der Erstellung dieser Arbeit.

Einen besonderen Dank möchte ich meiner Mutter, Katharina Merker, aussprechen, die mich immer unterstützt hat.

Schließlich danke ich der Deutschen Forschungsgesellschaft (DFG), die Teile dieser Arbeit finanziell gefördert hat.

# Ehrenwörtliche Erklärung

Hiermit erkläre ich,

- dass mir die Promotionsordnung der Fakultät bekannt ist,
- dass ich die Dissertation selbst angefertigt habe, keine Textabschnitte oder Ergebnisse eines Dritten oder eigenen Prüfungsarbeiten ohne Kennzeichnung übernommen und alle von mir benutzten Hilfsmittel, persönliche Mitteilungen und Quellen in meiner Arbeit angegeben habe,
- dass ich die Hilfe eines Promotionsberaters nicht in Anspruch genommen habe und dass Dritte weder unmittelbar noch mittelbar geldwerte Leistungen von mir für Arbeiten erhalten haben, die im Zusammenhang mit dem Inhalt der vorgelegten Dissertation stehen,
- dass ich die Dissertation noch nicht als Prüfungsarbeit für eine staatliche oder andere wissenschaftliche Prüfung eingereicht habe.

Bei der Auswahl und Auswertung des Materials sowie bei der Herstellung des Manuskripts haben mich folgende Personen unterstützt:

.....  
.....

Ich habe die gleiche, eine im wesentlichen Teilen ähnliche bzw. eine andere Abhandlung\* bereits bei einer anderen Hochschule als Dissertation eingereicht:     Ja / Nein\*.

(\* Zutreffendes unterstreichen)

Wenn Ja, Name der Hochschule: .....

Ergebnis: .....

Jena, den 17.07.2014

Unterschrift